Growth and characterisation of p-type delafossite transparent conducting thin films for heterojunction applications

Thesis submitted to

COCHIN UNIVERSITY OF SCIENCE AND TECHNOLOGY

in partial fulfillment of the requirements

for the award of the degree of

DOCTOR OF PHILOSOPHY

Vanaja.K.A

Department of Physics
Cochin University of Science and Technology
Kochi – 682 022, Kerala, India

May 2011

Growth and characterisation of p-type delafossite transparent conducting thin films for heterojunction applications

Ph.D thesis in the field of material science

Author:

Vanaja.K.A
Division for Research in Advanced Materials
Department of Physics
Cochin University of Science and Technology
Kochi – 682 022, Kerala, India
email: vanajajayaraj@gmail.com

Supervisor:

Dr. S.Jayalekshami
Professor
Division for Research in Advanced Materials
Department of Physics
Cochin University of Science and Technology
Kochi – 682 022, Kerala, India
email: jayalekshmi@cusat.ac.in

Front cover: Schematic of the transparent n-ZnO/p-$AgCoO_2$ pn heterojunction and its I-V characteristics
Back cover: TEM picture of α-$AgGaO_2$ thin film grown on carbon coated copper grid and the inset shows the atomic scale image of the film

May 2011

Dr.S.Jayalekshmi
Professor
Department of Physics
Cochin University of Science and Technology
Kochi – 682 022

May 4 2011

Certificate

Certified that the work presented in this thesis entitled "***Growth and characterisation of p-type delafossite transparent conducting thin films for heterojunction applications***" is based on the authentic record of research done by Smt Vanaja.K.A under my guidance in the Department of Physics, Cochin University of Science and Technology, Kochi – 682 022 and has not been included in any other thesis submitted for the award of any degree.

Dr. S.Jayalekshmi

(Supervising Guide)

Phone : +91 484 2577404 Fax: 91 484 2577595 email : jayalekshmi@cusat.ac.in

Declaration

Certified that the work presented in this thesis entitled "***Growth and characterisation of p-type delafossite transparent conducting thin films for heterojunction applications***" is based on the original research work done by me under the supervision and guidance of Dr. S.Jayalekshmi, Professor, Department of Physics, Cochin University of Science and Technology, Cochin-682022 and has not been included in any other thesis submitted previously for the award of any degree.

Kochi – 22
4 th May 2011

Vanaja.K.A.

Acknowledgement

I am deeply indebted to my guide, Dr. S.Jayalekshemi. for her constant encouragement and for sharing her knowledge with me throughout the course of my research. I am deeply indebted to her for the gentle and inspiring guidance, forbearance, constant encouragement and support.

I would like to express my sincere gratitude to the present and former Heads of the Department for permitting me to use the facilities. I gratefully acknowledge the help and inspiration from all the other faculty members of the Department of Physics.

I am thankful to all the office and library staff of the Department of Physics and the technical staff at USIC for all the help and cooperation.

I am thankful to the Department of Science and Technology, Government of India for the financial support under Women Scientist Scheme.

I remember with gratitude the sincere support I have received from all the research students of Optoelectronic Device Laboratory, especially the support from Dr.Nisha, Dr.Asha, Dr.Manoj, Dr.Ajimsha, Dr.Reshmi.and Dr Aneesh. I would also like to thank the research students of Advanced Materials Laboratory.
I would like to thank Prof.A.W.Sleight, and Prof J.Tate of Oregon State University for providing me a fellowship and introducing me to the field of p-type transparent oxides.

I would like to thank my husband Jayaraj and my daughters Anooja and Anjala for their support and patience
I am thankful to God Almighty for benevolently showering upon me this blessing in life

Contents

Preface xiii

Chapter 1 1

Introduction to transparent conducting oxides

1.1 Introduction 3

1.2 How can a material be transparent and conducting simultaneously? 5

1.3 Electrical and optical properties. 6

1.4 Properties of TCOs 8

1.4.1 Electrical properties 8

1.4.2 Optical properties and plasma frequency 10

1.5 Transparent p-type conducting oxides 11

1.5.1 Material consideration 11

1.5.2 Preferred crystal structure 13

1.6 Selection of the material for present study 16

1.7 An overview of p-type TCO thin films 19

References 27

Chapter 2 37

Experimental and analytical techniques

2.1 Introduction 39

2.2 Bulk synthesis 40

2.2.1 Solid state reaction 40
2.2.2 Ion exchange reaction 41
2.2.3 Hydrothermal synthesis 44
2.3 Thin film growth techniques 47
2.3.1 Thermal evaporation by resistive heating 48
2.3.2 Sputtering 49
2.3.3 Pulsed laser deposition (PLD) 56
2.4 Characterisation tools 62
2.4.1 Thin film thickness 62
2.4.2 Structural characterisation 63
2.4.3 Morphological analysis 65
i. Scanning Electron Microscope(SEM) 65
ii. Atomic Force Microscopy(AFM) 67
2.4.4 Compositional analysis 70
i. Energy dispersive x-ray (EDX) analysis 70
ii Transmission electron microscopy (TEM) 72
2.4.5 Electrical transport properties 74
i Hall effect measurements 74
ii Thermopower measurements 77
2.4.6 Optical studies 79
i Diffuse reflectance spectroscopy (DRS) 79
ii Transmission spectroscopy 80
References 82

Chapter 3 85

Synthesis of copper delafossites and growth of thin films

3.1 Introduction 87
3.2 RF magnetron sputtered $CuAlO_2$ thin films 88
  3.2.1 Experimental 89
  3.2.2 Results and discussion 90
3.3 Growth and characterisation of polycrystalline $CuYO_2$ and Ca doped $CuYO_2$ thin films 94
  3.3.1 Experimental 94
  3.3.2 Results and discussion 96
3.4 Growth and characterisation of $CuGaO_2$ and $CuGa_{1-x}Fe_xO_2$ thin films 102
  3.4.1 Experimental 103
  3.4.2 Results and Discussion 103
3.5 Conclusion 110
References 112

Chapter 4 115

Synthesis of $AgCoO_2$ and fabrication of p-$AgCoO_2$/n-ZnO heterojunction

4.1 Introduction 117
4.2 Experimental 118
4.3 Synthesis and characterisation of $AgCoO_2$ bulk powder and

thin films 119
4.4 Fabrication of the all transparent pn junction 126
4.4.1 Deposition of transparent conducting ITO thin films. 127
4.4.2 Deposition of n-ZnO thin films by sputtering 130
4.5 Conclusion 136
References 137

Chapter 5 141

Hydrothermal synthesis of p-type $AgGaO_2$ and fabrication n-ZnO/p-$AgGaO_2$ pn junction by pulsed laser deposition

5.1 Introduction 143
5.2 Synthesis of bulk $AgGaO_2$ powder 144
5.2.1 Characterisation of the $AgGaO_2$ powder material 145
5.3 Growth of $AgGaO_2$ thin films by PLD 150
5.4 Conclusion 158
References 159

Chapter 6 161

Summary and scope for future works

6.1 Summary 163
6.2 Scope for future work 165
References 166

Preface

"Transparent electronics" or "invisible electronics" and "flexible electronics" are some of the research areas which have undergone tremendous progress during the past decade. Metal oxides which have wide band gap, and are stable, environment friendly and abundant are being investigated as substitutes to silicon electronics. Some of the passive applications of these oxides are as transparent conductors and have become familiar examples in automatic teller machines, liquid crystal displays, solar cells, energy efficient windows and flat panel displays. Most of the useful oxide-based materials are *n*-type conductors that ideally have a wide band gap (>3 eV), can be doped to degeneracy, and have a conduction band shape that ensures that the plasma absorption edge lies in the infrared range. The transparency of the transparent conducting oxide(TCO) films in the visible region is a result of the wide band gap of the material and the n type conductivity is mainly due to the oxygen ion vacancies that contribute to the excess electrons in the metal atoms.

The application of TCOs has been restricted to transparent electrodes, notwithstanding the fact that TCOs are n-type semiconductors. The basic reason is the lack of p-type TCOs, and many of the active functions in semiconductors originate from the nature of *pn*-junction. In 1997, Kawazoe et al. from Tokyo Institute of Technology, Japan, reported for the first time, p-type conductivity in a highly transparent thin film of copper aluminum oxide ($CuAlO_{2+x}$). This has opened up a new field in optoelectronics device technology, the so-called *Transparent Electronics* or *Invisible Electronics* , where a combination of the

two types of TCOs in the form of a p-n junction could lead to a ''functional'' window, which transmits the visible portion of solar radiation, yet generates electricity by the absorption of the UV part. The non-stoichiometric and doped versions of various new types of p-type transparent conducting oxides with improved optical and electrical properties are being synthesised by various research groups. In the new class of delafossite films of AMO_2 structure where A is monovalent such as Cu, Ag, Pd and M is trivalent, like Al, Y, Sc etc all the films reported earlier were copper delafossite and the lone silver delafossite $AgInO_2$ film is a n-type conductor. In the present study the effort was to improve the p- type conductivity of various copper delafossite thin films by either doping or by oxygen intercalation. A low temperature hydrothermal synthesis was adopted for the synthesis of the silver delafossites like $AgGaO_2$ and $AgCoO_2$. Thin films of these silver delafossites were grown by pulsed laser deposition and by rf magnetron sputtering. These p-type oxides along with n-ZnO were used for the fabrication of all transparent pn junction diodes.

The first chapter gives general introduction to the transparent conducting oxides and the basic reasons for materials to exhibit simultaneously transparency and conductivity are also dealt with. A method called chemical modulation of valance band is reviewed and the criteria of material selection and preferred crystal structure for a p-type conductor is discussed. A review of literature on TCO in particular the p-type delafossite TCOs are described in this chapter.

The second chapter gives the techniques used for the synthesis of the material, their growth in thin film and various characterisation tools. The bulk materials, the copper delafossites were synthesised by high temperature solid state reaction whereas for the silver delafossites low temperature techniques like

hydrothermal and ion exchange reactions were adopted. The thin film growth, pulsed laser deposition and rf magnetron sputtering used for the film growth is discussed. A brief working principle of various characterisation tools used viz; XRD, SEM, AFM, TEM, UV-vis-nir spectrometer, and electrical characterisation techniques, etc are discussed in this chapter.

The third chapter describes the synthesis of various copper delafossite bulk material and the growth of these materials in thin film form. Various copper delafossite materials viz; $CuAlO_2$, $CuGaO_2$, $CuFeO_2$, $CuGa_{1-x}Fe_xO_2$, $CuYO_2$ and $CuCa_xY_{1-x}O_2$ were synthesised by solid state reaction technique. These copper delafossite materials were grown in thin film form by rf magnetron sputtering technique. In general copper delafossites exhibit good optical transparency. The conductivity of the $CuYO_2$ was improved by Ca doping or by oxygen intercalation by annealing the film in oxygen atmosphere. It has so far been impossible to improve the p-type conductivity of $CuGaO_2$ significantly by doping Mg or Ca on the Ga site. Reports show, oxygen intercalation or divalent ion doping on Ga site is not possible for $CuGaO_2$ thin films to improve the p-type conductivity. $CuFeO_2$ powder and crystals have been reported as the materials having the highest p-type conductivity among the copper and silver delafossites. However the $CuFeO_2$ films are found to be less transparent in the visible region compared to $CuGaO_2$. The solid solution between the $CuGaO_2$ and $CuFeO_2$ was effected by solid state reaction varying the Fe content. The $CuGa_{1-x}Fe_xO_2$ with Fe content x=0.5 shows an increase in conductivity by two orders compared to $CuGaO_2$ but the transparency is only about 50% in the visible region which is less than that of $CuGaO_2$.

$AgCoO_2$ thin films with 50% transparency in the visible region were deposited on single crystalline Al_2O_3 and amorphous silica substrates by RF

magnetron sputtering and the p type conductivity of $AgCoO_2$ was demonstrated by fabricating transparent p-n junction diode with $AgCoO_2$ as p-side and ZnO: Al as n-side using sputtering. Junction thus obtained was found to be rectifying with a forward to reverse current of about 10 at an applied voltage of 3 V. The present study shows that silver delafossite thin films with p-type conductivity can be used for the fabrication of active devices for transparent electronics applications. The results on the investigations on $AgCoO_2$ are presented in chapter four.

Chapter five describes the synthesis of $\alpha-AgGaO_2$ by two step process which involves the synthesis of β-$AgGaO_2$ by ion exchange reaction followed by the hydrothermal conversion of the β-$AgGaO_2$ into α-$AgGaO_2$. The trace amount of Ag has been reduced substantially in the two step synthesis compared to the direct hydrothermal synthesis Thin films of α-$AgGaO_2$ were prepared on silicon and Al_2O_3 substrates by pulsed laser deposition. These studies indicate the possibility of using this material as p-type material in thin film form for transparent electronics. We have grown wide band gap α-$AgGaO_2$ p-type conducting thin film by pulsed laser deposition. The room temperature conductivity was measured as 3.17×10^{-4} $Scm^{-1}$and the optical band gap was estimated as 4.12 eV. A transparent p-n junction thin film diode on glass substrate was fabricated using p-type α-$AgGaO_2$ and n-ZnO.

The final concluding chapter gives the summary and scope for future work. Transparent electronics which is an emerging area calls for the realization of new active devices with good performance efficiency which in turn requires the development of new materials and growth techniques.

Part of the work presented in the thesis has been published in various journals.

1. p-$AgCoO_2$/n-ZnO heterojunction diode grown by rf magnetron sputtering, K.A.Vanaja, U.M.Bhatta, R.S.Ajimsha, S.Jayalekshmi and M.K.Jayaraj Bull Mater.Sci 31(2000)753
2. Effect of Oxygen intercalation on the properties of sputtered $CuYO_2$ for potential use as p-type transparent conducting films, R. Manoj, M. Nisha, K.A. Vanaja, M.K. Jayaraj, Bulletin of Materials Science 31(1), 49 (2008
3. Pulsed Laser Deposition of p-type α-$AgGaO_2$ thin films. K. A. Vanaja, R. S. Ajmsha, A. S. Asha, K. Rajeev Kumar and M. K. Jayaraj, Thin Solid Films 516 (7), 1426 (2008)
4. Transparent p-$AgCoO_2$/n-ZnO Diode Heterojunction Fabricated by Pulsed Laser Deposition, R. S. Ajimsha, K. A. Vanaja, M. K. Jayaraj, P. Misra, V. K. Dixit and L. M. Kukreja. Thin solid film 515, 7352 (2007)
5. p-type electrical conduction in α-$AgGaO_2$ delafossite thin films, K.A. Vanaja, R.S. Ajmsha, A.S. Asha and M.K. Jayaraj, Applied Physics Letters 88, 212103 (2006)

Other publications

6. Nuclear Quadrupole Resonance Studies of Transparent Conducting Oxides, W. W. Warren, Jr., A. Rajabzadeh, T. Olheiser, J. Liu, J. Tate, M. K. Jayaraj, K. A. Vanaja, Solid State Nuclear Magnetic Resonance 26, 209 (2004)
7. Photoacoustic investigations on thermal diffusivity of $CuGa_{1-x}Fe_xO_2$, Jyotsna Ravi, M.K.Jayaraj, K.V.Vanaja,K.P.R.Nair and T.M.A.Rasheed, Semiconductor Science and Technology 18, 693(2003)

8. P-type oxides for use in transparent diodes. J. Tate, M.K.Jayaraj, A. D. Draeseke, T. Ulbrich, A. W. Sleight, K. A. Vanaja, R. Nagarajan, J. F. Wager, and R. L. Hoffman , Thin Solid Films 411, 119 (2002)
9. P-type conductivity in the delafossite Structure, R.Nagarajan, N.Duan, M.K.Jayaraj, J.Li, K.A.Vanaja, A.Yokochi, A.Draskee, J.Tate and A.W.Sleight, Int J. Inorganic Materials 3, 265(2001)
10. Synthesis of ZnO nanoparticles by hydrothermal method, P.M. Aneesh, K.A. Vanaja and M.K. Jayaraj, Proc. SPIE Vol. 6639, (Sep. 2007)
11. Growth of ITO thin films on polyamide substrate by bias sputtering, M. Nisha, K. A. Vanaja, K. C. Sanal, K. J. Saji, P. M. Aneesh and M. K Jayaraj, Materials Science in Semiconductor Processing, 13, 64 (2010)

Conference publications

1. Effect of oxygen intercalation on the properties of sputtered $CuY_{(1-x)}Ca_xO_2$ p-type transparent conducting oxides, R. Manoj, M. Nisha, K.A. Vanaja, M.K. Jayaraj, International conference on Materials for advanced technology ICMAT 2005
2. Transparent Electronics, M.K. Jayaraj, K.A. Vanaja, A.S. Asha, Rajeev Kumar, Invited talk International Conference on Optoelectronic materials and thin films for advanced technology, OMTAT-2005
3. Transparent p-$AgCoO_2$/n-ZnO junction fabricated by Pulsed Laser Deposition R.S.Ajmsha, K.A. Vanaja, M.K. Jayaraj, P.Misra and L.M.Kukreja DAE-BRNS 3rd National conference PLD 2005
4. Transparent p-$AgCoO_2$/n-ZnO pn junction K.A.Vanaja, M.Nisha, A.S.Asha, M.K.Jayaraj, Photonics 2004

5. Electrical and optical properties of α-$AgGaO_2$ synthesised by hydrothermal reaction, K.A.Vanaja., M.Nisha., A.S.Asha., M.K.Jayaraj, Solid state symposium 2004
6. rf magnetron sputtered calcium doped copper yttrium oxide p-type transparent semiconductor, Manoj.R, Sreejith S Pillai, Nisha.M, Vanaja.K.A and M.K.jayaraj, DAE solid state symposium, Gowaliar, December 2003
7. Thermal Characterisation of $CuGa_{1-x}Fe_xO_2$ using open photo-acoustic cell, J.Ravi, M.K.Jayaraj, Vanaja.K.A,K.P.Rajjappan Nair,T.M.A.Rasheed, Asia-Pacific optical and wireless conference Nov 2003, Whuan, China
8. NMR Relaxation Study of the p-Type Transparent Conductor $CuYO_2$:Ca, A. Rajabzadeh, T. Olheiser, V. Achuthan, M. K. Jayaraj, J. Tate, W. W. Warren, Jr presented at the *March Meeting of the American Physical Society*, Indianapolis, IN, March 2002. (B23.011)
9. NMR and NQR Studies of $CuMO_2$-based Transparent p-Type Conductors", A. Rajabzadeh, F. Monte, J. Liu, T. Olheiser, V. Achuthan, M. K. Jayaraj, J. Tate, W. W. Warren Jr., presented at the March Meeting of the American Physical Society, Seattle, WA, March 2001. (E30.006)
10. P-type transparent $CuGaFeO_2$ thin films, K.A.Vanaja, M.K.Jayaraj, T.Ulbrich, J.Tate and A.W.Sleight. ACS meeting 2001, Seattle, WA. June 2001
11. P-type oxides for use in transparent diodes. J. Tate, M. K. Jayaraj, A. D. Draeseke, T. Ulbrich, A. W. Sleight, K. A. Vanaja, R. Nagarajan, J. F. Wager, and R. L. Hoffman (Oregon Univ.) International symposium on Transparent Oxide thin films for electronics and optics, Tokyo, Japan (2001)

Chapter 1

Introduction to transparent conducting oxides

Abstract

*Transparent electronics is becoming a reality. Transparent pn hetrojunction diodes, UV light emitting diodes and transparent thin film transistors have become part of prototype commercial products. The developments in the field of transparent electronics call for understanding the basic properties of transparent conducting oxides. This chapter gives the description of the characteristic properties and applications of transparent conducting oxides, and basic principles of design of n-type and p-type transparent materials. A brief discussion on the recent developments in transparent electronics is also presente*d.

1.1 Introduction

Metal oxides have wide band gap because of significant contribution of ionic character to the chemical bonds between the metallic cations and oxide ions. Inorganic solids with wide band gap are usually insulators which find application as dielectrics and optical materials in industry. Metal oxides because of their ionic character suppress the formation of easily ionisable shallow donors or acceptors and enhance localisation of electrons and holes. Hence, in general metal oxides are not electrically conducting. However, current interest in material science is in unravelling the fundamental aspects of transparent conducting oxides and their applications as semiconducting and conducting transparent thin films. There are some exceptionally good conductive oxides with wide band gap [1] which are transparent to the visible region of electromagnetic waves. The p-block heavy metallic cations with ns^0 electronic configuration such as ZnO, CdO, Ga_2O_3, In_2O_3, SnO_2, PbO_2, Sb_2O_5 and their mixed oxides can be made n-type by electron doping. The electron doping can be easily achieved by making them oxygen deficient.

Badeker in 1907 was the first to report transparent conducting oxide (TCO) films prepared by thermal oxidation of cadmium [2]. The thin films of cadmium metal deposited in a glow discharge chamber could be oxidized to become transparent while remaining electrically conducting. Since then, the commercial value of these thin films has been recognized, and the list of potential TCO materials has expanded to include aluminium doped ZnO [3], SnO_2 [4], fluorine doped In_2O_3 [5] etc. Most of the research to develop highly

transparent and conducting thin films has focussed on n-type semiconductors consisting of metal oxides. Historically, TCO films composed of binary compounds were developed by means of physical and chemical deposition methods [6, 7] One of the advantages of using binary compound as TCO material is that their chemical composition in film deposition is relatively easier to control than that of ternary and multicomponent oxides. Until now, undoped and doped films such as SnO_2, In_2O_3, ZnO, CdO have been developed. These materials have a free electron concentration of the order of 10^{20} cm^{-3} provided by native donors such as oxygen vacancies and interstitial metal atoms. Since impurity doped materials can use both native and impurity donors, undoped binary materials have got limited range of applications. In addition to these binary compounds, ternary compounds such as Cd_2SnO_4, $CdSnO_3$ and $CdIn_2O_4$ have also been developed prior to 1980 [8, 9].

In order to get TCO films suited for specialized applications, new TCO materials have been studied actively. TCO materials consisting of multicomponent oxides have been developed in 1990s. In these material systems, TCO materials consisting of ternary compounds such as Zn_2SnO_4 [10], $MgIn_2O_4$ [11], $ZnSnO_3$ [12], $GaInO_3$ [13] as well as multicomponent oxides composed of combinations of these ternary compounds were developed. The advantage of the multicomponent oxide materials is the fact that their electrical, optical, chemical and physical properties can be controlled by altering their chemical compositions.

In 1999, Minami et al [14] reported $Zn_2In_2O_5$-$MgIn_2O_4$ multicomponent oxide as a new TCO material. Transparent conductors were prepared by magnetron sputtering of compounds such as $MgIn_2O_4$, $ZnSnO_3$, $GaInO_3$

$Zn_2In_2O_5$ and $In_4Sn_3O_{12}$.$In_{2-x}Sn_xO_3$ (ITO) thin films are commercially being used as a transparent electrode. Recently the electrical conductivity as high as 1.3×10^4 Scm^{-1} [15] has been reported in ITO thin films grown by pulsed laser deposition (PLD)**.** Thin films of (~10-20 nm) metals such as Au, Ag, Cu, Fe etc have also been found to have similar electrical and optical properties, however these films generally are not stable and require some protective coatings. On the other hand the stability and hardness of thin films based on wide band gap conducting oxides are far superior to those of metallic films.

The conductivity of the TCOs can be varied across a wide range from insulator, to metal. However, these TCOs are mainly n-type, where electrons are responsible for the electrical conduction. Fabrication of all transparent pn junction calls for the development of p-type TCOs. Transparent thin film FET has been fabricated using n-type TCOs [16, 17]. The transparent electronics requires TCOs with p-type and n-type conductivities. Design of TCOs with p-type and n-type materials calls for the need of understanding the basic properties of transparent conducting oxides. Some of them are described in the preceding sections.

1.2 How can a material be transparent and conducting simultaneously?

The optical transparency and electrical conductivity of the solids are antonyms to each other. This can be easily understood using the basic equations in electromagnetic theory [18, 19]. For electromagnetic waves passing through an uncharged semiconducting medium, the solution to Maxwell's equations gives the real and complex parts of the refractive index as

$$n^2 = \frac{\varepsilon}{2}\left[\left\{1+\left(\frac{2\sigma}{\upsilon}\right)^2\right\}^{\frac{1}{2}} + 1\right] \quad \text{and}$$

$$k^2 = \frac{\varepsilon}{2}\left[\left\{1+\left(\frac{2\sigma}{\upsilon}\right)^2\right\}^{\frac{1}{2}} - 1\right]$$

where n is the refractive index of the medium, k is the extinction coefficient, ε is the dielectric constant, σ is the conductivity of the medium and ν is the frequency of the electromagnetic radiation. In the case of an insulator $\sigma \to 0$, $n \to \varepsilon^{\frac{1}{2}}$ and $k \to 0$. This implies that an insulator is transparent to electromagnetic waves.

For a perfect conductor, the solution to the Maxwell's equations yields, the reflected and transmitted components of the electric field vector as $E_R = -E_I$ and $E_T = 0$. This means that the wave is totally reflected with a 180^0 phase difference. Or in other words, a good conductor reflects the radiations incident on it, while a good insulator is transparent to the electromagnetic radiations.

1.3 Electrical and optical properties

The optical phenomena in the IR range can be explained on the basis of Drude's theory for free electrons in metals[20-22]. When the free electrons interact with an electromagnetic field, it may lead to polarization of the field within the material. It affects the relative permittivity ε. For an electron of mass m moving in an electric field, the equation of motion can be written as,

$$m\left(\frac{d}{dt}+\frac{1}{\tau}\right)\delta \mathrm{v}(t) = F \tag{1.1}$$

where τ is the relaxation time and. δv is change in velocity

The force on an electron in an alternating field is given by

$$F = -eE\, e^{-i\omega t} \tag{1.2}$$

Let us assume a solution to (1.2) in the form $\delta v = \delta v\, e^{-i\omega t}$

Then (1.1) becomes, $m\left(-i\omega+\frac{1}{\tau}\right)\delta \mathrm{v} = -eE$

$$\text{or,} \qquad \delta \mathrm{v} = -\frac{e\tau/m}{1-i\omega\tau} \tag{1.3}$$

The current density is j = nqδv = $\frac{ne^2\tau}{m(1-i\omega\tau)}E$, where n is the electron concentration and q is the charge on the electron.

The electrical conductivity is $\sigma(\omega) = \frac{ne^2\tau}{m(1-i\omega\tau)} = \sigma_0 \frac{1+i\omega\tau}{1+(\omega\tau)^2}$ (1.4)

Here, $\sigma_0 = ne^2\tau / m$ is the dc conductivity.

At high frequencies, ωτ >>1,we can write,

$$\sigma(\omega) = \sigma_0\left(\frac{1}{(\omega\tau)^2}+\frac{i}{\omega\tau}\right) = \frac{ne^2}{m\omega^2\tau} + i\frac{ne^2}{m\omega} \tag{1.5}$$

In this equation the imaginary term is dominant and is independent of τ. Then we can express the result as a complex dielectric constant instead of expressing it as a complex conductivity.

The dielectric constant ε = 1+ (4πP/E) where $P = -\frac{ne^2/m}{\omega^2 + i\omega/\tau}E$.

Then,

$$\varepsilon(\omega) = 1 - \frac{4\pi ne^2/m}{\omega^2 + i\omega/\tau}. \tag{1.6}$$

This expression gives the dielectric constant of a free electron gas. For $\tau \to \infty$ the dielectric constant is positive and real if $\omega^2 > 4\pi ne^2/m$.

Electromagnetic wave can not propagate in a medium with negative dielectric constant because then wave vector is imaginary and the wave decays exponentially. Waves incident on such a medium are totally reflected. We can denote the cut off frequency as

$$\omega_p = \left(4\pi ne^2/m\right)^{1/2} \tag{1.7}$$

which is also known as the plasma frequency. The material is transparent to the em radiation whose frequency is greater than the plasma frequency. Plasma frequency depends on the carrier concentration n and is inversely proportional to the effective mass of the carrier. Plasma frequency in general is small in p-type materials owing to the large effective mass of holes.

1.4 Properties of TCOs

1.4.1 Electrical properties

Most of the research to develop highly transparent and conducting films has been focussed on n-type semiconducting metal oxides. In this section some of the factors governing the conduction in n-type TCOs are discussed.

Numerous investigations have been carried out on the electrical properties of transparent conducting oxide films to understand the conduction phenomena involved [23-25]. Systematic studies have been carried out the effect of various parameters such as the nature and temperature of the substrate, film thickness, dopant and its concentration etc[26-28] on the electrical properties of TCO films in order to optimize the growth conditions.

The high conductivity of the TCO films results mainly from stoichiometric deviation. The conduction electrons in these films are supplied from donor sites associated with oxygen vacancies or excess metal ions [29]. These donor sites can be easily created by chemical reduction. Unintentional doping which happens mainly in the case of film deposition by spray pyrolysis, intentional doping, contamination by alkali ions from the glass substrate etc can affect electrical conductivity.One of the major factors governing the conductivity of TCO films is the carrier mobility. The mobility of the carriers in the polycrystalline film is dependent on the mechanism by which carriers are scattered by lattice imperfections. The various scattering mechanisms involved in semiconducting thin films are acoustic deformation potential scattering, piezoelectric scattering, optical phonon scattering, neutral impurity scattering, ionized impurity scattering, electron-electron scattering and grain boundary scattering [30-32].

In the case of a polycrystalline film, the conduction mechanism is dominated by the inherent inter-crystalline boundaries rather than the intra-crystalline characteristics. These boundaries generally contain fairly high densities of interface states which trap free carriers by virtue of the inherent disorders and the presence of trapped charges. The interface states result in a

space charge region in the grain boundaries. Due to this space charge region, band bending occurs, resulting in potential barriers to charge transport.

1.4.2. Optical properties and plasma frequency

The optical properties of a transparent conducting film depend strongly on the deposition parameters, microstructure, level of impurities and growth techniques. Being transparent in the visible and NIR ranges and reflecting to IR radiations, they act as selective transmitting layers. The spectral dependence of a TCO is given in figure1.1.

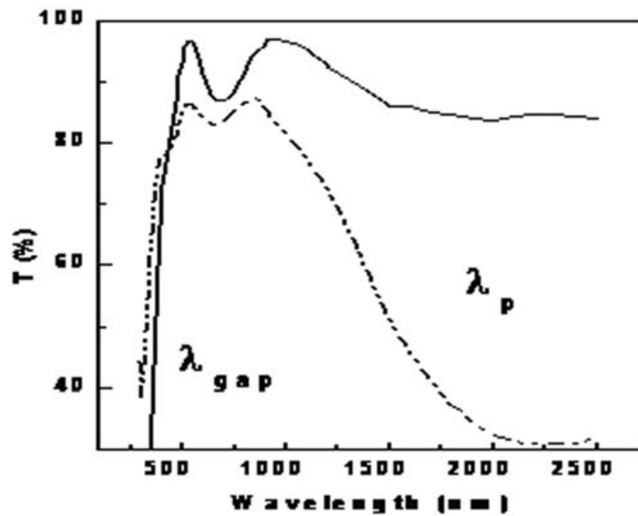

Figure 1.1. Typical transmission spectra of TCO thin film (ITO). (λ_{gap} indicates the absorption wavelength region corresponding to band gap, λ_p indicates plasma wavelength corresponding to the plasma frequency ω_p). The doted curve is the transmission spectrum of ITO film with higher carrier concentration compared to the solid curve and hence higher ω_p. The oscillations in the transmission spectra are due to the interference.

The spectral dependence shows that for wavelengths longer than plasma wavelength, the TCO reflects radiation while for shorter wavelengths TCO is transparent. At frequencies higher than the plasma frequency, the electrons cannot respond, and the material behaves as a transparent dielectric. At frequencies below the plasma frequency, the TCO absorbs incident radiation. For most TCO materials, the plasma frequency falls in the near-infrared part of the spectrum, and the visible region is in the higher, transparent frequency range. The plasma frequency increases approximately with the square root of the conduction electron concentration. The maximum obtainable electron concentration and the plasma frequency of TCOs generally increase in the same order as the resistivity [33].

1.5 Transparent p-type conducting oxides

1.5.1 Material consideration

Most of the existing and commercially available TCOs are n-type. The difficulty in ambipolar (p-type and n-type) doping of certain class of materials which is essential for the realisation of heterojunction devices is one of the important hurdles for the technological utilisation of these materials for electronic devices. As the band gap of the material increases (e.g Si→GaAs→ ZnSe→ ZnO) generally the ambipolar doping becomes increasingly difficult. Diamond can be doped p-type but n-type doping is rather difficult [34], while ZnO can be easily doped n-type, its p-type doping is very difficult [35]. Some theoretical guiding principle which has to be judiciously experimented for doping strategies for wide gap materials which are difficult to be doped is given by Zuger [35]**.** The possible reason for the difficulty in doping the binary wide band gap oxides with p-type conductivity has been suggested to be the

electronic structure of these metal oxides [35-39]. Strong localisation of holes at oxygen 2p levels or an upper edge of the valance band is due to the high electronegative nature of oxygen, that is localisation is due to the ionicity of metallic oxide

The non-existence of p-type transparent conducting oxides is thought to originate from a general characteristic in the electronic structure of oxides: the strong localization of the upper edge of the valence band to oxide ions. Therefore, any finding of a p-type conducting oxide must include modification of the energy band structure to reduce the localization behaviour, which in turn requires new insight into the relation between electronic structure and properties of oxide materials. In the technological field, finding such a material may open the way to new applications such as ultraviolet-emitting diodes.

The first problem is how to reduce the strong localisation behaviour of positive holes at the valance band edge of the oxide materials. The oxygen 2p levels due to the ionicity of metallic oxides generally lie far lower than the valance metallic atoms [36]. Consequently, the positive hole introduced by substitution localises on the single oxygen atom and cannot migrate with in the crystal lattice even under an applied field. The possible solution is introduction of covalency in the metal oxygen bonding to induce the formation of extended valance band structure. A method called chemical modulation of valance band (CMVB) was introduced by Yanagi et al [40] to realise p-type TCOs. The second problem to be considered is what kind of cationic species and crystal structures should be selected for favouring the covalency. If the localization behaviour in the valence band of typical oxides is to be modified, the cationic

species is required to have a closed shell whose energy is almost comparable to those of the 2*p* levels of oxygen anions.

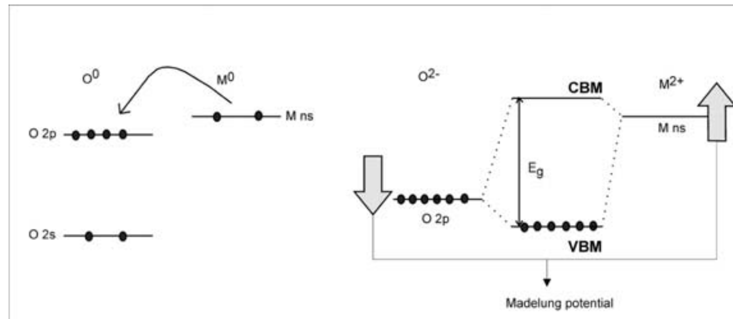

Fig.1.2. Formation of energy gap in ionic semiconductors.

The closed shell valence state is required to avoid coloration due to intra-atomic excitations. The cations that can be selected are Cu^+, Ag^+ and Au^+, which have the electronic configuration $d^{10}s^0$. Within the group of cations having the same electronic configuration, the energy of the d^{10} closed shell electrons is highest for these three cations, and is expected to overlap with that of the 2*p* electrons on oxide ions.

1.5.2 Preferred crystal structure

The second condition to be considered in the selection of the candidate oxide is the crystal structure which enhances the covalency in the bonding between the cation and oxide ion. One of the possible structures is the delafossite structure (Figure 1.3). The chemical formula of a delafossite is AMO_2 in which A and M are monovalent cation and a trivalent cation respectively. Delafossites have a hexagonal, layered crystal structure with the layers of A cations and MO_2 stacked alternately perpendicular to the c axis. There is no oxygen within the A cation layers, and only two oxygen atoms are

linearly coordinated to each cation in axial positions. The MO_2 layers consist of MO_6 octahedra, sharing edges. Each oxide ion is in pseudo-tetrahedral coordination.

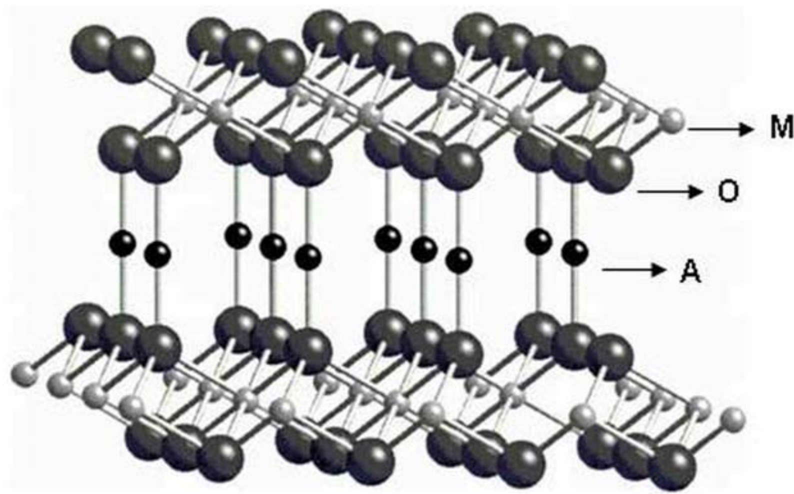

Figure 1.3 Delafossite structure

Recent interest has been directed to applications of p-type conductors that exploit their transparency in the infra red spectral range where they could serve as RF shields for IR sensors. In this case optical transparency is less important while good conductivity is essential. For photovoltaic applications transparency is of paramount importance. Transparency and conductivity co-exist in materials but one has to trade transparency for conductivity and vice versa. Unless carrier mobility is increased, this trade off will be more severe in the case of p-type materials. Several strategies have been adopted to expand the possibilities in the delafossite material AMO_2, and several have been implemented in thin film form.

Transparent, p-type semiconducting crystalline thin films have recently gained tremendous interest in the field of active devices. All-transparent junction devices have begun a new generation in the optoelectronics technology called *Invisible Electronics*. In 1997, Kawazoe et al. [38] from Tokyo Institute of Technology, Japan, reported for the first time, p-type conductivity in a highly transparent thin film of copper aluminium oxide ($CuAlO_{2+x}$). This has opened up a new field in optoelectronics device technology, the so-called *Transparent Electronics* or *Invisible Electronics*, where a combination of the two types of TCOs in the form of a p-n junction could lead to a ''functional'' window, which transmits visible portion of solar radiation yet generates electricity by the absorption of the UV part. The non-stoichiometric and doped versions of various new types of p-type transparent conducting oxides with improved optical and electrical properties are being synthesized by various research groups.

Now for diverse device applications, it is very important to prepare various new types of p-TCOs with superior optical and electrical characteristics, at least comparable to the existing, widely used n-TCOs, which have a transparency above 80% in the visible region and a conductivity of about 1000 S cm^{-1} or more. Extensive work has been done for the last five years in this direction to fabricate new p-TCOs by various deposition techniques. Intense work has been carried out for proper understanding of the structural, optical and electrical characteristics of p-TCOs.

P-type transparent $CuAlO_2$ semiconductor films were made by the spin-on technique from nanocrystals [41]. The nanocrystals were synthesized by a hydrothermal metathesis reaction. Scanning electron microscopy, X-ray diffraction and energy dispersive X-ray spectrometry suggest that the films

contain nano crystalline phases of $CuAlO_2$. Both the Hall technique and the Seebeck measurements reveal that the film is p-type and a very high room-temperature conductivity of 2.4 S cm^{-1} is achieved. This success in fabricating a high-conductivity transparent $CuAlO_2$ film indicates that nanotechnology will be helpful in enhancing the conductivity of p-type transparent semiconductors.

The sol-gel synthesis, wet chemical dipping of $CuAlO_2$ [42]and pulsed laser deposition (PLD)[43] of Cu_2SrO_2 opened up the possibility to make phase pure p-type TCOs by a variety of methods.For Cu_2SrO_2 by the chemical solution route, samples were made by spray deposition on quartz substrates using an aqueous solution of copper formate and strontium acetate. Phase pure materials were obtained by an optimum two stage annealing sequence. This initial work led to the development of good quality homogeneous films by a related sol-gel approach. They have also used pulsed laser deposition (PLD) to deposit Cu_2SrO_2 and $CuInO_2$ thin films on quartz substrates and obtained improved conductivities in the $CuInO_2$ thin films.

1.6 Selection of the materials for present study.

Taking into account the principle of chemical design by Yanagi et al [40] of p-type conducting wide band gap oxides, the A-A interaction will influence hole transport properties in these AMO_2 delafossite materials. The A-A distance depends on the ionic radius of M cation (fig 1.4). The smaller M cationic size will increase the A-A interaction. The p-type conductivity in AMO_2 delafossite can be induced either by substitution of divalent cation in the place of trivalent M ion or by oxygen intercalation.[44]. For effective oxygen intercalation the M ionic size should be larger. Oxygen intercalation has been found to be difficult in $CuGaO_2$ and $CuAlO_2$. Oxygen intercalation becomes easier with larger M

cations resulting in larger A-A distance and bigger volume in the cage like structure (Fig1.4). The excess oxygen is located in or near the A cation planes[45] and increases the A-A distance, thus decreasing the overlap of A metal orbitals and tending to decrease the conductivity. However A-O bonds formed may increase the conductivity by providing direct path. In principle each excess oxygen provides two holes, but it is not known if they are equally mobile as the holes created by divalent ion substitution in M cation sites. The divalent cation substitution in the M cation site, much further from the planes is the source of single hole. Since the M cation orbital does not contribute to the band structure near the Fermi level, the A-O-M-O-A linkages are not major contributors to hole conduction, and any hole produced by the divalent cationic substitution presumably immediately migrates to the A cationic planes [46].

Most of the work related to the delafossite compounds was based on Cu delafossite. There were no reports on p-type conduction in silver delafossite. Bulk $AgInO_2$ and $AgInO_2$ films were reported to be n-type[47,48]. A composite thin film of Ag_2O-In_2O_3 has been reported to show p-type conductivity [49, 50]. These films donot have delafossite structure and show 50% Ag_2O which itself is a p-type semiconductor. The larger M cations can help in intercalating oxygen and inducing p-type conductivity. $CuYO_2$ and $CuScO_2$ where Y and Sc have larger ionic radii allow the oxygen intercalation [51-53]. However, oxygen intercalation is found to be difficult in copper delafossite of $Ga^{3+}$and Al^{3+} whose radii are smaller in comparison with Y^{3+} and Sc^{3+}.

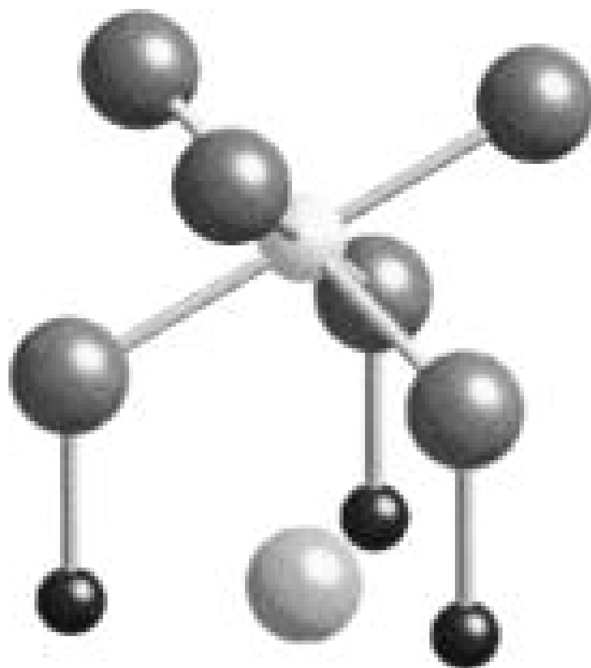

Fig. 1.4 Part of the AMO_2 delafossite structure showing the site of the O dopant. Small dark spheres are A atoms forming a triangle around the interstitial oxygen atom. The light sphere is M atom (for which divalent atom can be substituted) bonded to six oxygen atoms. In the 3R form, the interstitial oxygen atom is displaced by about 0.3 Å out of the A plane toward the M atom.

We have tried the synthesis of $AgYO_2$ compound by solid state reaction, ion exchange reaction and by hydrothermal synthesis and could not obtain the $AgYO_2$ compound. The conductivity in $AgGaO_2$ is three times larger than $AgInO_2$ [54]. The $AgInO_2$ films were n-type and p-type doping was not successful in these films. To realise p-type silver delafossite, $AgGaO_2$ and $AgCoO_2$ were synthesised. $AgGaO_2$ was synthesised by hydrothermal and ion

bexchange reactions. The phase pure delafossites of $AgGaO_2$ and $AgCoO_2$ compounds were stoichiometric as confirmed by electron probe micro analysis. The x-ray diffraction and the selective area electron diffraction of these samples show that there are no other binary phases or the β-phase of the silver compounds. The Seebeck coefficient measurements show that the holes are responsible for the conduction. The contribution to conductivity by silver ions has also been found to be negligible. These silver compounds have band gap larger than 4 eV and $AgCoO_2$ is slightly coloured due to the d-d transitions of Co^{3+}ions. These p-type TCOs were successfully utilised along with n-ZnO in the fabrication of p-n junctions.

1.7 An overview of p-type TCO thin films

The first report of a p-type TCO was NiO [55]. A 110 nm thick film had a conductivity of $0.14 Scm^{-1}$ and 40% transmission in the visible region.These films were used for the fabrication of p-n junction in combination with n-type ZnO. Yamamoto and co-workers have proposed, based on first principle calculation, that the co- doping of donor acceptor dopants (eg Ga and N) in ZnO can lead to p-type conduction in ZnO [56]. Joseph et al were the first to demonstrate experimentally the growth of p-type ZnO thin films[57].Thereafter numerous reports have appeared on various growth techniques of p-type ZnO films and the fabrication UV light emitting diodes (LED)[58,59] and blue LEDs using the p-ZnO and n-ZnO. In this section the major contributions of TCOs based on delafossite materials will be reviewed. The AMO_2 wide band gap semiconductors are isostructural with the mineral delafossite $CuFeO_2$. Many compounds share the delafossite structure, they are all of the type $A^{+}M^{3+}O_2$ where A can be Cu, Ag, Pt or Pd and B is Al, Ga, In, Sc. Cr, Fe or rare earths

[60]. Benko and Koffyberg were the first to report p-type conduction in these types of materials [61-64]. Kawazoe et al [38] reported the first p-type transparent conducting films of $CuAlO_2$ grown by pulsed laser deposition which generated much interest in this class of materials. Reports followed of similar p-type TCOs like $CuGaO_2$ [65], $CuScO_2$ [52], $CuYO_2$ [53], $CuCrO_2$ [66], $CuInO_2$ [67, 68] etc. All of them are copper delafossites exhibiting p-type conductivity. It has been demonstrated that $CuInO_2$ can be doped to both p-type and n-type and rectifying behaviour has been reported in homojunctions of n-$CuInO_2$:Sn/p-$CuInO_2$:Ca. All p-type delafossites reported so far are based on copper delafossites except for $AgCoO_2$ [69]. Acceptor doping of $AgInO_2$ [48] has not been successful in inducing p-type conductivity. We were successful in growing p-type $AgGaO_2$ thin films by pulsed laser deposition and heterojunctions were fabricated in conjunction with n-ZnO [70, 71]. Rectifying behaviour has also been observed in the p-n junctions of p-$AgCoO_2$/n-ZnO fabricated in the laboratory by PLD [72] as well as by sputtering [73]. In order to have more possibilities for transparent delafossite p-type conductors, the number of delafossite compounds can be expanded by double substitution. One way of expanding the chemistry is by double substitution on the M site of the compound AMO_2. Delafossite type $AM_{1/2}M'_{1/2}O_2$ are known where M and M' are divalent and tetravalent cations, respectively [44, 74, 75]. A new class of delafossite oxides has also been explored with a combination of divalent M and pentavalent M' cations in compositions such as $AM_{2/3}Sb_{1/2}O_2$ (A=Cu, Ag and M=Mn, Fe, Co, Ni, Cu, Zn, Mg) [76]. The choice of Sb^{5+} is based on the rationality that fifth row $d^{10}s^0$ cations with similar electronic configurations such as In^{3+} and Sn^{4+} were known to stabilise the delafossite structure. On a comparison between Cu-

based delafossites and Ag-based delafossites, it has been suggested [77] that copper delafossite should be a better candidate for TCs because of greater hole mobility owing to the Cu-3d character of valance band edge. However for Ag based delafossites the valance band edge possesses O-2p character and d-manifold holes are more mobile than p-manifold [44]. The optical and electrical properties of the delafossite p-type compounds grown by various methods are summarised in Table 1.1

The development of p-type TCO has opened up an entirely new field of research called "transparent electronics or Invisible Electronics [78, 79]. The all transparent active devices with p and n-type TCOs can be used for the fabrication of "functional windows" which would absorb UV part of the solar spectrum to generate electricity yet transmit visible radiation. Since the TCOs have wide band gap, they can also be used for the fabrication of UV and blue light emitting diodes.

Table1.1 Electrical and optical properties of copper and silver delafossite thin films

Material	Dopant	Thick-ness (nm)	T (%)	Band gap eV	σ_{RT} Scm^{-1}	S_{RT} μVK^{-1}	Reference
$CuAlO_2$	Undoped	230	70	3.5	0.340	214	99
$CuGaO_2$	Undoped	500	80	3.6	0.063	500	65
CuGa1-xFexO_2	Fe	150	60	3.4	1.0	480	69
$CuIn_{1-x}Ca_XO_2$	Ca	170	70	~3.9	0.028	--	67
$CuCrO_2$	Undoped	250	40	~3.1	1.0	150	66
$CuCr_{1-x}Mg_XO_2$	Mg	270	50	3.1	220.0	--	44,66
$CuYO_2$	Undoped	200	60	~3.5	0.025	275	44,53
$CuY_{1-x}CaO_2$	Ca	240	50	3.5	1.05	275	44,53
$CuScO_2$	Undoped	110	40	~3.3	30.0	-	52
$CuSc_{1-x}Mg_XO_2$	Mg	220-250	15-80	3.3-3.6	0.07-20.0	120	69,100
$CuNi_{1-x}Sb_xSn_yO_2$	Sb and Sn	~200	60	3.4	0.05	250	69
$AgCoO_2$	Undoped	150]	50	4,15	0.2	220	69
$AgGaO_2$	Undoped	180	50	4.12		70	70

Just after the report of the first p-type delafossite $CuAlO_2$ films, numerous reports on p-n and p-i-n junctions based on delafossites [53, 80-88] and also on homojunctions [68], have appeared. Some of the all transparent p-n junctions and the various related parameters are given in table 1.2.

Various research groups have focussed on p-type TCOs other than delafossite structures. Layered oxides, oxysulphides and orthorhombic structured $BaCu_2S_2$ thin films are also being investigated as p-type TCOs. The electrical and optical properties of some of these p-type TCOs are summarised in table 1.3.

Thin-film transistors based on TCOs have attracted much attention over the last several years because of the following several potentials towards future electronic and optoelectronic applications (1) replacing conventional amorphous-Si thin film transistors (TFT)[17] (2)Transparent thin film transistors are the building blocks for the realisation of transparent electronics.

Among the various TCOs, amorphous oxide semiconductors (amorphous TCO) appear as promising materials for the channel layer [17]. The amorphous oxides are attractive especially for large area deposition on flexible substrates. The use of non fragile soft substrates, like plastics and foils in TFT fabrication will help in reducing the weight and the fragile nature due to the use of glass substrates. Amorphous oxides have emerged as alternatives to organic TFTs and a-Si TFTs.

Table 1.2 All transparent pn junctions and the related various parameters

Device structure		n-ZnO/ p-$SrCu_2O$	n-ZnO/ p-$SrCu_2O$:K	n-$CuInO_2$:Sn/ p-$CuInO_2$:Ca	n-ZnO:Al/ p-$CuYO_2$:Ca	n-ZnO:Al/ p-$CuAlO_2$
Thickness (nm)	p-layer	300	200	400	300	400
	n-layer	300-1000	200	400	250	400
Carrier Concentration (cm-3)	p-layer		$1x10^{17}$	$\sim 1x10^{18}$		
	n-layer		$5X10^{18}$	$\sim 1x10^{18}$		
Deposition technique	p-layer	Reactive Evaporation In O_2 atmosphere	PLD	PLD	Reactive evaporation in O_2 atmosphere	PLD
	n-layer	Magnetron sputtering	PLD	PLD	rf magnetron Sputtering	PLD
Substrate		Glass	YSZ(111)	YSZ(111)	Glass	Glass
Electrode	p-side	ITO	Ni	ITO	In	ITO
	n-side	n^+-ZnO	ITO	ITO	ITO	n^+-ZnO
Reference		81	82	68	53	87

Table 1.2 continue

Table 1.2 All transparent pn junctions and the related various parameters

Device structure		n-ZnO:Al/	n-ZnO/	n-ZnO/	n-ZnO:Al/	p-Cu_2O/	p-NiO/ i-ZnO
		p-$AgCoO_2$	p-$AgGaO_2$	p-ZnO	p-ZnO:As	i-ZnO/n-ITO	n-ZnO:Al
Thickness (nm)	p-layer	250	200	5000	~1500	4000 (1-ZnO-300)	195(i-ZnO-216)
	n-layer	200	200	5000	600	2000	400
Carrier Concentration (cm^{-3})	p-layer	~$1x10^{18}$					$1x10^{18}$
	n-layer	$5x10^{19}$					$7X10^{20}$
Deposition technique	p-layer	rf magnetron sputtering	rf magnetron sputtering	rf magnetron sputtering	rf magnetron sputtering	Electrodeposition	rf Magnetron Sputtering
	n-layer	rf Magnetron sputtering	PLD	rf Magnetron sputtering	rf magnetron sputtering		rf Magnetron Sputtering
Substrate		Glass	Glass	Si(100)	GaAs(001)	Glass	Glass
Electrode	p-side	In	In	Au/Al	In	Au	Al
	n-side	ITO	ITO	Au/Al	In	Au	Al
Reference		73	70	80	42	109	55

Table 1.3 p-type TCO thin films(other than delafossites) and their electrical and optical properties

Material	Dopant	Thickness (nm)	T (%)	Band Gap eV	σ_{RT} Scm^{-1}	S_{RT} μVK^{-1}	Reference
$CuSr_2O_2$	Undoped	150	75	~3.1	0.004	260	80
$CuSr_{1-x}K_xO_2$	K	120	75	~3.25	0.040	260	80
$NiCo_2O_2$	Undoped	100	~65		~16.67		101
LaCuOS	Undoped	150	70	~3.1	$6.4x10^{-5}$	713	102
$(La_{1-x}Sr_xO)CuS$	Sr	150	60	~3.1	20.0	44	102
$(LaO)CuS_{1-x}Se_x$	Se	~150	~60	>3.1	0.6-25	250	103
$(La_{1-x}Mg_xO)CuSe$	Mg	~150			24-140		103
In_2O_3-Ag_2O	Undoped	300	~20		100.0		49,50
NiO	Undoped	111	40	~3.8	7.00		55
p-ZnO	Ga&N		90		0.2		57
CuO	Undoped	270			0.0		104
Cu_2O	Undoped	1370			0.02		104
AgO	Undoped	50-100			0.2		105
SnO	Undoped			2.7		2.4 cm^2/Vs (mobility	106
$BaCu_2S_2$	Undoped	430	90	2.3	17	3.5cm^2/Vs (mobility)	107
BaCuSF	Undoped	250	85	3.2	0.1		108

References

1. K.L.Chopra,S.Major and T.K.Pandya, *Thin Solid Films***102**(1983)1
2. K.Badeker, and Ann,*Phys* **22**(1907) 749.
3. A.J.Freeman, K.R.Poeppelmeir, T.O.Mason,R.P.H.Chang, and T.J.Marks *M.R.S.Bulletin* **25**(2000)45
4. Mohammed-Mehdi Bagheri-Mohagheghi and Mehrdad Shokooh-Saremi *J.Phys D.Appl.Phys*. **37**(2004)1248
5. Y.Shigesato, N.Shin, M. Kamei, P.K.Song, and I.Yasui, *Jpn.J.Appl.Phys. Part***1**, **11**(2000)6422
6. K.L.Chopra, S.Major and D.K.Pandya, *Thin Solid Films* **102**(1983)1
7. A.L.Dawar and J.C.Joshi, *J.Mater.Sci*.**19**(1984)1
8. T.J.Coutts, X.Wu, W.P.Mulligan and J.M.Webb , *J.Electron.Mater*. **25**(1996)935
9. T.Minami, *MRS Bulletin25* (2000)38
10. H.Enoki, T.Nakayama and ,J.Echigoya, *Phys.Stat.Sol.(a)* **29**(1992)181
11. H.Un'no, N.Hikuma, T.Omata, N.Ueda, T.Hashimoto and H.Kawazoe*, Jpn.J.Appl.Phys.Part2,* Lett **32**(1992)l1260
12. T.Minami, H.Sonohara, S.Takata, and H.Sato, Jpn.*J.Appl.Phys., Part2,* Lett.**33**(1994)L1963
13. R.J.Cava, J.M.Phillips, J.Kwo, G.A.Thomas, R.B.van Dover, S.A.Carter, J.J.Karjewski, W.F.Peck,J.M.Marshall,and D.H.Rapkine, *Appl.Phys.Lett* **649**(1994)2071

14. T.Minami, S.Takata, T.Kakumu,and H.Sonohara, *Thin Solid Films* **270**(1995)22
15. H.Ohta, M.Orita,M.Hirano,H.Tanji, H.Kawazoe and H.Hosono *Appl. Phys. Lett* **77**(2000)475
16. K.Nomura, H.Ohta, A.Takagi, T.Kamiya, M.Hirano and H.Hosono, *Nature* **432**(2004)488
17. K.J Saji, M.K.Jayaraj, K.Nomura, T.Kamiya and H.Hosono *J.electro.chem Soc* **155**(2008)H390
18. D.Griffiths, *Introduction to Electrodynamics,Prentice –Hall,New Jersey 1999*
19. Jordan and Balmain, *Electromagnetic Waves and Radiating Systems,Prentice Hall India*
20. C.Kittel, *Introduction to Solid State Physics*, 7th Edn ,Wiley Eastern Ltd (1996)
21. Ali Omar, *Elementary solid State Physics*: Principles and Applications, Addison Wesely Publishing company Inc (1999)
22. H.L.Hartnagel, A.L.Dawar, A.K.Jain ,and C.Jagdish, *Semiconducting Transparent Thin films*, IOP Publishing Ltd, Bristol (1995)
23. J.C.C.Fan,and J.B.Goodenough,*J.Appl.Phys*. **48**(1977)3524
24. I.Hamberg,C.G.Granqvist,K.F.Berggreen,B.E.Sernellius,and L.Engstrom, *Phys.Rev.B*. **30**(1984)3240
25. O.N.Marysov,and A.J.Freeman, *Phys.Rev.B.* **64**(2001)233111-1
26. H.Ohta, M.Orita, M.Hirano, H.Tanji, H.Kawazoe, and H.Hosono, *Appl.Phys. Lett.* **70**(2000)2740

27. N.S.Murty, G.K.Bhagawat, and S.R.Jawalekar, *Thin Solid Films* **92**(1982)347
28. Y.Shigesato, and D.C.Paine, *Appl.Phys.Lett*.**62**(1993)1268
29. K.Sreenivas, T.Sudersana Rao, A.Mansingh and S.Chandra, *J.Appl.Phys* **57**(1985)384
30. J.Bardeen,and W.Shockley, *Phys.Rev.* **80**(1950)72
31. A.R.Huston, *J.Appl.Phys.* **32**(1961)2287
32. H.Ehrenreich, *J.Appl.Phys* **32**(1961)2155
33. T.J.Coutts, D.L.Young, X.Li, *MRS Bulletin* **25**(2000)58
34. R.Kalish, and Dimond *Relat.Mater* **10** (2001)1749
35. A.Zuger *Appl. Phys. Lett.* **83**(2003)57
36. D.A.DeVault *J.Chem Edu* **21**(1944) 526
37. H.Kawazoe, H.Yanagi,K.Ueda and H.Hosono *MRS Bulletin 25*(2000) 28
38. H.Kawazoe, M.Yasukawa. H.Hyodo, M.Kurita, H.Yanagi and H.Hosono *Nature* **389** (1997) 939.
39. S.Fraga, J.Karwoswski and K.M.S.Saxena, *Handbook of Atomic Data* Elsevier, Amsterdam,(1976)p259
40. H Yanagi, H.Kawazoe, A.Kudo, M.Yasukawa and H.Hosono *J. Electroceramics* **4** (2000) 407
41. S.Gao,Y.Zhao,P.Gou,N.Chen,Y.Xie *Nanotechnology*, **14**(2003) 538.
42. A.N.Banerje and K.K.Chattopadhyay *Progress in Crystal Growth and Charactersiation of Materails* **50**(2005)52
43. A.Kudo, H.Yanagi, H.Hosono and H.Kawazoe *Appl. Phys. Lett* **73**(1998)220

44. R.Nagarajan, N.Duan,M.K.Jayaraj, J.Li, K.A.Vanaja, A.Yokochi, A.Draeseke, J.Tate and A.W.Sleight *International J Inorganic Materials* **3**(2001) 265.
45. J.Li, A.F.T.Yokochi and A.W.Sleight, *Solid State Sci* **6**(2004)831.
46. R.Kykneshi,B.C.Nielsen, J.Tate, J.Li and A.W.Sleight, *J. App. Phys.* **96**(2004)6188.
47. T.Otabe, K.Ueda, A.Kudoh, H.Hosono and H.Kawazoe, *Appl. Phys.Lett.,* **72** (1998) 1036.
48. S.Ibuki, H.Yanagi, K.Ueda, H.Kawazoe and H.Hosono, *J.Appl Phys.*, **88** (2000) 3067.
49. J.Asbalter and A.Subrahmanyam *J.Vac.Sci and Technology* vol **18** (2000)1672 .
50. T.Minami, K.Shimokawa and T.Miyata, *J.Vac.Sci.Technol.A,* **16**(1998) 1218
51. R.J.Cava, H.W. Zandbergen, A.P.Ramirez, H.Takagi, C.T.Chen, J.J.Krajewski, W.F.Pecj Jr, J.V.Waszczak, G.Meigs, R.S.Roth and L.F.Schneemeyer*, J. Solid State Chem.,* **104** (1993) 437.
52. N.Duan, A.W.Sleight, M.K.Jayaraj, and J,Tate, *Appl.Phys.Lett* **77** (2000) 1325.
53. M.K.Jayaraj, A.D.Draeseke, J.Tate and A.W.Sleight*, Thin Solid Films* **397**(2001) 244.
54. D.B.Rogers, R.D.Shannon, C.T.Prewitt and J.L.Gillson, *Inorg.Chem.,* **10**(1971) 723.
55. H.Sato, T.Minami, S.Takata and T.Yamada, *Thin Solid Films* **236** (1993) 27.

56. T.Yamamoto, and H.K.Yoshida, *Jpn.J.Appl.Phys*. **38**(1999)L166-L169.
57. M.Joseph, H.Tabata,and T.Kawai *Jpn.J.Appl.Phys***.** **38**(1999)L1205-L1207.
58. L.Kakuya, F.Paul, M.Koji, Y.Akimasa, N.Shigeru and N.Ken, US Patent US6638846 (2003)
59. H.W.White, S.Zhu, and Y.Ryu, US Patent US7033435 (2006)
60. R.D.Shannon, D.B.Rogers and C.T.Petwitt *Inorg.Chem*. **10**(1971) 713.
61. F.A Benko and F.P.Kofyberg, *Can J.Phys.* **63**(1985) 1306.
62. F.A Benko and F.P.Kofyberg, *J.Phys.Chem.Solids* **48**(1987) 431.
63. F.A Benko and F.P.Kofyberg, *Phys. Stat Sol(a)* **94**(1986) 231.
64. F.A Benko and F.P.Kofyber*, Mater. Res. Bull.,* **21**(1986) 753.
65. K.Ueda,T.Hase,H.Yangi.H.Kawazoe, H.Hosono, H.Ohta, M.Orita, and M.Hirano, *J.Appl.Phys* **89**(2001) 1790.
66. R.Nagarajan, A.D.Draeseke, A.W.Sleight and J.Tate *J.Appl.Phys.* **89**(2001)8022.
67. H.Yanagi,T.Hase, S.Ibuki, K.Ueda, And H.Hosono, *Appl.Phys.Lett.,* **78**(2001)1583.
68. H.Yanagi, K.Ueda, H.Ohta, M.Orita, M.Hirano, H.Hosono, *Solid State Comm* **121**(2001) 15.
69. J.Tate, M.K.Jayaraj, A.D.Draeseke, T.Ulbrich, A.W.Sleight, K.A.Vanaja,R.Nagarajan, J.F.Wager and R.L.Hoffman, *Thin Solid Films* **411**(2002)119.

70. K.A. Vanaja, R.S. Ajmsha, A.S. Asha and M.K. Jayaraj, *Appl.Phys.Lett.* **88** (2006)212103
71. K. A. Vanaja, R. S. Ajmsha, A. S. Asha, K. Rajeev Kumar and M. K. Jayaraj, *Thin Solid Films* **516**(2008)1426
72. R. S. Ajimsha, K. A. Vanaja, M. K. Jayaraj, P. Misra, V. K. Dixit and L. M. Kukreja. *Thin solid film* **515**(2007)7352
73. K.A.Vanaja, U.M.Bhatta, R.S.Ajimsha, S.Jayalekshmi and M.K.Jayaraj *Bull Mater.Sci* **31**(2000)753.
74. J.P.Doumerc, A.Ammar, A.Wichainchai, M.Pouchard and P.Hagenmuller, *J.Phys.Chem. Solids* **48**(1987) 37.
75. Y.J Shin, J.P.Doumerc, M.Pouchard and P.Hagenmuller *Mater Res Bull.* **28** (1993) 159.
76. R.Nagrajan, S.Uma, M.K.Jayaraj, J.Tate and A.W.Sleight *Solid State Sciences* **4**(2002)787.
77. H.C.Kandpal and R.Seshadri, *Solid Stste Sci.* **4**(2002)1045.
78. J.F.Wager, Transparent Electronics. *Science* **300**(2003) 1245.
79. G.Thomas, Materials science: Invisible circuits. *Nature* **389**(1997) 907.
80. A.Kudo , H.Yanagi ,K. Ueda ,H. Hosono and Y .Yano. *Appl. Phys. Lett***75**(1999): 2851.
81. H.Ohta, K.Kawamura ,M. Orita ,N. Sarukura ,M. Hirano and , H.Hosono, *Electron. Lett* **36**(2000)984.
82. H.Ohta, K.Kawamura ,M. Orita, M. Hirano, N. Sarukura and H.Hosono. *Appl. Phys. Lett.***77**(2000) 475
83. H.Ohta, M.Orita and M.J.Hirano, *Appl. Phys.,* **89**(2001)5720.

84. H.Hosono ,H.Ohta, K.Hayashi, M.Orita and M.J.Hirano *Cryst. Growth,* **237-239**(2002)496.
85. R.L.Hoffman, J.F.Wager, M.K.Jayaraj and J.Tate *J. Appl. Phys*., **90**(2001) 5763.
86. M.K.Jayaraj,A.D.Draeseke, J.Tate, R.L. Hoffman and J.F.Wager *Mat. Res. Soc. Proc.,* **666**(2001) F4.1-F4.5
87. K.Tonooka, H.Bando, and Y.Aiura. *Thin Solid Films*, **445**(2003)327.
88. A.N.Banerjee, S,Nandy, C.K.Ghosh,and K.K.Chattopadhyay *Thin Solid Films*,**515**(2007)7324.
89. M.W.J.Prins, K.O.Grosse-Holz, G.Müller, J.F.M.Cillessen, J.B.Giesbers, R.P.Weening and R.M.Wolf *Appl. Phys. Lett.,* **68** (1996) 3650.
90. M.W.J Prins,S.E.Zinnemers, J.F.M.Cillessen and J.B.Giesbers, *Appl. Phys. Lett.* **70**(1997) 458.
91. R.L.Hoffman, B.J.Norris and J.F. Wager *Appl. Phys. Lett*. **82**(2003) 733.
92. S.Masuda, K.Kitamura, Y.Okumura, S.Miyatake, H.Tabata and T. Kawai *J. Appl. Phys* **93**(2003) 1624.
93. P.F.Carcia, R.S.McLean, M.H.Reilly and G.Nunes Jr *Appl. Phys. Lett.* **82** (2003)1117.
94. K.Nomura, H.Ohta, K.Ueda, T.Kamiya, M.Hirano and H.Hosono, *Thin-Film Science* **300**(2003) 1269.
95. H.Ohta, K.Nomura, H.Hiramatsu, K.Ueda, T.Kamiya,M.Hirano and H.Hosono, *Solid-State Electronics* **47**(2003) 2261.

96. E.M.C.Fortunato,P.M.C. Barquinha, A.C.M.B.G. Pimental, A.M.F.Gonc¸alves, A.J.S.Marques, L.M.N.Pereira L M N and R.F.P.Martins, *Adv. Mater.* **17**(2005)590.
97. S.Masuda, K.Kitamura, Y.Okumura, S.Miyatake, H.Tabata and T.Kawai, *J. Appl. Phys.* **93(**2003)1624.
98. R.L.Hoffman, B.J.Norris and J.F.Wager, *Appl. Phys. Lett.***82** **(**2003)733.
99. H.Yanagi, S.Inoue, K. Ueda, H.Kawazoe, H. Hosono and N.Hamada *J. Appl. Phys* ***88*** (2000)4159
100. H.Yanagi, S.Park, A.D Draeseke, D.A Keszler and J .Tate *J.Solid State Chem* **175**(2003)34
101. C.F Windisch Jr,K.M Ferris and G.J Exarhos *J.Vac.Sci.Technol.A* **19**(2001)1641
102. H.Hiramatsu, K.Ueda, H.Ohta, M.Orita M, M.Hirano and H.Hosono *Thin Solid Films* **411(**2002)125
103. H.Hiramatsu, K.Ueda, H.Ohta M.Hirano, T. Kamiya and H.Hosono *Appl.Phys.Lett* **82** **(**2003) 1048
104. A.Parreta, M.K. Jayaraj, A. Di Nocera, S.Loreti L.Quercia,A.Agati *Phys.state.sol. a***155**(1996)399
105. A.J. Varkey, A.F.Fort *Solar Energy Materials and Solar cells* **290(**1993)253
106. Y.Ogo, H.Hiramatsu,K .Nomura, H.Yanagi, T.Kamiya, M.Hirano, H.Hosono *Appl.Phys.Lett* **93**(2008)032113
107. S.Park, D.A.Kezer, M.M.Valencia, R.L.Hoffman, J.P.Bender, J.F.*Wager Appl.Phys.Lett* **80**(2002) 4393

108. H.Yanagi, S.Park, A.D.Draeseke, D.A.Kezeler, J.Tate, *J.Solid State Chem*. **175** (2003) 34
109. D.K.Zhang,Y.C.Liu, Y.L.Liu,H.Yang *Physica B* **351**(2004) 178

Chapter 2

Experimental and analytical techniques

Abstract

Various techniques have been used for the synthesis of the bulk delafossite materials. Silver delafossite requires the synthesis through a low temperature route. Hydrothermal or ion exchange technique has been used for the synthesis of silver delafossites. This chapter describes the preparation techniques of bulk materials and the pulsed laser deposition technique and rf magnetron sputtering utilized for the growth of thin films. A brief description of various analytical tools used for the structural, compositional, electrical and optical properties of the films as well as bulk materials is also included.

2.1 Introduction

The growth techniques play an important role in determining the characteristics of crystals, bulk powders as well as thin films. It has been observed that various physical constants, characteristic to a bulk material, may not be reproduced as the same in their corresponding thin films. The structural, electrical and optical properties of thin films are found to be highly sensitive to the techniques adopted, the substrates chosen, deposition conditions, the presence of defects and impurities and the film thickness. The appropriate choice of an experimental technique thereby helps in tailoring a material with controlled, reproducible and well defined properties so as to suit a technological application. For example the $AgCoO_2$ thin films grown by pulsed laser deposition were amorphous where as highly oriented growth has been achieved by growing the films by rf magnetron sputtering

The present work is primarily related to studies on new p-type delafossite oxides. Though many reports on the synthesis of copper delafossite exist in literature, synthesis of p-type silver delafossites is sparingly few. The silver delafossites cannot be grown by the high temperature solid state reaction because the decomposition temperatures of these compounds are low. These factors make the synthesis of silver delafossites some what tricky. In the present work the copper delafossites were synthesized by the high temperature solid state reaction. For the synthesis of silver delafossite oxides, two methods viz., hydrothermal synthesis and ion exchange reaction were successfully used. The ABO_2 wide band gap delafossite oxides thus synthesized in the laboratory were used for the deposition of thin films. Deposition techniques such as pulsed laser deposition (PLD) and radio frequency (rf) magnetron sputtering were employed

for the growth of these oxide thin films. Thermally evaporated metal electrodes (aluminum, indium) were used to make contacts for electrical characterisation of the films and pn junctions. The present chapter describes the various methodologies especially the hydrothermal and ion exchange reaction adopted for bulk synthesis and thin film growth. It also briefs on the different analytical tools used in the present study.

2.2 Bulk synthesis

The polycrystalline materials in the powder form were synthesised mainly by three techniques, viz., solid state reaction, ion exchange reaction and hydrothermal synthesis. The powders thus synthesised were sintered at high temperature to make targets for growth of thin films by PLD and sputtering techniques.

2.2.1 Solid state reaction

For preparing bulk p-type delafossite powders, and some of the starting precursors for ion exchange reactions, stoichiometric quantities of the oxides of the starting materials were thoroughly mixed in alcohol medium using an agate mortar and pestle. The dried mixture was then placed in an alumina boat and introduced into the hot temperature zone of a horizontal tube furnace equipped with a proportional integral differential (PID) controller. The firing was done at the requisite temperature over a fixed time. All the oxides were preheated to 300^0C before weighing which ensures the powders to be dry. A two step firing process is usually adopted for pellet synthesis. The constituent materials, after thorough mixing, are calcined to complete the reaction and compound

formation. These powders are then pressed into pellets and then sintered at higher temperature.

A solid and highly condensed pellet with reduced porosity is desirable for pulsed laser deposition to arrest cracking due to high thermal conductivity on exposure to the high energy laser. A large press loading can reduce porosity in the target but overloading during pressing results in a cracked target. The pore density can be measured from the following relation,

Pore density = Actual mass density / Theoretical mass density

where,

Actual mass density = Target weight / Target Volume

Theoretical mass density = Weight of all atoms in the primary cell / Volume of the primary cell

2.2.2 Ion Exchange reaction

Inorganic reactions can be divided into roughly three types**:**

1) Ion Exchange Reactions: Ion exchange is a reversible chemical reaction wherein an ion (an atom or molecule that has lost or gained an electron and thus acquired an electrical charge) from solution is exchanged for a similarly charged ion attached to an immobile solid particle.

2) Redox Reactions: These are characterised by changes in oxidation state of elements 3) Reactions involving complex ions

Ion Exchange Reactions

For an ion exchange reaction: AB(aq) + CD(aq) → AD + CB to occur, the products cannot both be soluble (ie. a strong electrolyte). One of the products must be one of the following as described in the following examples

1. An insoluble compound $AgNO_3(aq) + NaCl\ (aq) \rightarrow AgCl\ (s) + NaNO_3(aq)$ AgCl is insoluble and so forms a precipitate.

2. A weak electrolyte $HCl\ (aq) + NaOH\ (aq) \rightarrow H_2O\ (l) + NaCl\ (aq)$: No precipitate is formed here.

3. A compound that dissociates to form a gas $Na_2CO_3(aq) + 2\ HCl\ (aq) \rightarrow 2NaCl\ (aq) + H_2O + CO_2(g)$ In this reaction, the following has occurred:

$Na_2CO_3(aq) + 2\ HCl\ (aq) \rightarrow 2\ NaCl\ (aq) + H_2CO_3(aq)$ The H_2CO_3 immediately decomposes to $H_2CO_3\ (aq) \rightarrow H_2O + CO_2(aq) \rightarrow H_2O + CO_2(g)$

Ion exchange reactions are also called double displacement reactions. An example of an ion exchange reaction is

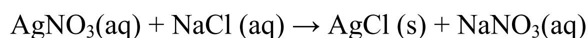

$AgNO_3(aq) + NaCl\ (aq) \rightarrow AgCl\ (s) + NaNO_3(aq)$

When $AgNO_3$ and NaCl dissolve in water, they dissociate completely to their component ions

$AgNO_3(aq) \rightarrow Ag^+(aq) + NO_3^-(aq)$

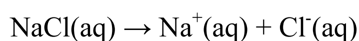

$NaCl(aq) \rightarrow Na^+(aq) + Cl^-(aq)$

In the reaction it can easily be seen that it is a double displacement reaction since both the cations (Ag^+ and Na^+) and the anions (NO_3^- and Cl^-) exchange. As the Ag^+ and Cl^- ions meet, they react to form insoluble AgCl which we observe as a precipitate.

If we re-write the reaction equation in terms of the ions that are present, we obtain:

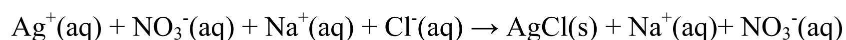

$Ag^+(aq) + NO_3^-(aq) + Na^+(aq) + Cl^-(aq) \rightarrow AgCl(s) + Na^+(aq) + NO_3^-(aq)$

Both Na^+ and NO_3^- remain unchanged through the reaction and so are called spectator ions . If we exclude these ions from the reaction equation we obtain the net ionic equation:

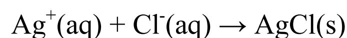

$Ag^+(aq) + Cl^-(aq) \rightarrow AgCl(s)$

How one make sure there is an ion exchange reaction?

In an ion exchange reaction, the cations and anions inter change as in this typical example

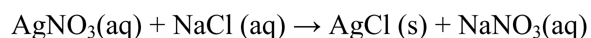

$AgNO_3(aq) + NaCl\ (aq) \rightarrow AgCl\ (s) + NaNO_3(aq)$

So Ag^+ will react with Cl^- and Na^+ will react with NO_3^- :

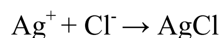

$Ag^+ + Cl^- \rightarrow AgCl$

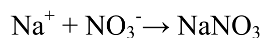

$Na^+ + NO_3^- \rightarrow NaNO_3$

Then check if AgCl or $NaNO_3$ are soluble. If they are, then the ions will remain in solution and there will be no reaction. Silver Chloride, AgCl, is insoluble and so there is an ion exchange reaction.

In the present work the $AgGaO_2$ bulk powder has been synthesized through ion exchange reaction. $AgGaO_2$ has two polymorphos α-$AgGaO_2$ and β-$AgGaO_2$.

2.2.3 Hydrothermal synthesis

The term ‘hydrothermal’ is purely of geological origin. Hydrothermal processing can be defined as any heterogeneous reaction in the presence of aqueous solvents or mineralizers under high pressure and temperature conditions to dissolve and recrystallize (recover) materials that are relatively insoluble under ordinary conditions. Recently, Byrappa and Yoshimura have defined hydrothermal [1] as any heterogeneous chemical reaction in the presence of a solvent (whether aqueous or non-aqueous) above the room temperature and at a pressure greater than 1 atm in a closed system. Hydrothermal method is a non-conventional method to obtain nanocrystalline inorganic materials. High temperature, high pressure apparatus called ‘auto-claves’ or ‘bombs’ are needed for hydrothermal synthesis. For hydrothermal experiments, the requirements for starting materials are (1) accurately known composition, (2) as homogeneous as possible, (3) as pure as possible and (4) as fine as possible, etc.

Generally the method is claimed as solvothermal, which means that water, and other solvents are also used in accordance with the general process principle. Polar solvents or even non-polar solvents can be used for the dissolution-recrystallisation process. These solvents have specific disadvantages concerning mainly their toxicity and corrosion problems for the autoclave materials.

The major advantages of processing the materials by hydrothermal method over other methods for powder preparations are 1) materials are formed directly from solution 2) materials can be obtained as anhydrous, crystalline or

amorphous. 3) It is possible to control the particle size and shape by varying hydrothermal temperature. 4) Chemical composition, stoichiometry, etc can be controlled by processing parameters. 5) Powders obtained by hydrothermal technique are highly reactive in sintering and in many cases, powders do not need calcination and milling process.

The grain size of the powders synthesized by hydrothermal method is less than I µm. We can make composites like organic/ inorganic mixtures and materials which have very high vapor pressure by hydrothermal method. Both physical and chemical parameters are effective during hydrothermal processing in such a way that direct precursor - product correlation can be established. Temperature, pressure and time of reaction are the three physical parameters in the hydrothermal synthesis. Temperature plays an important role in the kinetics of product formation as well as on the thermodynamic stability of the product phase. Pressure is essential for solubility, the supersaturation range directing to the crystallization process as well as for the thermodynamic stability of the product phase. Time is also an important parameter because the synthesis of kinetically stable phases are favored in short term processes while thermodynamically stable phases are formed in long term experiments, corresponding to a suitable temperature and pressure. The fundamental roles of temperature, pressure, precursors, and time on crystallization kinetics of various compounds are defined empirically [1]

At a given hydrothermal temperature and pressure suitable for the synthesis, the precursor materials are continuously dissolved in hydrothermal fluid. The formation of gels is not observed at any time during the process. Bigger molecular units are hydrolyzed at elevated temperature and pressure.

In the hydrothermal synthesis, the precursor materials are taken in a container with solid to water proportions of about 1:10. The closed containers are placed into the sealed stainless steel autoclaves and put into the furnace. Applying the desired hydrothermal synthesis temperature, an autogenous pressure is formed. The external pressure is adjusted as soon as the temperature equilibrium is achieved within the autoclave. By the installation of the hydrothermal pressure, the reaction process takes place. Temperature fluctuations of the furnace have negative consequences because a rise in the temperature leads to a higher dissolution rate disturbing the dynamic equilibrium of dissolution-crystallization, while lowering of temperature leads to higher supersaturation.

A key limitation to the conventional hydrothermal method has been the need for time consuming empirical trial and error methods as a means for process development. Material processing under hydrothermal conditions requires a pressure vessel capable of containing a highly corrosive solvent at high temperature and pressure. Ideal hydrothermal apparatus popularly known as an autoclave should have the following characteristics:

i) Inertness to acids, bases and oxidizing agents.

ii) Ease of assembly and disassembly.

ii) Sufficient length to obtain a desired temperature gradient.

iv) Leak-proof with unlimited capabilities to the required temperature and pressure

v) Rugged enough to bear high pressure and temperature experiments for long periods with no damage so that no machining or treatment is needed after each experimental run.

Figure 2.1.General purpose autoclave fabricated for hydrothermal synthesis. The Parr bomb used in the present study is a home made teflon lined stainless steal bomb. Since the lining used is teflon the reaction temperate is limited to less than 300^0C. For higher temperature a platinum lining is advisable.

2.3 Thin film growth techniques

A 'thin film' has one of its linear dimensions very small compared to the other two and is characterised by a large surface to volume ratio. Any thin film deposition process involves the following sequential steps:

1) Transition of the condensed phase (solid or liquid) into the gaseous state (atomic/molecular/ionic species)
2) Transport of the vapor from the source to the substrate
3) Condensation of the vapor upon arrival on the substrate

The deposition techniques are broadly classified into two - physical and chemical - depending on how the atoms/molecules/ions/clusters of species are created for condensation process [2].

Various chemical methods have been realized for thin film deposition of phosphor materials. Some of them are sol-gel synthesis [3,4], solvent evaporation epitaxy method [5], electrophoresis [6], spray pyrolysis [7,7] and dip-coating [9]. Thermal and electron beam evaporation, pulsed ion beam evaporation [10], chemical vapor deposition (CVD) [11], PLD, rf sputtering, and atomic layer epitaxy (ALE) fall under the stream of physical methods, generally adopted for thin film phosphor growth.

The following sections give a brief outline of the various thin film deposition techniques used in the present work.

2.3.1 Thermal evaporation by resistive heating

Thermal evaporation is a simple and convenient technique widely used for the deposition of thin films of metals, alloys and many compounds. The process, in general, involves heating up of a source material until it evaporates and condenses on a cold target surface, referred to as the substrate. If carried out in vacuum, the evaporation temperature can be considerably lowered and the formation of oxides and incorporation of impurities in the growing layer can be avoided. Moreover, at pressures as low as 10^{-6} or 10^{-5} Torr, the mean free path of vapor atoms shall be of the same order as the vacuum chamber dimensions. Hence, the particles can travel in straight lines from the evaporation source towards the substrate without being significantly scattered [12].

In thermal evaporation technique, the average energy of vapor atoms reaching the substrate surface is generally low (of the order of kT ie. less than

tens of eV). Here, a refractory metal (tungsten or tantalum) strip or shaped filaments are heated directly by attaching the ends to a low voltage, high current supply to evaporate the charge. The characteristics and quality of the deposited film shall depend on the substrate temperature, rate of deposition, substrate to target distance, base pressure, etc. The homogeneity of the film depends on the geometry of the evaporation source and the distance from the source material to the substrate. Excellent and detailed reviews on the know-how of the technique have been discussed by Holland [13].

In the present work, the deposition of metal electrodes (In) was done using thermal evaporation via resistive heating.

2.3.2 Sputtering

Sputtering is one of the most versatile techniques used for the deposition of high quality thin films over a larger area with better control of composition and thickness, greater adhesion and homogeneity. The process involves the creation of inert gas plasma, usually of argon [14], by applying a high voltage between electrodes. The target holder is generally taken as the cathode and the substrate holder as the anode. The source material is subjected to intense bombardment by heavy argon ions. By momentum transfer, particles are knocked out from the target surface and they travel across the system to condense onto the substrate surface. The process, if carried out in vacuum, becomes more efficient since the sputtered material will arrive at the substrate surface without suffering collisions with the residual gas with energy enough to produce a fine coating. Sputtering is normally performed at a pressure of 10^{-2} to 10^{-3} Torr. At such high residual gas pressures, the sputtered material is seldom transferred towards the

substrate without many collisions. This gives rise to very slow deposition rate and poor quality coating.

Sputtering may be carried out in a variety of systems, which may differ in sputtering configuration, geometry, target type etc. Experimental sputtering systems usually have small targets and low production rates, whereas commercial production systems have large targets and rapid substrate transport to maximize production rate. Irrespective of the sputtering system used, the basic sputtering process remains the same. A schematic diagram of the rf sputtering system used in the present study is shown in figure 2.2.

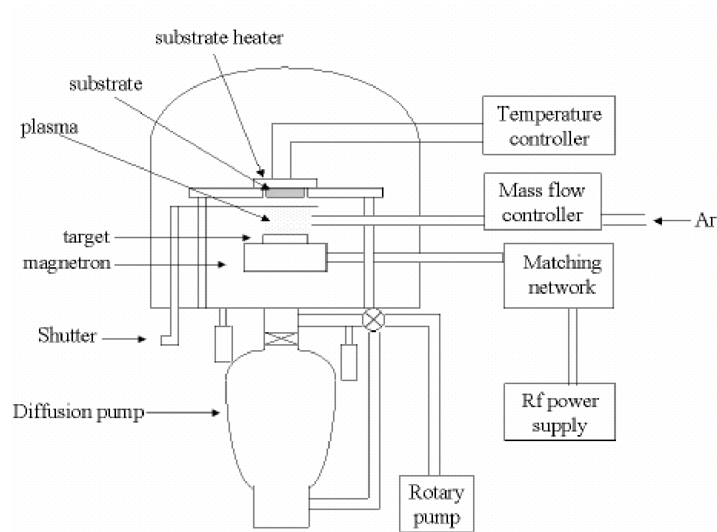

Figure 2. 2. Schematic of rf sputter deposition system used for film deposition.

Normally there are two modes of powering the sputtering system - dc and rf biasing. In dc sputtering, a direct voltage is applied between the cathode and the anode. This method is restricted for conducting materials only. The process is

inadequate for the deposition of dielectric films because of charging, arcing, and very low deposition rates. Radio frequency (rf) sputtering is suitable for both conducting and nonconducting materials. A high frequency generator (13.56 MHz) is connected between the electrodes of the system. The oscillating rf potential applied between the anode and cathode modifies the electron motions, which produces better energy coupling to the electrons as well as higher plasma densities. A large capacitor (500-2000 pF), placed in series between the rf power supply and the powered electrode, allows a significant negative bias to develop on the cathode, typically half of the value of the applied peak-to-peak rf voltage. This bias is then the acceleration voltage for ions from the plasma, which move much too slowly to respond to the applied rf potentials. In addition to the series capacitor, usually, two other tuning components help in matching the impedance of the plasma to the output impedance of the rf power supply. These components, usually a shunt capacitor to ground and a series inductor, are located along with the series capacitor in the "matching network". The inductor is fixed, and both of the capacitors (shunt and series) are variable. The reflected power is minimized by adjusting these variable capacitors in the tuning network. In rf sputtering, the substrates function as partial cathodes in the circuit and are bombarded by ions from the plasma, but at a lower rate than the primary cathode.

Magnetron sputtering uses a magnetic field to confine the electrons close to the cathode, making it easier to sustain an electrical discharge at low pressure. The conventional, circular planar cathode is characterized by high levels of erosion on the cathode surface in the form of a ring. This technique is particularly useful when high deposition rates and low substrate temperatures are required [15]. Both reactive and nonreactive forms of dc, rf and magnetron sputtering

have been employed for the deposition of compound semiconductors. In reactive sputtering, the reactive gas is introduced into the sputtering chamber along with argon to deposit thin films. For example to deposit metal oxide thin films pure metal target is sputtered in a mixture of argon and oxygen atmosphere. The deposition rates and properties of the films strongly depend on the sputtering conditions such as the partial pressure of the reactive gas, the sputtering pressure, substrate temperature and substrate to target spacing.

In sputter deposition, the material arrives at the substrate mostly in atomic or molecular form. The atom diffuses around the substrate with a motion determined by its binding energy to the substrate, which is influenced by the nature and temperature of the substrate. The depressions on the substrate surface act as adsorption sites for the diffusing atoms. At each hop, the atom will either jump over the barrier into an adjacent site or will re-evaporate. After a certain time, the atom will either evaporate from the surface or will join another diffusing single atom to form a doublet. These doublets will be joined by other single atoms to form triplets, quadruplets and so on. This stage is known as the nucleation stage of thin film growth and it leads to the formation of quasi-stable islands. The islands will grow in size and it will lead to the coalescent stage. Coalescence proceeds until the film reaches continuity.

The process of rf sputter deposition is made possible due to the large difference in mass, and hence mobility, of electrons and inert gas ions. Being less massive than ions, electrons attain much greater velocities and travel much further than ions during each cycle of the applied rf voltage waveform. Hence they eventually accumulate on the target, substrate and chamber walls such that the plasma is the most positive potential in the system. These induced negative

voltages or "sheath voltages" [16] cause acceleration of positive ions toward the negatively charged surfaces, which subsequently leads to sputtering events. The volume adjacent to the cathode surface relatively free of electrons leads to a "dark space" because electrons are not available to excite gas atoms. The target is selectively sputtered by controlling the relative surface areas of the target and the substrate holder. If space charge limited current is assumed, the ion current flux, J can be estimated by the Child-Langmuir equation [17],

$$J = \frac{KV^{3/2}}{D^2 m_{ion}} \tag{2.1}$$

where, D is the dark space thickness, V is the sheath voltage, m_{ion} is the ionic mass and K is the proportionality constant. Since the positive ion current must be equal at both the electrodes,

$$\frac{A_A V_A^{3/2}}{D_A^2} = \frac{A_B V_B^{3/2}}{D_B^2} \tag{2.2}$$

where, A_A and A_B are the surface areas of cathode and anode A and B respectively. If positive ion current densities are assumed to be equal, there would be a much greater positive ion current flowing during one half cycle of the applied voltage waveform than the other due to the much greater area of the grounded substrate electrode. Here, as the system is assumed to be in steady state, the total positive ion current per half cycle should be the relevant quantity.

The glow discharge itself is a region where large quantities of positive and negative charges exist and can be modelled as a wire. Since most of the voltage in the glow discharge is dropped across the dark space, and they have very low conductivities, they can be modelled as capacitors such that the capacitance C,

$$C \alpha A/D \tag{2.3}$$

Furthermore, an ac voltage will divide across the two series capacitors such that,

$$\frac{V_A}{V_B} = \frac{C_B}{C_A} \tag{2.4}$$

$$\therefore \frac{V_A}{V_B} = \left(\frac{A_B}{A_A}\right)^2 \tag{2.5}$$

This equation tells that smaller area will see larger sheath voltage, whereas larger area will see a smaller sheath voltage by a power of 2. The usefulness of this result is that $A_B > A_A$ must hold to selectively sputter the target. This is done in practice by grounding the substrate holder to the entire chamber resulting in a very large A_B. For this reason it is extremely important that the substrate holder and the system are well grounded to ensure that re-sputtering of the growing film does not occur.

Sputtering yield is defined as the quantity of the material sputtered per ion (atoms/ion or grams/ion) [18]. Main features observed for the sputtering technique are:

1) Sputtering yield differs with the nature of the element ie., the yield increases as the reciprocal of the binding energy of the surface atoms.
2) Sputtering yield decreases as the surface damage increases i.e. the yield from a rougher surface is lower than that from a smoother surface.
3) As the mass of the sputtering species increases, the sputtering yield increases.
4) Lighter mass ions penetrate deeper into the target than heavier mass ions.

5) As sputtering energy increases, the sputtering yield increases up to an energy of 100 keV. At higher energies, the sputtering yield again decreases since the ions penetrate into the target. Since smaller particles penetrate further into the target, the energy when the yield starts to decrease is lower for lighter particles.
6) For multicomponent samples, the lightweight particle is usually preferentially sputtered if the binding energies of the components are similar. The sputtering rate of each component increases as the reciprocal of the binding energy and mass of that component.
7) Sputtering of oxide targets results in preferential depletion of oxygen.
8) Sputtering yield of metal oxide is less than that of corresponding metals.
9) For oxide samples, sputtering in an oxygen rich environment decreases the sputtering yield; the sputtering yield does not vary in other environments (for example, CO and N_2) indicating that adsorption without chemical bonding is not enough to reduce the sputtering yield.

In the present study, an in-house assembled magnetron has been used for rf magnetron sputtering. A magnet of 2000 gauss was used to deflect the ions. A schematic diagram of the magnetron is shown in figure 2.2. The vacuum system consists of a 6" diameter diffusion pump backed by a rotary pump (make - Indovision, Bangalore). The rf supply was connected to the magnetron through a capacitive matching network (Digilog Instruments, Bangalore). The flow of argon gas into the vacuum chamber was controlled using a mass flow controller (Bronkhorst, Holland).

2.3.3 Pulsed laser deposition (PLD)

Lasers are energy sources in the form of monochromatic and coherent photons, enjoying ever increasing popularity in diverse and broad applications. The laser has become an irreplaceable tool in metallurgy, medical technology and electronic industry. In material science, lasers play a significant role either as a passive component for process monitoring or as an active tool by coupling its radiation energy to the material being processed. Lasers, are therefore, extremely useful in a wide variety of applications such as localized melting during optical pulling, laser annealing of semiconductors, surface cleaning by desorption and ablation, laser induced rapid quench to improve surface hardening etc. Finally, pulsed laser deposition (PLD) has emerged as one of the premier thin film deposition technologies [19].

PLD is the deposition method of choice when one needs to deposit materials with complex stoichiometry. PLD was the first technique successfully used to deposit a superconducting $YBa_2Cu_3O_{7-d}$ thin film. Since then, many materials, especially multi element oxides, normally difficult to be deposited by other methods, have been deposited by PLD. This technique offers many potential applications, from integrated circuits and optoelectronics to micro mechanics and medical implants.

In a typical PLD process, a focused train of high energy laser pulses, derived from a UV nanosecond pulse width laser source, such as the frequency tripled (355 nm) or quadrupled (266 nm) solid state Nd:YAG laser, or the KrF (248 nm) or ArF (193 nm) excimer laser, is rastered over either a metal, a single crystal oxide or a compressed oxide powder target in a vacuum chamber. The high energy laser pulses interact with the target generating a plume comprised of

atomic and molecular species ablated from the target. A substrate, often heated, is placed at a short distance from the target in the direction of the advancing plume (figure 2.3). Though the actual physical process of material removal is quite complex, one can consider the ejection of material to occur from rapid explosion of the target surface by superheating. Unlike thermal evaporation, which produces a vapor composition dependent on the vapor pressures of elements in the target material, the laser induced expulsion produces a plume of material with stoichiometry similar to the target. The best quality films can be deposited by controlling the fundamental criteria such as the substrate temperature, the relative and absolute arrival rates of atoms and the energy of the depositing flux. PLD offers the best control over these criteria than other vacuum deposition techniques.

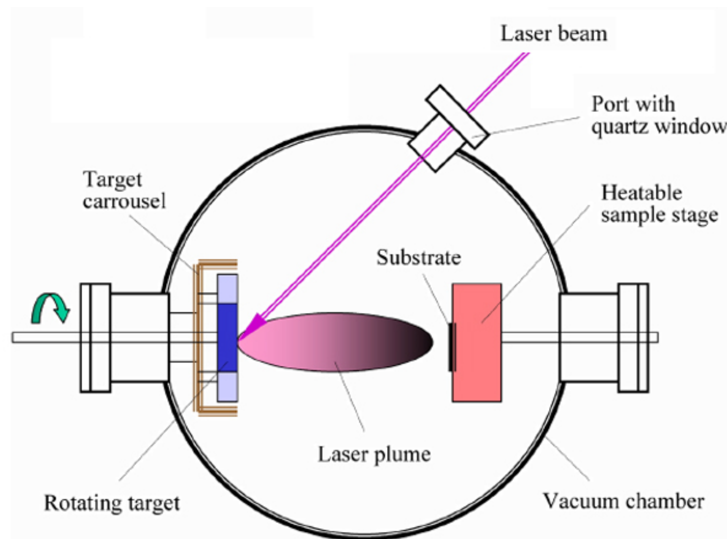

Figure. 2.3. Schematic diagram of PLD chamber

The main advantages of pulsed laser deposition are:

1) **conceptually simple**: a laser beam vaporizes a target surface, producing a film with the same composition as the target.
2) **versatile**: many materials can be deposited in a wide variety of gases over a broad range of gas pressures.
3) **cost effective**: one laser can serve many vacuum systems.
4) **fast**: high quality samples can be grown reliably in 10 or 15 minutes.
5) **scalable:** as complex oxides move toward volume production.

The mechanism of pulsed laser deposition, in contrast to the simplicity of the setup, is a very complex physical phenomenon. It not only involves the physical process of the laser-material interaction, but also the formation of plasma plume with high energetic species and even the transfer of the ablated material through the plasma plume onto the substrate surface. Thus the thin film formation in PLD generally can be divided into the following four stages.

1) Laser radiation interaction with the target
2) Dynamics of the ablated materials.
3) Deposition of the ablation materials on the substrate.
4) Nucleation and growth of a thin film on the substrate surface

Each stage in PLD is critical to the formation of quality epitaxial, crystalline, stoichiometric and uniform thin films.

In the first stage, the laser beam is focused onto the surface of the target. At sufficiently high flux densities and short pulse duration, all elements in the target are rapidly heated up to their evaporation temperature. Materials are dissociated from the target surface and ablated out with stoichiometry as in the target. The instantaneous ablation rate is highly dependent on the fluences of the

laser shining on the target. The ablation mechanisms involve many complex physical phenomena such as collision, thermal and electronic excitation, exfoliation and hydrodynamics.

During the second stage, the emitted materials tend to move towards the substrate according to the laws of gas dynamics and show the forward peaking phenomenon. The spatial thickness varies as a function of $\cos\theta$. The spot size of the laser and the plasma temperature have significant effects on the deposited film uniformity. The target-to-substrate distance is another parameter that governs the angular spread of the ablated materials. A mask placed close to the substrate can reduce the spreading. Typical plasma temperature measured by emission spectroscopy during initial expansion of the plume is ≈ 10,000 K, which is well above the boiling point of most materials (≈ 3000 K). Heating of the plasma to these temperatures is thought to occur by inverse Bremsstrahlung absorption of the laser light in a free transition of electron ion pair. This high temperature would evaporate the surface layer of the target thereby producing exact composition in the thin films.

The third stage is important to determine the quality of thin film. The ejected high energy species impinge onto the substrate surface and may induce various types of damage to the substrate. These energetic species sputter some of the surface atoms and a collision region is formed between the incident flow and the sputtered atoms. Film grows after a thermalized region is formed. The region serves as a source for condensation of particles. When the condensation rate is higher than the rate of particles supplied by the sputtering, thermal equilibrium condition can be reached quickly and films grow on the substrate surface at the

expense of the direct flow of the ablation particles and the thermal equilibrium obtained.

The effect of increasing the energy of the adatoms has a similar effect of increasing substrate temperature on film growth. Typical power densities involved in PLD are approximately 50 $MWcm^{-2}$ for a reasonable growth rate. (> 1 A^o/shot) If plasma is formed during laser target interaction in vacuum or in air then an explicit laser-plasma interaction occurs due to which ions in the plasma are accelerated to as much as 100-1000 eV [20].

Nucleation and growth of crystalline films depend on many factors such as the density, energy, ionization degree, and the type of the condensing material, as well as the temperature and the physio-chemical properties of the substrate. The two main thermodynamic parameters for the growth mechanism are the substrate temperature T and the supersaturation D_m related by the following equation:

$$D_m = kT \ln(R/R_e) \qquad (2.6)$$

where, k is the Boltzmann constant, R is the actual deposition rate, and R_e is the equilibrium value at the temperature T.

The nucleation process depends on the interfacial energies between the three phases present - substrate, the condensing material and the vapour. The critical size of the nucleus depends on the driving force, i.e. the deposition rate and the substrate temperature. For the large nuclei, a characteristic of small supersaturation, they create isolated patches (islands) of the film on the substrate, which subsequently grow and coalesce together. As the supersaturation increases, the critical nucleus shrinks until its height reaches on atomic diameter and its shape is that of a two dimensional layer. For large supersaturation, the layer-by-layer nucleation will happen for incompletely wetted foreign substrates.

The crystalline film growth depends on the surface mobility of the adatom (vapour atoms). Normally, the adatom will diffuse through several atomic distances before sticking to a stable position within the newly formed film. The surface temperature of the substrate determines the adatom's surface diffusion ability. High temperature favours rapid and defect free crystal growth, whereas low temperature or large supersaturation crystal growth may be overwhelmed by energetic particle impingement, resulting in disordered or even amorphous structures.

The mean thickness, (N), at which the growing thin and discontinuous film reaches continuity, is given by the formula:

$$N = A(1/R)^{1/3} \exp(-1/T) \qquad (2.7)$$

where A is a constant related to the materials and R is deposition rate. In the PLD process, due to the short laser pulse duration (~ 10 ns) and hence the small temporal spread (≤ 10 ms) of the ablated materials, the deposition rate can be enormous (~10 nm/s). Consequently a layer-by-layer nucleation is favoured and ultra-thin and smooth film can be produced. In addition, the rapid deposition of the energetic ablation species helps to raise the substrate surface temperature. In this respect, PLD tends to demand a lower substrate temperature for crystalline film growth.

In the present study, PLD was used to deposit the oxide films at room temperature. The process was carried out in a vacuum chamber pumped by a 6” diffusion pump backed by a rotary pump (Indovision, Bangalore). The source used was the third(355 nm) harmonic of Nd:YAG laser (Spectra Physics model GCR 150). The flow of oxygen into the chamber was controlled using a mass flow controller (Bronkhorst, Holland).

2.4 Charactersation tools

Once the films are grown, the structural, compositional, morphological, optical and electrical analytical tools give a better understanding of the film behavior and characteristics. On the reverse, the characterisation techniques help in optimizing the growth conditions to get device quality films. In the following sections, the techniques used for the film characterisations in the present study are discussed briefly.

2.4.1 Thin film thickness

Film thickness has a crucial role in determining its properties unlike a bulk material. The properties of the thin films can be reproduced if thickness, along with other deposition parameters, is kept constant. Film thickness may be measured either by in situ monitoring of the rate of deposition or after the film deposition. The thickness of the thin films prepared for the work presented in this thesis was measured by a stylus profiler (Dektak 6M).

The stylus profiler takes measurements electromechanically by moving the sample beneath a diamond tipped stylus. The high precision stage moves the sample according to a user defined scan length, speed and stylus force. The stylus is mechanically coupled to the core of a linear variable differential transformer (LVDT). While in contact over the moving sample surface, surface variations cause the stylus to be translated vertically. Electrical signals corresponding to the stylus movement are produced as the core position of the LVDT changes. The LVDT scales an ac reference signal proportional to the position change, which in turn is conditioned and converted to a digital format through a high precision, integrating, analog-to-digital converter [21].

To measure the film thickness, a region of the substrate has to be masked during film deposition. This creates a step on the sample. The thickness of the sample can then be measured accurately by measuring the vertical motion of the stylus over the step.

2.4.2 Structural characterisation

The crystallographic nature of a sample very well influences its electrical and optical properties. X-ray diffraction (XRD) studies are generally used for structural analysis. Any material has a characteristic diffraction pattern, whether present in pure state or as one constituent of a mixture of substances. This fact is made useful in the diffraction method of chemical analysis. The advantage of the technique is that it discloses the presence of a substance, as that substance actually exists in the sample and not in terms of its constituent chemical elements. Hence, diffraction analysis is useful whenever it is necessary to know the state of chemical combination of the elements involved or the particular phase in which they are present. Compared with ordinary chemical analysis the diffraction method has the advantage that it is usually much faster, requires only very small quantity of sample and is non-destructive.

The basic law involved in the diffraction method of structural analysis is the Bragg's law. When monochromatic beam of x-rays impinges upon the atoms in a crystal lattice, each atom acts as a scattering source. The crystal lattice presents a series of parallel reflecting planes to the incident x-ray beam. The intensity of the reflected beam at certain angles will be maximum when the path difference between two reflected waves from two different crystal planes is an integral multiple of λ.This condition is termed as Bragg's law and is given by,

$$n\lambda = 2d\sin\theta \tag{2.8}$$

where, n is the order of diffraction, λ is the wavelength of x-rays, d is the spacing between consecutive parallel planes and θ is the glancing angle (or the complement of the angle of incidence) [22].

X-ray diffraction studies give a whole range of information about the crystal structure, orientation, average crystalline size and stress in the powder. Experimentally obtained diffraction patterns of the sample are compared with the standard powder diffraction files published by the International Centre for Diffraction Data (ICDD).

In the present study, the bulk and thin film samples were structurally characterized by recording their XRD patterns using an automated Rigaku X-ray diffractometer. The filtered copper K_{α} radiation (λ = 1.5414 A^0) was used for recording the diffraction pattern. The average grain size, t, of the film can be calculated using the Scherrer's formula,

$$t = \frac{0.9\lambda}{\beta \cos\theta} \qquad (2.9)$$

Here, β is the full width at half maximum in radians.

The lattice parameter values for a cubic crystallographic system can be calculated from the following equation using the (hkl) parameters and the interplanar spacing d.

Cubic system,
$$\frac{1}{d^2} = \frac{h^2 + k^2 + l^2}{a^2} \qquad (2.10)$$

2.4.3 Morphological analysis

Surface morphology is an important property while going for multilayer device fabrication. Roughness of the thin film surface plays a vital role, especially while making interfaces. Some of the characterisation tools used to study about the surface of thin films is described below.

i. Scanning Electron Microscope (SEM)

The scanning electron microscope (SEM) uses electrons rather than light to form an image. SEM has several advantages over an ordinary light microscope [23]. The SEM has a large depth of field, which allows a large amount of the sample to be in focus at a time. The SEM also produces images of high resolution, which means that closely spaced features can be examined at a high magnification. Preparation of the samples is relatively easy since most SEMs only require that sample should be conductive. The combination of higher magnification, larger depth of focus, greater resolution, and ease of sample observation makes the SEM one of the most heavily used instruments in current research areas.

In a typical SEM, electrons are thermionically emitted from a tungsten or lanthanum hexaboride (LaB_6) cathode and are accelerated towards an anode. Alternatively, electrons can be emitted via field emission. The most common is the tungsten hairpin gun. Tungsten is used because it has the highest melting point and lowest vapour pressure of all metals, thereby allowing it to be heated for electron emission.

A voltage is applied to the loop, causing it to heat up. The anode, which is positive with respect to the filament, forms powerful attractive forces for electrons. This causes electrons to accelerate toward the anode. The anode is

arranged, as an orifice through which electrons would pass down to the column where the sample is held.

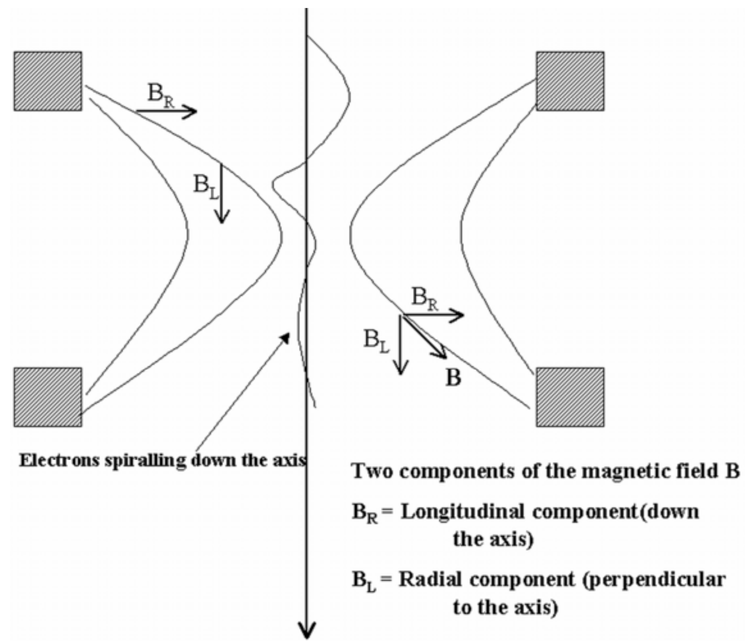

Figure 2.4. The focusing of electrons in SEM

The electron beam, which typically has an energy ranging from a few hundred eV to 100 keV, is attracted through the anode, made to pass through a condenser lens, and focused to very fine point on the sample by the objective lens (figure 2.4). The electron beam hits the sample, producing secondary electrons from the sample. These electrons are collected by a secondary detector or a backscatter detector and converted to voltage, and amplified. The amplified voltage is applied to the grid of the CRT that causes the intensity of the spot of

light to change. The image consists of thousands of spots of varying intensity on the face of a CRT that corresponds to the topography of the sample.

The spatial resolution of the SEM depends on the size of the electron spot, which in turn depends on the electron energy and the magnetic electron-optical system which produces the scanning beam. To ensure that the information recorded in the image arises only from the sample surface, the column must always be at vacuum. Or else, there are chances for contamination of the sample and the electron beam, instead of being directed onto the sample, would induce ionisation in any background gas that would effect the measurement being made on the sample.

In the present studies, JEOL JSM 5600 was used for SEM analysis.

ii. Atomic Force Microscopy (AFM)

The atomic force microscope (AFM) is a very high resolution type of scanning probe microscope, with resolution of fractions of a nanometer, more than 1000 times better than the optical diffraction limit. It can, therefore, probe into understanding the fine details of a sample surface [23].

In atomic force microscopy, a tip integrated to the end of a spring cantilever, is brought within the inter atomic separations of a surface, such that the atoms of the tip and the surface are influenced by inter atomic potentials. As the tip is rastered across the surface, it bounces up and down with the contours of the surface. By measuring the displacement of the tip (*i.e.* the deflection of the cantilever), one can theoretically map out the surface topography with atomic resolution.

The AFM is essentially identical in concept to the scanning profilometer, except that the deflection sensitivity and resolution are improved by several orders of magnitude. The AFM can operate well in ambient air or in a liquid environment making it an important tool in studying biological systems, polymers and a host of insulator and semiconductor materials.

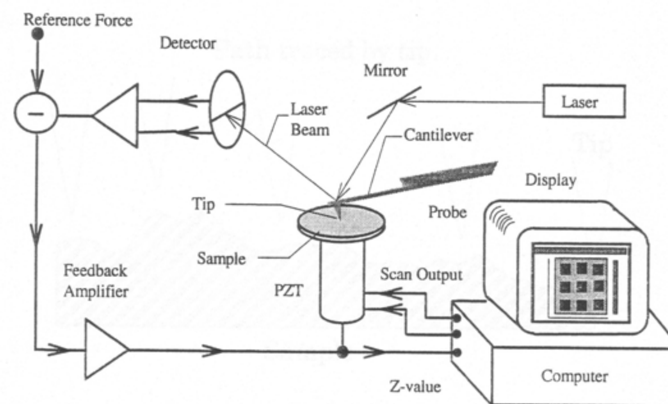

Figure 2.5. The essential elements of an AFM

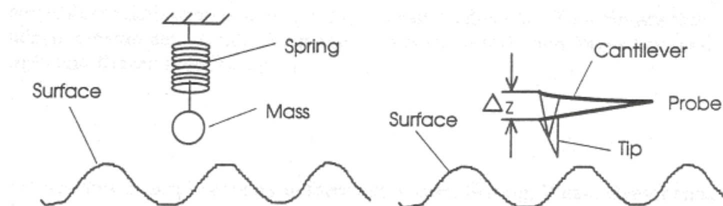

Figure 2.6. Attachment of the tip to the cantilever in an AFM

An AFM images a surface in a manner analogous to the gramophone stylus sensing the groves of gramophone disk. The essential elements of an AFM are shown in figure 2.5. The tip is attached to a cantilever type spring as shown in

figure 2.6. As the tip and sample interact, forces act on the tip and cause the cantilever (spring) to deflect. The cantilever position is monitored by a position detector. The output of the detector is connected to a feedback controller that regulates the force between the sample and the tip by moving the sample up or down. The sample is moved by a PZT scanning actuator. The cantilever must be soft enough to deflect a measurable amount without damaging the surface features of the sample. The amount of deflection is proportional to the force acting on the tip:

$$F_{spring} = -k \cdot \Delta Z \qquad (2.11)$$

where, F is the force on the sample, k is the spring constant of the cantilever, and, ΔZ is the deflection of the cantilever.

Two important modes of an AFM are contact mode and the tapping mode. In the contact mode, the static tip deflection is used as the feedback signal. In the tapping mode, the cantilever is externally oscillated at or close to its resonance frequency. The oscillation amplitude, phase and resonance frequency are modified by tip-sample interaction forces; these changes in oscillation with respect to the external reference oscillation provide information about the sample's characteristics.

The AFM provides us with a true three dimensional surface profile compared to the two dimensional SEM image, with atomic resolution in ultra high vacuum environments. But an AFM can only image a maximum height of the order of micrometres and a maximum scanning area of around 150 by 150 micrometres whereas SEM can image an area of the order of millimetres by millimetres with a depth of field of the order of millimetres.

In the present work, AFM from Veeco was used for the morphological study.

2.4.4 Compositional analysis

Compositional analysis helps to check the stoichiometry of the deposited films. Some of the characterization tools used in the present investigation is described below.

i. Energy dispersive x-ray (EDX) analysis

Energy dispersive x-ray (EDX) analysis is used for determining the elemental composition of a specimen. It often works as an integrated feature of a SEM, and cannot operate on its own without the latter. During EDX analysis, the specimen is bombarded with an electron beam inside the scanning electron microscope. The bombarding electrons (primary electrons) collide with the specimen, knocking some of them off in the process. The vacancy in the specimen atoms created by the ejection of an inner shell electron is eventually occupied by a higher energy electron from an outer shell. During this transition, the transferring electron gives up its excess energy in the form of x-rays.

The amount of energy released by the transferring electron depends on which shell it is transferring from, as well as which shell it is transferring to. Furthermore, the atom of every element releases x-rays, unique in energy during the transferring process, characteristic of that element. Thus, by measuring the energy of the x-rays emitted by a specimen during electron beam bombardment, the identity of the atom from which the x-ray was emitted can be established.

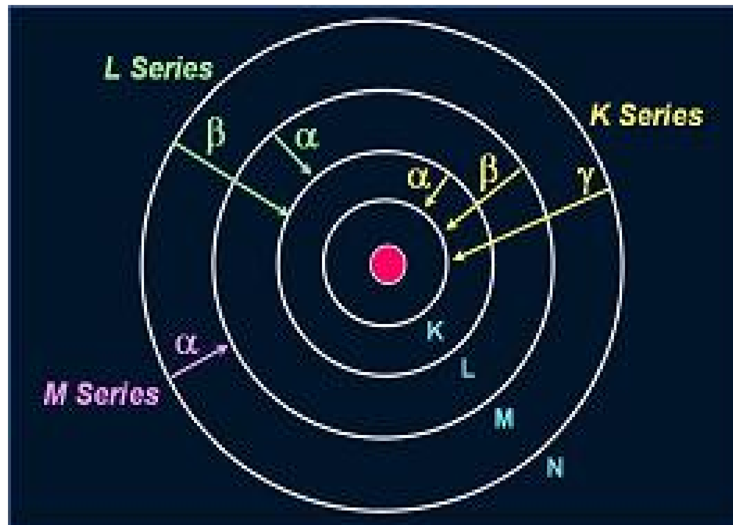

Figure 2.7. Electronic transitions giving rise to x-ray emission

The output of an EDX analysis is an EDX spectrum, which is a plot of how frequently an x-ray is received for each energy level. An EDX spectrum normally displays peaks corresponding to the energy levels for which the most x-rays had been received. Each of these peaks is unique to an atom, and therefore corresponds to a single element. The higher a peak in a spectrum, the more concentrated the element is in the specimen. An EDX plot not only identifies the element corresponding to each of its peaks, but the type of x-rays to which it corresponds as well. For example, a peak corresponding to the amount of energy possessed by x-rays emitted by an electron in the L-shell going down to the K-shell is identified as a K_{α} peak. The peak corresponding to x-rays emitted by M-shell electrons going to the K-shell is identified as a K_{β} peak as shown in figure 2.7.

ii. Transmission electron microscopy (TEM)

Transmission electron microscopy (TEM) is an imaging technique whereby a beam of electrons is focused onto a specimen causing an enlarged version to appear on a fluorescent screen or layer of photographic film or to be detected by a CCD camera. The first practical transmission electron microscope was built by Albert Prebus and James Hillier at the University of Torondo in 1938 using concepts developed earlier by Max Knoll and Ernst Ruska. Electrons are generated by a process known as thermionic discharge in the same manner as the cathode in a cathode ray tube, or by field emission; they are then accelerated by an electric field and focused by electrical and magnetic fields onto the sample. The electrons can be focused onto the sample providing a resolution far better than possible with light microscopes, and with improved depth of vision. Details of a sample can be enhanced in light microscopy by the use of stains. Similarly with electron microscopy, compounds of heavy metals such as osmium, lead or uranium can be used to selectively deposit in the sample to enhance structural details. The electrons that remain in the beam can be detected using a photographic film, or fluorescent screen [24]. So areas where electrons are scattered appear dark on the screen, or on a positive image.

An additional class of these instruments is the electron cryomicroscope, which includes a specimen stage capable of maintaining the specimen at liquid nitrogen or liquid helium temperatures. This allows imaging specimens prepared in vitreous ice, the preferred preparation technique for imaging individual molecules or macromolecular assemblies. Another type of TEM is the scanning transmission electron microscope (STEM), where the beam can be rastered across the sample to form the image. In analytical TEMs the elemental

composition of the specimen can be determined by analysing its X-ray spectrum or the energy-loss spectrum of the transmitted electrons. Modern research TEMs may include aberration correctors, to reduce the amount of distortion in the image, allowing information on features on the scale of 0.1 nm to be obtained (resolutions down to 0.08 nm has been demonstrated, so far). Monochromators may also be used which reduce the energy spread of the incident electron beam to less than 0.15 eV.

From TEM images, size of the nanoparticles can be determined. Parallel lines in the high resolution transmission electron micrograph (HRTEM) represent planes in the crystal lattice and distance between them corresponds to d spacing. By comparing these d spacing values with the JCPDS data, one can identify the orientation of the planes in the synthesized material. Selective area electron diffraction (SAED) is the map of the reciprocal lattice which will also give the signature of various planes in which material has been grown. Depending on the crystalline nature of the material, the SAED pattern will be orderly arranged spots, distinguishable rings or fused rings. But in the case of quantum dots concentric rings are observed in the SAED. The d spacing of the planes corresponding to the rings can be determined by the following equation

$$(Dd) = CL\lambda \qquad (2.12)$$

where L is the effective camera length, λ is the de-Broglie wavelength of the accelerating electrons, D is the ring diameter of a standard electron diffraction pattern and d is the interplanar spacing [24]. The term on the right hand side of the equation is referred to as the camera constant. TEM, JEOL operating at an accelerating voltage of 200 kV was used for the confirmation of the formation of nanorods in the present work.

2.4.5 Electrical transport properties

i. Hall effect measurement

The Hall effect measurement technique is widely applied in the characterisation of semiconductor materials as it gives the resistivity, the carrier density, type of carriers and the mobility of carriers. When a magnetic field is applied to a conductor perpendicular to the current flow direction, an electric field will be developed perpendicular to the direction of magnetic field and the current. This phenomenon is known as Hall effect and the developed voltage is called Hall voltage.

The force acting on a charge (q) moving with a velocity v in the presence of electric (E) and magnetic (B) fields is given by the vector expression

$$\vec{F} = q(\vec{E} + \vec{v} \times \vec{B}) \tag{2.13}$$

For n-type and p-type samples, the electrons and holes respectively deflect to the same side of the sample for the same current direction because electrons flow in the opposite direction to holes and have opposite charge.

The Hall coefficient R_H is defined as

$$R_H = \frac{V_H d}{BI} \tag{2.14}$$

where d is the sample dimension in the direction of magnetic field B, V_H is the Hall voltage and I is the current through the sample [23]. Hall coefficient is related to hole (p) and electron (n) densities by the equation:

$$p = \frac{1}{qR_H}; \quad \textit{and} \quad n = -\frac{1}{qR_H} \tag{2.15}$$

Equation 2.15 is derived under the assumption of energy independent scattering mechanisms. With this assumption relaxed, the expressions for the hole and electron densities become

$$p = r/qR_H; \quad and \quad n = -r/qR_H \qquad (2.16)$$

where r is the Hall scattering factor, defined by $r = \langle \tau^2 \rangle / \langle \tau \rangle^2$, with τ being the mean time between carrier collisions. The scattering factor depends on the type of scattering mechanism in the semiconductor and generally lies between 1 and 2. For lattice scattering, $r = 1.18$, for impurity scattering $r = 1.93$, and for neutral impurity scattering $r = 1$. The scattering factor is also a function of magnetic field and temperature and can be determined by measuring R_H in the high magnetic field limit, i.e.,

$$r = R_H(B) / R_H(B = \infty) \qquad (2.17)$$

In the high field limit $r \rightarrow 1$.

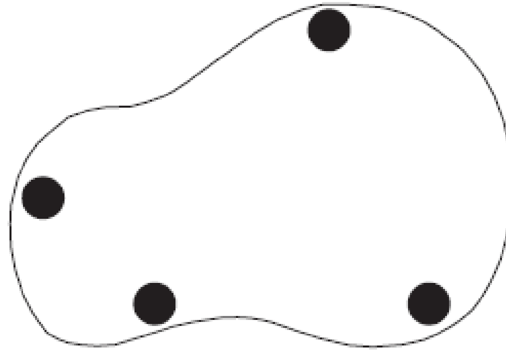

Figure 2.8: Lamella-type van der Pauw Hall sample.

The Hall mobility *H* is defined by

$$\mu_H = \frac{|R_H|}{\rho} = |R_H|\sigma \quad (2.18)$$

substituting the value of σ for hole and electron, the equation 1.6 becomes

$$\mu_H = r\mu_p; \quad and \quad \mu_H = r\mu_n \quad (2.19)$$

for extrinsic p- and n-type semiconductors, respectively. Hall mobilities can differ significantly from conductivity mobilities since *r* is generally larger than unity. For most Hall-determined mobilities, *r* is taken as unity.

A more general geometry is the irregularly shaped sample in figure 2.8. The theoretical foundation of Hall measurement evaluation for irregularly shaped samples is based on conformal mapping developed by van der Pauw. He showed how the resistivity, carrier density, and mobility of a flat sample of arbitrary shape can be determined without knowing the current pattern if the following conditions are met: contacts should be point contacts located symmetrically on the periphery of the sample, the sample is uniformly thick, and does not contain isolated holes. This is not achievable in practice, and some error is introduced thereby. Hall effect measurements are simple to interpret for uniformly doped samples. However in delafossite compounds it was very difficult to determine the hall coefficient owing to the low mobility values. The efforts to measure the carrier concentration in p-type delafossites did not succeed due to the observation of unpredictable dependence of Hall voltage on magnitude and direction of applied magnetic field. The hall voltage showed a non linear behaviour as function of applied magnetic field and did not change sign with reversing the direction of the applied magnetic field. Such an electrical behaviour has been attributed to mixed conduction. Hence in the case of p-type conductors, the type

of carriers was determined by the thermopower measurement which showed positive Seebeck coefficient. The hall coefficient of n-type carriers was determined as described using van der Paw geometry.

The pn junctions were investigated by fabricating the heterojunctions and studying their current voltage characteristics using the Keithley source measure unit SMU236.

ii. Thermopower measurements

The sample holder for the thermopower measurement is similar to the one reported by Young et. al. [25]. The sample holder is made from copper and can be thermally attached to a closed cycle two stage cryostat. The copper blocks ‘F’ and ‘G’ are electrically isolated from each other and also from the sample-holder stage, but thermally connected via a sheet of 2 mm thick teflon. The heating element in the blocks is carbon resistance (100Ω) mounted with stycast^{TM} epoxy in hole bored through the centre of the heating blocks parallel to its axis. Embedded in, but electrically isolated from, the heater block is a type ‘K’ differential thermocouple made from chromel alumel. The junctions of the chromel alumel differential thermocouple are located as close as possible (Below 1mm from the surface of the blocks F,G where the samples are mounted) to the mounting surface of the heater block and are thermally anchored which stycast^{TM} epoxy .

All the thermocouple junctions are located just under the surface of the copper blocks exactly where the sample is loaded. Both of them are drilled and tapped with holes on the inside of the channel between the blocks. All of the wires exiting the sample holder are wound in twisted pairs to minimise magnetic

interference and these pairs are wound around the cryostat expander arm multiple times to minimise heat conduction [26].

The two ends of the thermocouple and the ends of the heater resistor are connected to the PID – temperature controller which controls the temperature gradient between the blocks.

The objective of the temperature controller is to maintain a temperature difference of 1^0C between the two copper blocks of the experimental set-up in order to facilitate the thermo e.m.f. measurement of the thin film sample A differential thermocouple. (type K, cromel-alumel) is used owing to the convenience it offers in the measurement of temperature difference and also due to its low thermal inertia which supports good control. However, the sensitivity of a thermocouple is relatively low, only about $40\mu V/^0C$ in the case of a type-K thermocouple. This is a serious challenge, as it demands a high performance amplifier capable of amplifying microvolt level signal with the required accuracy. It is not easy to construct such an amplifier using locally available components hence an existing micro voltmeter (Model – KEITHLY 2000) is used for temperature measurement. A personnel computer is used to implement the control function, which communicates with the micro voltmeter through IEEE-488 interface. The heater voltage is calculated using PID control algorithm and it is sent to the heater through a D/A channel of an analogue interface which is inserted into one of a bus expansion slot of the PC. The entire control programme that also includes provision for a real-time graphical display of the control parameter is written in C-language.

2.4.6 Optical studies

i. Diffuse reflectance spectroscopy (DRS)

In the present study, diffuse reflectance spectroscopy and transmission spectroscopy were used to determine the band gap of powder and thin film samples respectively.

Diffuse reflection is the reflection of light from an uneven or granular surface such that an incident ray is seemingly reflected at a number of angles. Diffuse reflected rays from a sample do not obey the Snell's law as do the ordinary mirror-like specular reflections. The measurement of radiation diffusely reflected from a surface constitutes the area of spectroscopy known as diffuse reflectance spectroscopy (DRS). Specular reflection is due to the reflection at the surface of single crystallites while diffuse reflection arises from the radiation penetrating into the interior of the solid and re-emerging to the surface after being scattered numerous times. Thus, the DRS spectra can exhibit both absorbance and reflectance features due to contributions from transmission, internal and specular reflectance components as well as scattering phenomena in the collected radiation.

Based on the optical properties of the sample, several models have been proposed to describe the diffuse reflectance phenomena. The Kubelka-Munk (KM) model put forward in 1931 [27, 28] is widely used and accepted in DRS. The KM theory is based on a continuum model where reflectance properties are described by differential equations for infinitesimally small layers. When the depth of the sample is infinite, the theory is solved to arrive at the remission function or the so-called KM function,

$$f(r_\infty) = \frac{(1 - r_\infty)^2}{2r_\infty} = \frac{k}{s} \qquad (2.20)$$

where, $r_\infty = R_\infty(\text{sample})/R_\infty(\text{standard})$, R_∞ denotes the diffuse reflectance. Here the standard used is $BaSO_4$. R_∞(standard) is taken as unity. The intensity of the diffusely reflected light therefore depends on the scattering coefficient s and the absorption coefficient k. The band gap is estimated from the plot of $\{(k/s).h\nu\}^2$ versus $h\nu$ ($h\nu$ is the photon energy) by extrapolating the graph to the x axis.

DRS was carried out using Jasco V 500 spectrophotometer in the present studies.

ii. Transmission spectroscopy

Intrinsic optical absorption of a single photon across the band gap is the dominant optical absorption process in a semiconductor. When the energy of the incident photon ($h\nu$) is larger than the band gap energy the excitation of electrons from the valence band to the empty states of the conduction band occurs. The light passing through the material is then absorbed and the number of electron hole pairs generated depends on the number of incident photons $S_0(\nu)$ (per unit area, unit time and unit energy). The photon flux $S(x,\nu)$ decreases exponentially inside the crystal according to the relation,

$$S(x, \nu) = S_0(\nu) \exp(-\alpha x) \qquad (2.21)$$

where, the absorption coefficient α, ($\alpha(\nu) = 4\pi k\nu/c$) is determined by the absorption process in semiconductors and k is the extinction coefficient.

For the parabolic band structure, the relation between the absorption coefficient (α) and the band gap of the material is given by [29],

$$\alpha = \frac{A}{h\nu}(h\nu - E_g)^r \qquad (2.22)$$

where, r = 1/2 for allowed direct transitions, r = 2 for allowed indirect transitions, r = 3 for forbidden indirect transitions and r = 3/2 for forbidden direct transitions. A is the parameter which depends on the transition probability. The absorption coefficient can be deduced from the absorption or transmission spectra using the relation,

$$I = I_0 e^{-\alpha t} \qquad (2.23)$$

where, I is the transmitted intensity and I_0 is the incident intensity of light and t is the thickness of the film. In the case of direct transition, $(\alpha h\nu)^2$ will show a linear dependence on the photon energy (hν). A plot of $(\alpha h\nu)^2$ against hν will be a straight line and the intercept on energy axis at $(\alpha h\nu)^2$ equal to zero will give the band gap energy.The transmission of the thin films was recorded using Jasco V570 spectrophotometer in the present studies. Further details of the experimental techniques are described in the respective chapters.

References

1. Hand book of Hydrothermal Technolgy, K.Byrappa and M.Yoshimura, Noyes publications New jerky USA (2001)
2. J. George, *Preparation of Thin Films*, p.1, Marcel Dekker Inc., New York (1992).
3. T. Sei , Y. Nomura and T. Tsuchiya, *J. Non-Cryst. Solids* **218** (1997) 135
4. Z. Ji, L. Kun, S. Yongliang and Y. Zhizhen, *J. Cryst. Growth* **255** (2003) 353
5. Z. Yan, M. Koike and H. Takei, *J. Cryst. Growth* **165** (1996) 183.
6. S. H. Yang, *J. Electrochem. Soc.* **150** (2003) H250
7. Z. Lou and J. Hao, *Appl. Phys. A* **80**(2005) 151
8. J. Hao, Z. Lou, I. Renaud and M. Cocivera, *Thin Solid Films* **467**(2004) 182.
9. T. Miyata, T. Nakatani and T. Minami, *Thin Solid Films* **373**(2000) 145
10. N. Honda, T. Suzuki, T. Yunogami, H. Suematsu, W. Jiang and K. Yatsui, *Jpn. J. Appl. Phys.*, **44**(2005) 695
11. T. Minami, Y. Kuroi, S. Dakata, *J. Vac. Sci. Technol. A* **14**(1996) 1736
12. L. I. Maissel and R. Glang, *Handbook of Thin Film Technology*, p.22, McGraw-Hill, New York (1970).
13. L. Holland, *Vacuum Deposition of Thin films*, p.104, John Wiley & Sons Inc., New York (1956).
14. D. L. Smith, *Thin-film deposition*, p.431, Mc Graw - Hill, New York (1995).
15. F. L.Akkad, A. Punnose and J. Prabu, *J. Appl. Phys.*, **71**(2000) 157
16. M. Ohring, *Materials Science of Thin Films*, Second edition, p.161, Academic Press, San Diego (2002).
17. B. Chapman, Glow Discharge Processes, p.108, John Wiley & Sons Inc., New York (1980).

18. V. S. Smentkowski, *Prog. Surf. Sci.*, **64** (2000) 1
19. T. Venkatesan and S. M. Green, *The industrial physicist*, **2** (1996) 22
20. D. B. Chrisey and G. K. Hubler, *Pulsed Laser Deposition of Thin Films*, p.229, John Wiley and sons Inc., New York (1994).
21. Veeco Dektak 6M Manual 2004.
22. B. D. Cullity and S. R. Stock, *Elements of X ray diffraction*, Third edition, p.170, Prentice Hall, New Jersey (2001).
23. D. K. Schroder, *Semiconductor material and device characterization*, Second edition, p.651, John Wiley & Sons Inc., New York (1998).
24. P. E .J. Flewit and R. K. Wild, *Physical methods for material characterization*, Second edition, p.501, IOP publishing, London (2003).
25. D.L.Young and T.J.Coutts and V.I. Kaydanov, Review of Scientific instruments **71**(2000) 462.
26. J.Yeager and M.A. Hrusch-Tupta, Low level measurements,Precision dc Current,Voltage and Resistance measurements, 5th Ed. Keithley Instruments Inc. Cleveland, 1997.
27. P. Kubelka and F. Munk, *Zh. Tekh. Fiz.*, **12**(1931) 593
28. P. Kubelka, *J. Opt. Soc .Am.*, **38** (1948) 448
29. A. Goswami, *Thin Film Fundamentals*, p.418, New Age International (P) Limited, New Delhi (1996).

Chapter 3

Synthesis of copper delafossites and growth of thin films

Abstract

Various copper delafossite materials viz; $CuAlO_2$, $CuGaO_2$, $CuFeO_2$, $CuGa_{1-x}Fe_xO_2$, $CuYO_2$ and $CuCa_xY_{1-x}O_2$ were synthesised by solid state reaction technique. These copper delafossite materials were grown in thin film form by rf magnetron sputtering technique. The conductivity of the $CuYO_2$ could be improved by Ca doping or by oxygen intercalation by annealing the film in oxygen atmosphere. Reports show that oxygen intercalation or divalent ion doping on Ga site is not possible for $CuGaO_2$ thin films to improve the p-type conductivity. $CuFeO_2$ sintered powder and crystals have been reported as the materials having the highest p-type conductivity among the copper and silver delafossites. However the $CuFeO_2$ films are found to be less transparent in the visible region compared to $CuGaO_2$. The solid solution between the $CuGaO_2$ and $CuFeO_2$ was effected by solid state reaction, varying the Fe content. The $CuGa_{1-x}Fe_xO_2$ with Fe content $x=0.5$ shows an increase in conductivity by two orders compared to $CuGaO_2$ but the transparency is only about 50% in the visible region which is less than that of $CuGaO_2$.

3.1 Introduction

Transparent conducting oxide (TCO) thin films have a wide range of applications in optoelectronic devices [1], because of their unique transparent and conducting properties. Most of the TCOs exhibit n-type electrical conductivity. Indium tin oxide (ITO) and aluminum doped ZnO which has a band gap > 3 eV, transmission >80% in the visible region and conductivity of the order of 10^4 Scm^{-1} are n type conductors. These n-type TCOs have wide range of applications but limited as passive components such as transparent electrodes and IR reflection coatings. The development of p-type TCOs will open up new applications in optoelectronic devices. The theoretical prediction of the possibility of producing p-type conducting ZnO [2] by co-doping with nitrogen and gallium has aroused much interest in the field of TCOs. There are several reports in the recent literature on the growth of p-type ZnO [3-9]. However the reproducibility of good p-type ZnO, TCO material remains a difficult task. P-type conductivity has also been reported in NiO films [10] which has 30% transparency in the visible region. The $CuAlO_2$ thin film having a delafossite structure has shown a transparency of 80% in the visible region and infrared region with electrical conductivity $1Scm^{-1}$ [11]. This has generated much interest in p-type conducting transparent thin films [12, 13]. P-type conductivity has been found in a number of delafossite compound thin films like $CuYO_2$ [14, 15], $CuScO_2$ [16], $CuCrO_2$ [17], $CuGaO_2$ [18, 19] $CuInO_2$ [20] and $CuAlO_2$ [21].

$CuYO_2$ is a p-type semiconductor having wide bandgap isostructural with $CuAO_2$ delafossite (where A= Fe, Co, Rh, Ga, Sc, Y or lanthanides) [22]. Intercalation with oxygen to form $CuAO_{2+\delta}$ phases is possible for compounds

with large A^{3+} cations. Cava et al [23, 24] have investigated the properties of polycrystalline $CuYO_{2+\delta}$ and $CuLaO_{2+\delta}$ phases. The $CuYO_{2+\delta}$ doped with calcium shows conductivity as high as 10 Scm^{-1} after the oxygen intercalation. Similar observation of increase in conductivity has been reported for $CuScMgO_{2+\delta}$ films on oxygen intercalation [25]. But the oxygen intercalation results in the reduced transmittance in these films. The cause of p-type conductivity shown by these types of materials is due to excess oxygen (or metal deficit) within the crystallite sites of the material i.e. the defect chemistry plays an important role. This deviation from the stoichiometric composition of the can be controlled by regulating the preparation conditions of the materials. Intercalation of excess oxygen ions in the interstitial sites may trap electrons, leaving behind empty states in the valence band, which act as holes. The formula for oxygen-excess delafossite films may be written as $CuYO_{2+x}$. The value of x i.e. the percentage of excess oxygen may be not more than 25% in $CuYO_{2+x}$ polycrystalline powder. [26]. In the present investigation, bulk copper delafossites of $CuAlO_2$, $CuGaO_2$, $CuFeO_2$, $CuGa_{1-x}Fe_XO_2$, $CuYO_2$ and Ca doped $CuYO_2$ were synthesized by high temperature solid state reaction. Thin films of these copper delafossites were grown by rf magnetron sputtering.

3.2 RF magnetron sputtered $CuAlO_2$ thin films

3.2.1 Experimental

Polycrystalline $CuAlO_2$ powder was synthesized by heating a stoichiometric mixture of Cu_2O and Al_2O_3 at 1373K for 10h [27]. The powder was again reground and pressed into 2inch diameter pellets by a cold isostaic press at 600Kg cm^{-2} and then sintered at 1473 K for 10 h. These pellets were

used as the sputtering targets for the preparation of thin films by rf magnetron sputtering. The synthesized powder could be identified as the delafossite structure with R3m space group by XRD analysis (fig 3.1) Films of $CuAlO_2$ were prepared by rf magnetron sputtering at an rf power of 100watts using the sintered $CuAlO_2$ targets. The sputtering was carried out in a 80:20 mixture of argon and oxygen at a total pressure of 100mTorr. The substrate, amorphous silica was heated at 100^0C placed at 3cm above the target. The films were subjected to post deposition annealing after sputtering at 700^0C under the deposition ambient for 90 minutes.

3.2.2 Results and discussion

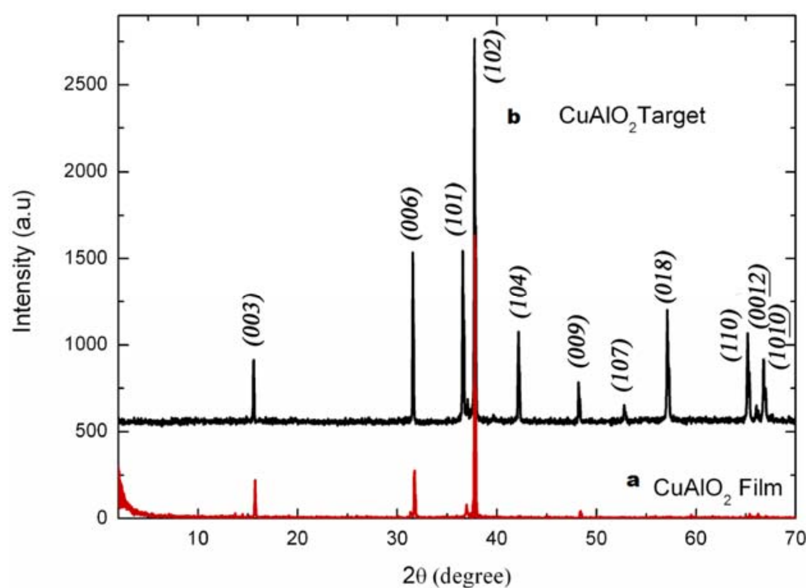

Figure 3.1 X-ray diffraction patterns of a) $CuAlO_2$ thin film and b) the ceramic target used for sputtering.

Figure 3.1 shows the diffraction patterns of the thin film (a) and the target (b) of $CuAlO_2$. The crystalline phase in the ceramic target and thin films is identified as delafossite structure with R3m space group. Figure 3.2 shows the transmission spectrum of the $CuAlO_2$ thin film in the visible and near infrared (NIR) region. Relatively high transmittance greater than 55% at 500nm is observed in the case of polycrystalline Cu thin films. The bandgap of the $CuAlO_2$ films is calculated from the transmission spectra by assuming a parabolic band structure for the material. The absorption coefficient and bandgap can be related by the expression $\alpha h\nu = A(h\nu\text{-}E_g)^{1/N}$ where E_g is the bandgap energy and α is the absorption coefficient corresponding to frequency ν [28]. The constant N depends on the nature of electronic transition. In the case of $CuAlO_2$ films N is equal to 2, for direct allowed transition. The band gap of the films is determined from the plot of $(\alpha h\nu)^2$ versus $h\nu$ by extrapolating the linear portion of the curve to $h\nu$ equal to zero. The direct allowed optical band gap evaluated from the plot is 3.77 eV (Figure 3.3) Banko and Koffyberg reported the indirect allowed band gap as 1.65 eV by photochemical measurements [29]. In the present study the indirect band gap estimated from the plot of $(\alpha h\nu)^{1/2}$ vs $h\nu$ is observed to be 1.68 eV (fig 3.4)

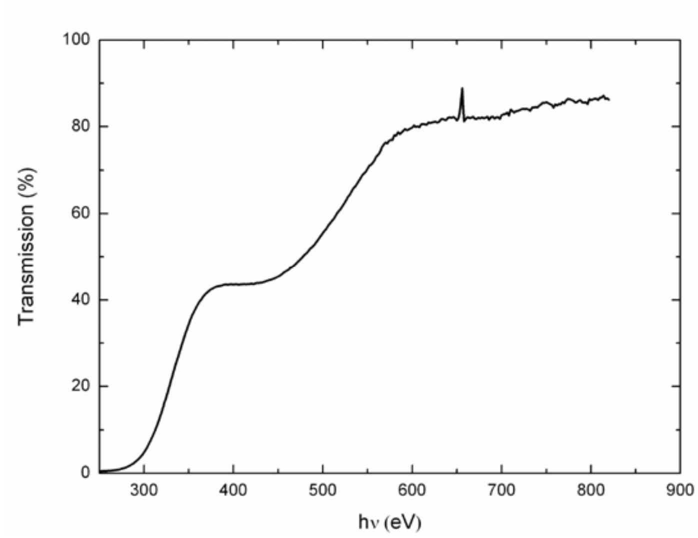

Fig 3.2 Transmission spectrum of $CuAlO_2$ thin film

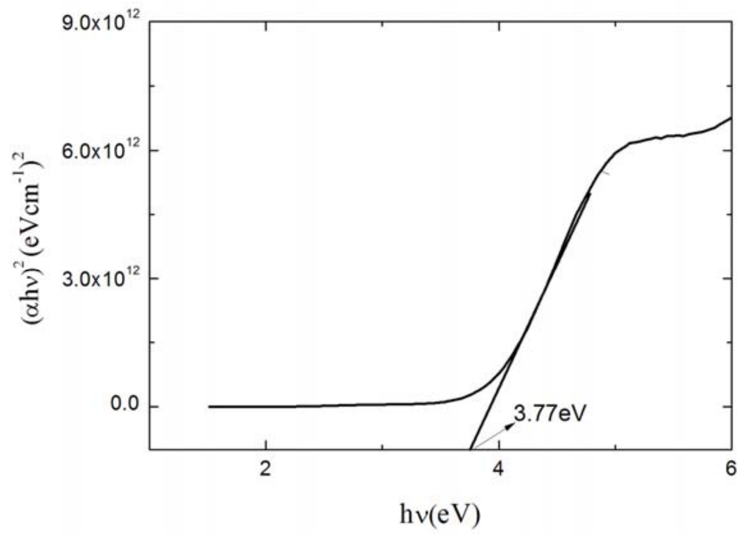

Fig 3.3 $(\alpha h\nu)^2$ vs hν plot of $CuAlO_2$ thin film

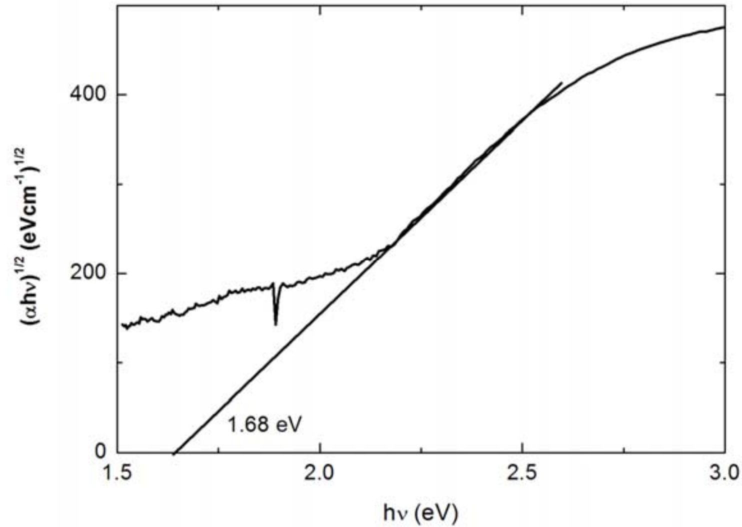

Fig 3.4 $(\alpha h\nu)^{1/2}$ vs hν plot of $CuAlO_2$ thin film

The samples show p-type electrical conductivity as confirmed by the hot probe method. The room temperature (300K) electrical conductivity is about $3x10^{-3}$ Scm^{-1}. The temperature dependence of conductivity shows a semiconducting behaviour The room temperature conductivity is very low which further decreases at low temperatures. Due to the low conductivity the temperature dependence did not give a reliable data. The hot probe measurement shows p-type electrical conduction. Though no intentional doping was carried out in the preparation of the samples, the positive holes in the $CuAlO_2$ are presumed to be generated from ionized Cu vacancies and interstitial oxygen as in Cu_2O [30] which is a well known p-type oxide semiconductor. Both Cu_2O and $CuAlO_2$ have crystal structures composed of O-Cu-O dumbbell units. The dumbbell units are three dimensionally connected in Cu_2O, while in $CuAlO_2$

these dumbbells have orientation parallel to c-axis (refer fig 1.3) and the layers are two dimensional. The layers are sandwiched by the sheets of AlO_6 octahedron in $CuAlO_2$. The difference in the crystal structure seems to control the degree of mixing between the Cu 3d and O 2p orbitals in the valance band edge. Four Cu ions coordinate to each O ion in Cu_2O, where as a Cu ion does in $CuAlO_2$. Therefore, it is considered that mixing and interactions between Cu 3d and O 2p orbitals in Cu_2O are rather greater than those in $CuAlO_2$ which lead to larger dispersion of the valance band in Cu_2O than in $CuAlO_2$. The larger dispersion of the valance band top in Cu_2O results in large mobility and narrower band gap (2eV) in comparison with that of $CuAlO_2$. As a consequence, it is found that $CuAlO_2$ has an appropriate dispersion in the valance band for enlarging the band gap which gives rise to an optical transparency.

The second neighboring distance, Cu-Cu distance in $CuAlO_2$ (0.286nm) is shorter than in Cu_2O (0.302nm), since Cu-Cu interaction also contributes to the dispersion of the valance band to some extent. The Cu-Cu interaction will influence hole transport properties in these materials. In delafossite single crystals anisotropy in electrical conductivity has been observed. The conductivity perpendicular to c-axis is larger than that parallel to c-axis [22]. Therefore epitaxial growth of $CuAlO_2$ films would show higher mobility than polycrystalline films obtained here. The conductivity and the transmission of the films in the visible region are low in comparison with the $CuAlO_2$ films grown by Kawozoe et al [11]. The trials to increase conductivity by substituting divalent cations (Mg^{2+} and Ca^{2+}) in place of trivalent Al^{3+} ions did not give any positive results. It has also been observed that the oxygen intercalation in $CuAlO_2$ was also not possible due to smaller size of the Al ions which results in

smaller space in the cage like structure (refer fig 1.4). Cava et al [23, 24] has reported improved conductivity in $CuYO_2$ by calcium doping and by oxygen intercalation in bulk powders. Hence further investigations were carried out in the growth of $CuYO_2$ films.

3.3 Growth and Characterisation of Polycrystalline $CuYO_2$ and Ca doped $CuYO_2$ thin films

3.3.1 Experimental

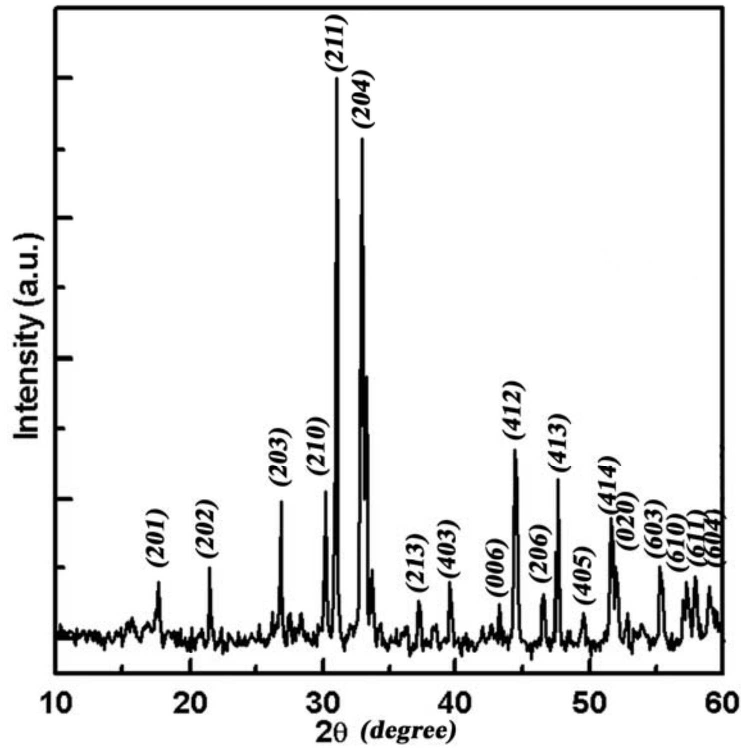

Figure 3.5 XRD pattern of ($Cu_2Y_2O_5$:Ca) powder.

Ca doped and undoped $CuYO_2$ were synthesized in the laboratory from a mixture of CuO and Y_2O_3 and CaO. This mixture was pelletized and heated at 1100^oC for 24 hours in air. The powder thus synthesized was found to be polycrystalline $Cu_2Y_{1.96}\,Ca_{0.04}O_5$ (Fig.3.5) [24].

This powder was again heated in a flow of argon at 1050^0C for 70 hours producing $CuY_{0.98}Ca_{0.02}O_2$. The sputtering target was prepared by pressing the Ca doped $CuYO_2$ powder into a 2 inch diameter pellet and heating at 1100^0C for 12 hrs. The sputtering was carried out by on-axis geometry on to fused quartz substrates. Initially when the films were sputtered at room temperature, the substrate temperature was found to increase up to 80^0C.Hence all the subsequent sputtering was carried out at a substrate temperature of 100^0C.

The sputtering chamber was initially pumped down to a pressure of $2x10^{-5}$ mbar, then filled with argon gas up to 0.008 mbar. Pre sputtering was carried out for 20 minutes before each deposition. The as deposited films were dark coloured and insulating. The films were subjected to a post deposition annealing at 700^0C in air for 10 minutes followed by 10 minutes annealing in argon atmosphere at 900^0C, which resulted in transparent Ca doped $CuYO_2$ films. The oxygen intercalation was achieved by annealing the films at various oxygen partial pressures. The annealing chamber was initially evacuated to $5x10^{-6}$ mbar and oxygen was fed into the chamber through a mass flow controller during annealing. The crystal structure of the films was analysed by Rigaku x-ray diffractometer in $\theta-2\theta$ geometry using Cu K_α radiation. All the as deposited films were amorphous. The composition of the target as well as the sputtered films was analysed using energy dispersive x-ray (EDX) studies. The EDX analysis shows that the films have the same compositions of the target with

Cu/(Y+Ca) ratio equal to one. The conductivity was measured by two-probe method using the silver electrodes in the planar geometry using a Keithley source measure unit (SMU 236). The transmission spectra of the films were recorded using a UV-Vis-NIR spectrophotometer (Hitachi U – 3410), The Ca doped $CuYO_2$ films showed p-type conductivity that was confirmed by thermoelectric power measurements.

3.3.2 Results and discussion

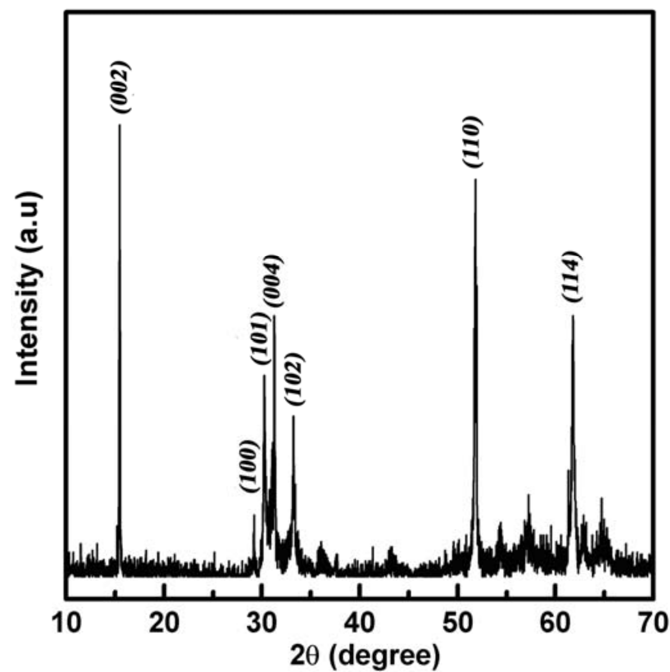

Figure 3.6 X-ray diffraction pattern of the Ca doped $CuYO_2$ target used for sputtering.

Figure 3.6 shows the x-ray diffraction (XRD) pattern of the Ca doped $CuYO_2$ target used for sputtering. The XRD pattern is consistent with delafossite structure belonging to R3m or P63/mmc [31]. The as deposited films were found to be amorphous by XRD (fig 3.6). These films when subjected to a post deposition annealing at 700 ^{o}C in air for 10 minutes formed $Cu_2Y_2O_5$ phase which on reduction in argon atmosphere at 900 ^{o}C for ten minutes, resulted in delafossite structure belonging to 2H or 3R polytype (fig 3.7).

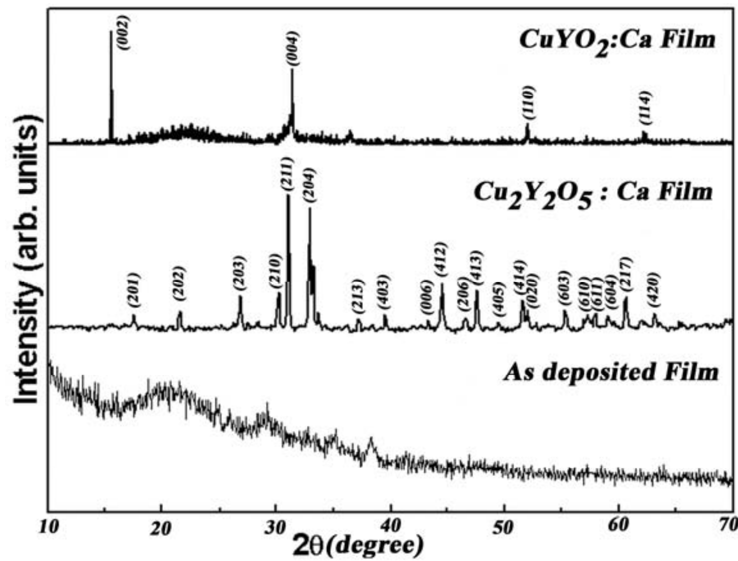

Figure 3.7 XRD patterns of as deposited film, $Cu_2Y_2O_5$:Ca phase and $CuYO_2$:Ca thin film

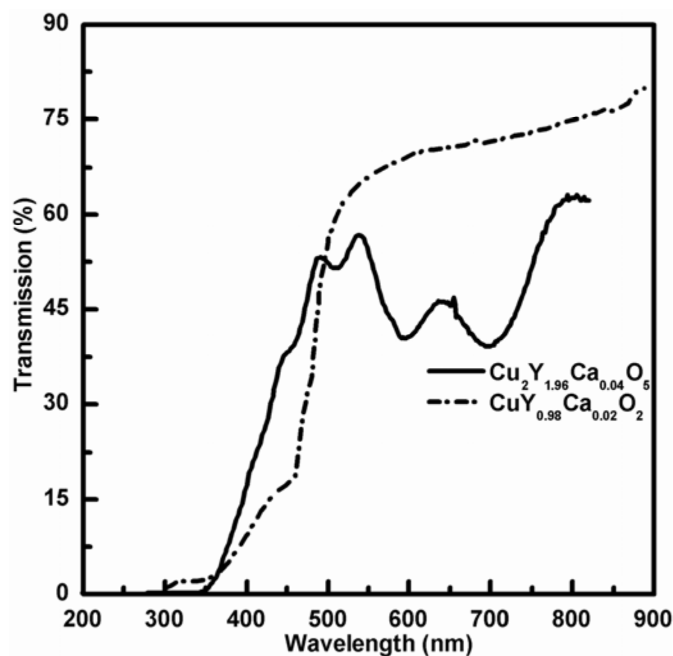

Figure 3.8. Transmission spectra of Ca doped $CuYO_2$ and $Cu_2Y_2O_5$.thin films

Oxygen intercalation by annealing the films at 420°C at an oxygen pressure of one atmosphere did not result in decomposition of the delafossites into the more stable $Cu_2Y_2O_5$ phases.The transmission spectrum of Ca doped $CuYO_2$ films recorded in the range of 200-900 nm is shown in figure 3.8. The films are transparent yellow in colour. The Ca doped $CuYO_2$ films before oxygen intercalation is transparent in the visible range with average transmission of about 60%. The transparency in the visible region is found to decrease with oxygen intercalation in to the films. The highly transparent films are less conducting and the conductivity increases with oxygen intercalation at the expense of transparency. The band gap of the Ca doped $CuYO_2$ films was

calculated from the transmission spectra by assuming a parabolic band structure for the material. The absorption coefficient and band gap can be related by the expression $\alpha h\nu = A(h\nu - E_g)^{1/N}$ where E_g is the band gap energy and α is the absorption coefficient corresponding to frequency ν [28]. The constant N depends on the nature of electronic transition. In the case of Ca doped $CuYO_2$ films N is equal to 2, for direct allowed transition. The band gap of the films was determined from the plot of $(\alpha h\nu)^2$ versus $h\nu$ by extrapolating the linear portion of the curve to $h\nu$ equal to zero (fig.3.9).

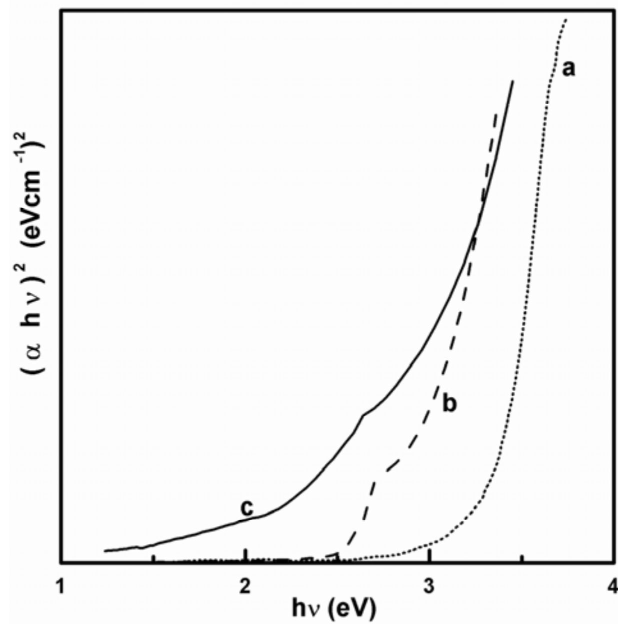

Figure 3.9 Plot of $(\alpha h\nu)^2$ vs $h\nu$ for the thin films of a) $Cu_2Y_2O_5$ (3.37eV) b) Ca doped $CuYO_2$ (3.01 eV) and c) Oxygen intercalated Ca doped $CuYO_2$ (2.88 eV)

.

In the present study the band gap of $Cu_2Y_2O_5$ is found to be 3.37 eV and that of Ca doped $CuYO_2$, obtained after annealing the as deposited films in oxygen atmosphere at 700°C followed by annealing in argon atmosphere at 900°C for 10 minutes each, to be 3.01eV. The absorption edge is not sharp both in the case of $CuYO_2$ films and oxygen intercalated films. The crystallinity of these films is also very poor. This indicates that the tail states extent to the band gap due to the defects and non stoichiometry.

The electrical properties of the films also show a dependence on the oxygen partial pressure during the annealing. The films before oxygen intercalation showed high resistivity. The resistivity as well as the transmission of the $CuYO_2$ films is found to decrease with the oxygen partial pressure during the annealing. The highest conductivity at room temperature, 8 Scm^{-1} was observed for films annealed at one atmosphere oxygen pressure. The temperature dependence of the conductivity of oxygen intercalated, Ca doped $CuYO_2$ films is shown in figure 3.10. The activated behaviour is typical of $CuAO_2$ (where A=Al, Ga, Fe, Y etc) p-type oxides [14, 16, 17]. The activation energy values obtained from the plot of ln σ versus $10^3/T$ plot are 0.59eV and 0.19eV at high and low temperatures respectively. The ln σ versus $10^3/T$ plot (Fig.3.10) is not a well fit by straight line. However ln σ vs $T^{-1/4}$ plot (inset fig.3.10) is close to a straight line suggesting a variable range hopping model for the conduction [35].

All the films were p-type as confirmed by the measurement of Seebeck coefficient. The highest value of Seebeck coefficient (+274μVK^{-1}) was obtained for films annealed in oxygen at atmospheric pressure at 420^{0}C for 20 minutes (Fig 3.11).

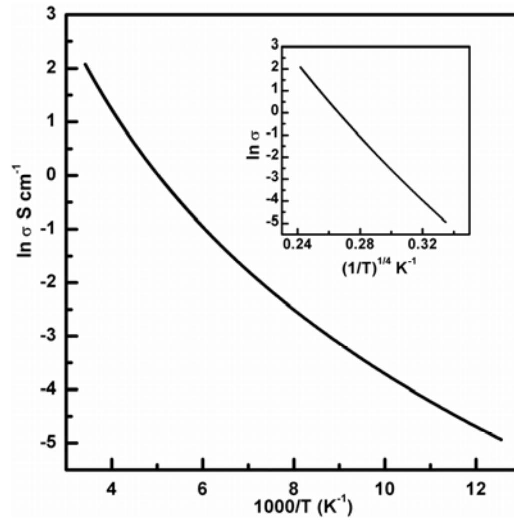

Figure 3.10. The temperature dependence of the conductivity of oxygen intercalated Ca doped $CuYO_2$ films. Inset shows the ln σ vs $T^{-1/4}$ plot.

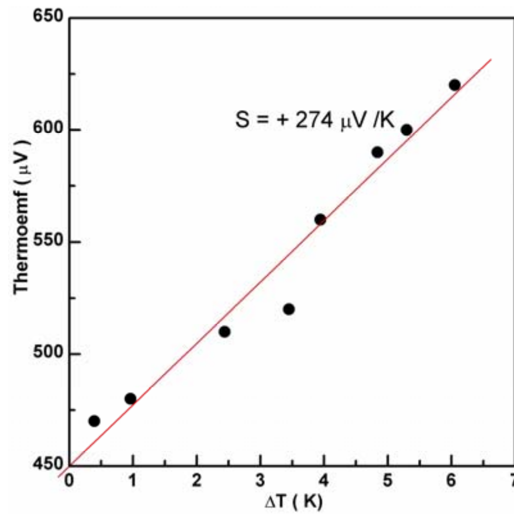

Figure 3.11. Thermopower of Ca doped $CuYO_2$ thin films annealed at 420°C under 1 atm oxygen pressure

3.4 Growth and characterization of $CuGaO_2$ and $CuGa_{1-x}Fe_x O_2$ thin films

3.4.1 Experimental

The $CuGaO_2$ thin films grown epitaxially on $\alpha-Al_2O_3$ (001) single crystal substrates showed enhanced conductivity of $6x10^{-2}$ Scm^{-1}, which was an improvement over the $2x10^{-3}$ Scm^{-1} obtained on a polycrystalline $CuGaO_2$ film [12] grown on a glass substrate. It has so far been impossible to improve the p-type conductivity of $CuGaO_2$ significantly by doping Mg or Ca on the Ga site. The p-type conductivity is presumed to be due to oxygen intercalation or Cu vacancies [11]. Reports in literature show oxygen intercalation or divalent ion doping on Ga site is not possible for $CuGaO_2$ thin films to improve the p-type conductivity. $CuFeO_2$ sintered powder and crystals have been reported as the materials having the highest p-type conductivity [37, 38] among the copper and silver delafossites. However the $CuFeO_2$ films are found to be less transparent in the visible region compared to $CuGaO_2$. The solid solution between the $CuGaO_2$ and $CuFeO_2$ could result in higher conductivity and transparency. In this chapter the synthesis and characterisation of p-type conducting $CuGaO_2$ in bulk and thin film forms are presented. Higher conductivity has been achieved by making solid solution with $CuFeO_2$.

The $CuGaO_2$ thin films and the $CuGa_{0.5}Fe_{0.5}O_2$ films were prepared by rf magnetron sputtering of the sintered targets. The polycrystalline $CuGa_{1-x}Fe_xO_2$ for x= (0 to 0.5) targets were prepared from an intimate mixture of 99.9% pure Cu_2O, Ga_2O_3 and Fe_2O_3. The mixture was pelletized and heated at 1100^0C for 24 hours in argon atmosphere. X-ray diffraction of this product shows that the solid

solution of $CuGa_{1-x}Fe_xO_2$ in delafossite structure can be formed for x=0 to 0.5 in the studied range.For the film preparation targets of $CuGaO_2$ and $CuGa_{0.5}Fe_{0.5}O_2$ were chosen. The background pressure was maintained at 100mTorr. The substrate used was amorphous silica heated to 100^0C. The substrate to target distance was kept at 3 cm and the sputtering gas used was a mixture of 80% argon and 20% oxygen. These films were then subjected to post deposition annealing in nitrogen at 800^0C for 90 minutes.Electrical conductivity measurements were made on films using four probe technique. The type of conductivity in the film was confirmed by Seebeck coefficient measurement. The composition of the film was estimated by the electron probe micro analysis (EPMA). The transmittance was measured using UV-Vis-NIR spectrometer in the wavelength range 190nm o 820 nm. Film thickness was measured by a surface stylus profiler. The surface roughness was estimated using atomic force microscope (AFM).

3.4.2 Results and Discussion

The possibility of mixing trivalent cations of Fe and Ga on the M site of the AMO_2 delafossite structure may allow compromise between the desirable properties of each of the $CuGaO_2$ and $CuFeO_2$ if a solid solution can be achieved. The ionic radius of octahedrally coordinated Ga^{3+} is 62pm and that of Fe^{3+} is 64.5pm (high spin) and 55pm (low spin) [39]. The solid solution of $CuGaO_2$ and $CuFeO_2$ might combine the excellent transparency of $CuGaO_2$ with higher conductivity of $CuFeO_2$. We have demonstrated that the solid solution of $CuGa_{1-x}Fe_xO_2$ is achievable in powders and thin films. The polycrystalline powder prepared by mixing the constituent oxides, Cu_2O, Ga_2O_3 and Fe_2O_3 was fired at 1100^0C for 24 hours in argon atmosphere.A solid solution of $CuGa_{1-}$

${}_{x}Fe_xO_2$ with delafossite structure was formed for x=0 to 1 and the composition was verified by EPMA. The x-ray diffraction patterns (fig.3.12) of these $CuGa_{1-x}Fe_xO_2$ show no impurity phase peaks. The chemical analysis of $CuGaO_2$ thin films by EPMA gave the atomic ratio Ga/Cu as 1.03. Higher Cu content or Ga content results in small impurity peaks of Cu_2O and Ga_2O_3 respectively. The EPMA analysis on $CuGa_{0.5}Fe_{0.5}O_2$ gave a Ga+Fe/Cu ratio as 1 in the sintered powder and 1.02 in the thin film. Figure 3.12 shows the x-ray diffraction patterns of $CuGaO_2$, $CuGa_{0.5}Fe_{0.5}O_2$ sintered ceramics. The $CuGa_{1-x}Fe_xO_2$ crystallises with the 3R delafossite structure (space group R3m). The unit cell volume and lattice parameter ***a*** increase with increase of Fe compositions, as shown in figure 3.13. This indicates that Fe^{3+} is in the high spin state, since the low spin state has a smaller radius than octahedrally coordinated Ga^{3+} and one would expect the ***a*** parameter to decrease with increase of Fe composition in this case. The lattice parameter c is nearly independent of x (fig. 3.14). This is reminiscent of the behaviour reported for $RCuO_2$ (R=rare earth) delafossite compounds [40], where large changes in the cation radius, from Eu^{3+} (0.947nm) to La^{3+} (1.022pm) result in considerable change in a- axis parameter, but comparatively little change in the c-axis lattice parameter. From the examination of the delafossite structure we might expect that changing the size of the M cation would have similar impact on both the ***a*** and ***c*** cell edges. It is, however, the edge sharing of the MO_6 octahedra in the ***ab*** plane which causes a change in size of M to impact primarily the ***a*** and *b* cell edges.

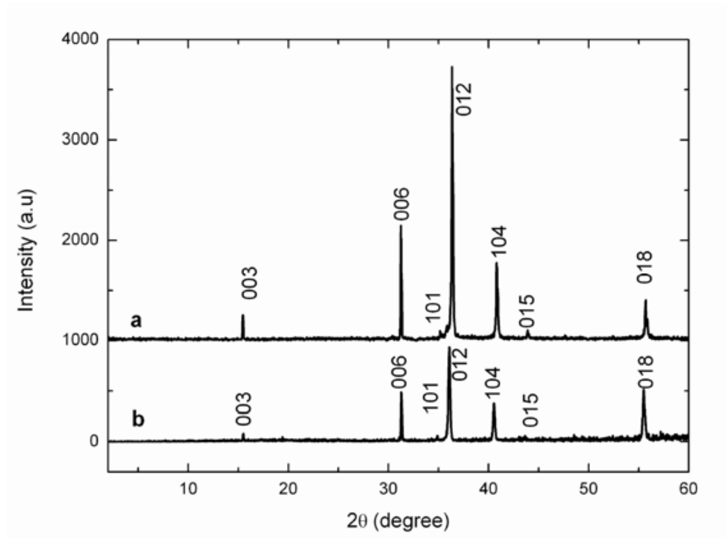

Figure 3.12 X-ray diffraction pattern of the sintered targets a) $CuGaO_2$ and b) $CuGa_{0.5}Fe_{0.5}O_2$.

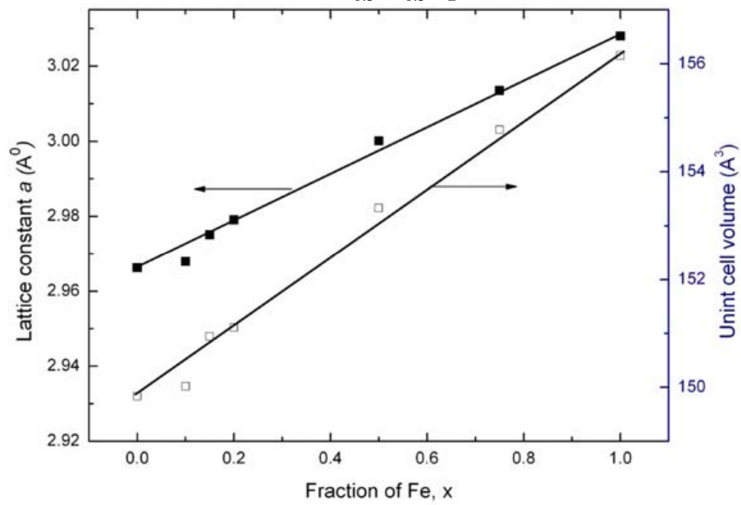

Figure 3.13 Variation of unit cell volume (open square) and the lattice constant ***a*** (solid square) of powder $CuGa_{1-x}Fe_xO_2$ solid solutions as function of Fe content x.

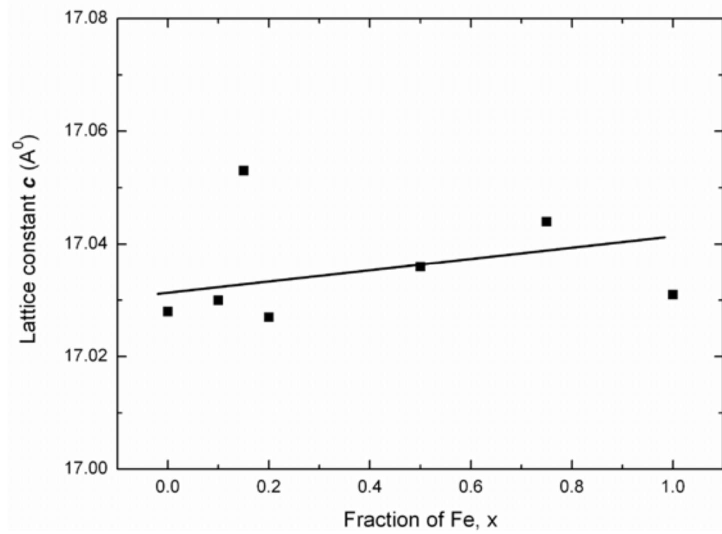

Figure 3.14 Variation of the lattice constant ***c*** of powder $CuGa_{1-x}Fe_xO_2$ solid solutions as function of Fe content x.

The strong repulsion of M^{3+} cations across the shared edges distorts the octahedra bringing the oxygen atoms on the shared edge to what can be regarded as a contact distance. As the M cation becomes larger, the M-O distance increases but the O-O contact distance of shared edge increases only slightly and therefore there is little impact on the ***c*** cell edge. This effect has been noted and modeled in other structures such as cordierite and b-eucryptite [41].

Figure 3.15 shows the x-ray diffraction patterns of the post annealed $CuGaO_2$ and $CuGa_{0.5}Fe_{0.5}O_2$thin films. All the diffraction peaks observed in the sintered ceramics as well as thin films could be indexed by assuming delafossite structure. As deposited thin films were amorphous as indicated by the XRD. A post deposition annealing was necessary to induce crystallinity in the film. The

optimum annealing condition was 800^0C for 90 minutes under nitrogen atmosphere.

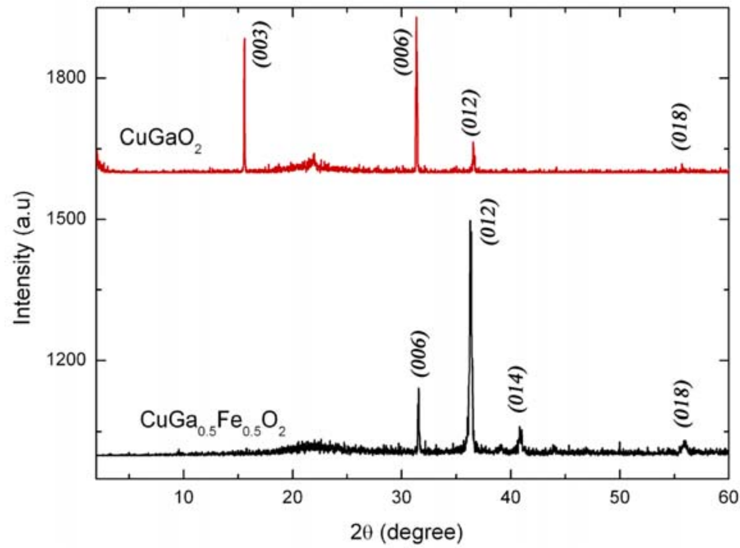

Figure 3.15 X-ray diffraction patterns of $CuGaO_2$ and $CuGa_{0.5}Fe_{0.5}O_2$ thin films grown by rf magnetron sputtering.

The optical transmission spectra of post annealed and sputtered $CuGaO_2$ and $CuGa_{0.5}Fe_{0.5}O_2$ are shown in figure 3.16. The fundamental absorption in $CuGaO_2$ thin films starts at about 310nm. The band gap was estimated by plotting $(\alpha h\nu)^2$ vs $h\nu$ and extrapolating the linear portion near the onset of the absorption edge to the energy axis (fig.3.17). This gives a direct band gap of 3.66 eV for the $CuGaO_2$ thin films which is in good agreement with the values reported in literature. The absorption edge in $CuGa_{0.5}Fe_{0.5}O_2$ films is at longer wavelength compared to the $CuGaO_2$ thin films. The direct band gap for $CuGa_{0.5}Fe_{0.5}O_2$ was estimated as 3.3 eV. This is close to the band gap values reported for $CuGaO_2$ (3.6eV) and $CuFeO_2$ (3.3eV) [37,42].

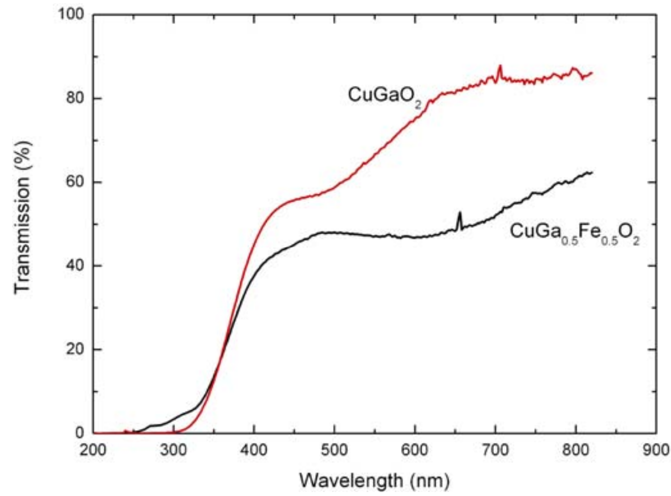

Figure.3.16 Transmission spectra of $CuGaO_2$ (150nm) and $CuGa_{0.5}Fe_{0.5}O_2$ (120nm) thin films

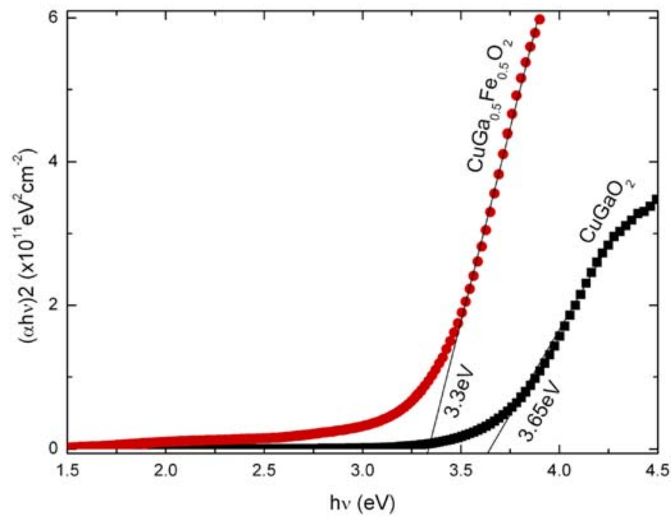

Figure 3.17 The plot of $(\alpha h\nu)^2$ vs energy hν for $CuGaO_2$ and $CuGa_{0.5}Fe_{0.5}O_2$ thin films.

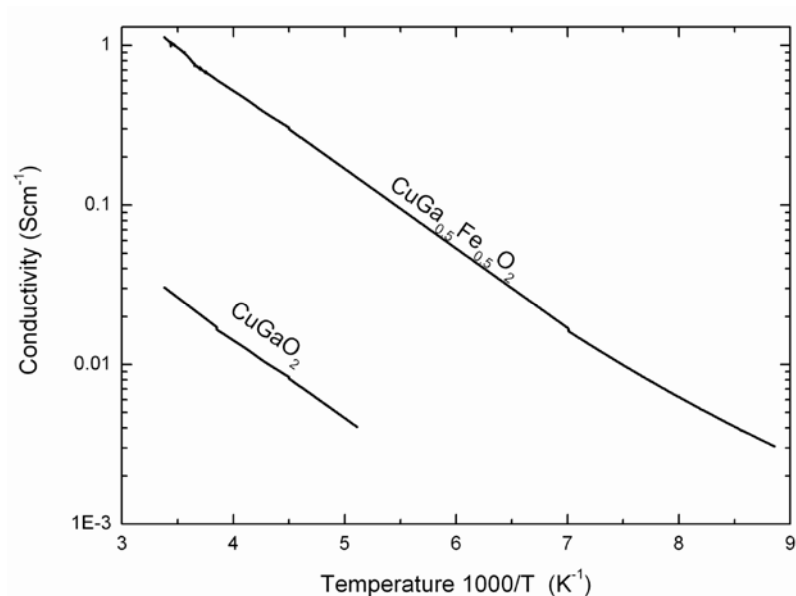

Figure.3.18 Temperature dependence of electrical conductivity of $CuGaO_2$ and $CuGa_{0.5}Fe_{0.5}O_2$ thin films.

The temperature dependence of dc electrical conductivity is depicted in figure 3.18. The thermally activated behaviour is typical of $CuMO_2$ p-type delafossite oxides. The activation energies extracted from the slope of the logσ vs 1000/T plots at high temperature are 0.25eV for $CuGaO_2$ film and 0.27eV $CuGa_{0.5}Fe_{0.5}O_2$ film respectively. The conductivity at room temperature is about $2x10^{-2}$ Scm^{-1} after the post deposition annealing of $CuGaO_2$ films. The sputtered $CuGa_{0.5}Fe_{0.5}O_2$films after annealing at 800^0C in nitrogen show a room temperature conductivity of $1Scm^{-1}$.

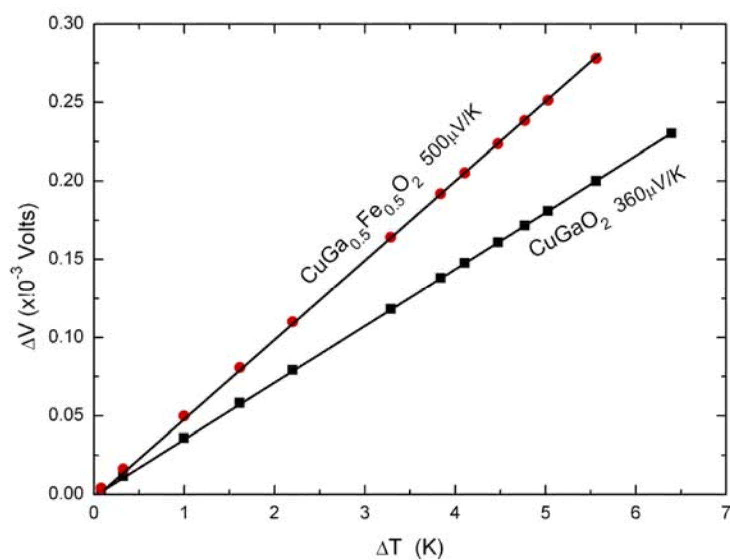

Figure 3.19. The plot of thermo emf verses ΔT for the $CuGaO_2$ and $CuGa_{0.5}Fe_{0.5}O_2$ thin films.

The Seebeck coefficient at room temperature was found to be +360μV/K for the $CuGaO_2$ thin films, where as the $CuGa_{0.5}Fe_{0.5}O_2$ films show a Seebeck coefficient of +500μV/K(fig 3.19). The positive sign indicates that both $CuGaO_2$ and $CuGa_{0.5}Fe_{0.5}O_2$ films are p-type conductors. Hall measurement in a vander Pauw configuration did not yield carrier type at room temperature.

3.5 Conclusion

P-type transparent conducting $CuMO_2$ (M=Al, Ga, Y and Fe) thin films were prepared by rf magnetron sputtering. The bulk powders of these compounds were synthesised in the laboratory by high temperature solid state reaction technique. The conductivity in the copper delafossite $CuYO_2$ could be enhanced by doping with divalent ions on the trivalent M site or by oxygen

intercalation. Oxygen intercalation was very difficult in the case of delafossite compounds with smaller M^{3+} ions such as $CuAlO_2$ and $CuGaO_2$ compounds of the present study. In the case of $CuYO_2$ it was possible to enhance the conductivity either by Ca^{2+} doping on the sites of Y^{3+} sites or by oxygen intercalation owing to the larger size of the Y^{3+} ions. The mixing of trivalent cations of Fe and Ga on the M site of the AMO_2 delafossite structure was found to allow compromise between the desirable properties of each of the $CuGaO_2$ and $CuFeO_2$. The solid solutions between $CuGaO_2$ and $CuFeO_2$ could be achieved. The conductivity of the $CuGaO_2$ could be improved by using solid solutions of $CuGaO_2$ and $CuFeO_2$. However the transparency of the films was found to decrease. The sputtered $CuGa_{0.5}Fe_{0.5}O_2$ films show a room temperature conductivity of $1Scm^{-1}$ while the transmission is about 50% in the visible region. All the copper delafossite films grown by sputtering which are transparent in the visible region, have moderate conductivity. These films exhibit p-type conduction as confirmed by thermopower measurements. These films can be used as transparent semiconducting films for the fabrication of devices like pn heterojunctions.

Reference:

1. K.L Chopra, S. Major, and D. K. Pandya, *Thin solid films* **102**(1983) 1
2. T. Yamamoto and H. K Yoshida , *Jpn.J.Appl.Phys* **38**(1999) L166.
3. D. C. look, D. C. Reynolds, C. W. Litton, R. C. Jones, D. B. Eason and G. Cantwell, *Appl Phys Lett*. **81**(2002) 1830.
4. M. Joseph, H. Tabata, H. Sacki, K. Ueda and T. Kawai , *Physica B* **302-303** (2001) 140.
5. K. Minegishi, Y. Koui and K. Kikuchi, *Jpn J Appl Phys* **36**(1997) L1453.
6. X. L. Gao, H. Tabata and T. Kawa, *J Cryst Growth* **223**(2001) 135.
7. Y. R. Ryu, S. Zhu, D. C. Look, J. W. Wrobel, H. W. Joeng and H. W. White, *J.Cryst Growth* **216**(2001) 330
8. Y. Ryu, T. S. Lee and H. W. White, *Appl Phys Lett*. **83**(2003) 87.
9. K. K. Kim, H. S. Kim,D. K. Hawang, J. H. Lim and S. J. Park, *Appl Phys Lett*. **63**(2003) 63.
10. H. Sato, T. Minami, S. Takata and T. Yamada, *Thin Solid films* **236**(1993) 27.
11. H. Kawazoe, M. Yasukawa, H. Hyodo, M. Kurita, H. Yanagi and H. Hosono, *Nature* **389**(1997) 939.
12. G. Thomas, *Nature* **389**(1997) 907.
13. Banerjee A.N, Chattopadhyay and K. K, Prog. *Cryst. Growth Charact. Mater*. **50**(2005) 52.
14. M.K.Jayaraj, A. D. Draeseke, J.Tate and A.W.Sleight, *Thin solid films* **397**(2001) 244
15. R. L. Hoffman, J. F. Wager, M. K. Jayaraj and J.Tate , *J.Appl Phys* **90** (2001) 5763

16. N. Duan, A. W. Sleight, M. K.Jayaraj and J.Tate, *Appl Phys Lett* **77**(2000) 1325.
17. R. Nagarajan, A. D. Draeseke, A. W. Sleight and J.Tate, *J.Appl.Phys* **89** (2001) 8022.
18. H. Kawazoe, H. Yanagi, K. Uede and H. Hosono, *MRS Bull* **25**(2000)28.
19. J. Tate, M. K. Jayaraj, A. D. Dareseke, T. Ulbrich, A. W. Sleight, K. A. Vanaja, R. Nagarajan and J. F. Wager, *Thin Solid Films* **411**(2002) 119.
20. H. Yanagi, K. Ueda, H. Ohata, M. Orita, H. Hirano and H. Hosono, *Solid State communication* **121**(2001) 15.
21. Brian.J, I, Gabriela B. G, Thomas O. M, Dean Y. S. Antoine B, Donggeun K and Kenneth R.P, *Chem. Mater.* **16**(2004) 5616
22. R. D. Shannon, D. B. Rogers and C.T. Prewitt, *Inorg Chem* **10**(1971) 713.
23. R. J. Cava, H. W. Zandbergen, A. P. Ramierz, H. Takagi, C. T. Chen, J. J. Krajewski, W. F. Peck.jr, J. V. Waszczak, G. Meigs, R. S. Roth and L. F. Schneemeyer, *J. Solid state chem*. **104**(1993)437.
24. R. J. Cava, W. F. Peck.jr, J. J. Krajewski, S. W. Chenog and H. Y. Hwang, *J.Mater Res* **9**(1994)314.
25. H. Yanagi, S. Park, A. D. Draeseke, D. A. Keszler and J.Tate, *J. Solid state chem* **175**(2003)34.
26. R.Nagarajan , N. Duan , M.K Jayaraj, J.Li ,K.AVanaja ,A. Yokochi, A.D. Draeseke , J.Tate and A.W Sleight *.Int. J. Inorg. Mater.***3**(2001)265
27. T.Ishiguro, A.Kitazawa, N.Miztani and M.Kato, *J.Sold State Chem*. **40** (1981)170

28. J.Bardeen, F.J.Blatt and L.H. Hall, in: Proceedings of Photoconductivity Conf. (1954, Atlantic City), (Eds) R.Breckenridze, B.Russel and T.Hahn, J.Wiley and Chapman and Hall, New York, (1956)
29. F.A.Banko and F.P.Koffyberg *J Phys,Chem.Solids* **45**(1984)57
30. O.Porat and I.Riess, *Solid State Ionics* **81**(1995) 29
31. JCPDS 37-930 and JCPDS 39-0224.
32. P. Y. Yu, M. Cardona Fundamentals of semiconductors: Physics and material properties, Springer, Berlin 1996.
33. B. E. Sernelius, K. F. Berggren, Z. C. Jin, I. Hamberg, and C. G. Granqvist, *Phys. Rev. B* **37**(1988)10244.
34. K. F. Berggern and B. E. Sernelius, *Physical Review B* **24**(1981)1971.
35. N. F. Mott Metal-insulator transitions, Taylor and Francis, London, 1974.
36. A. Jacob, C.Parent, P. Boutinaud, G.L. Flem, J. P. Doumerc, A. Ammar, M.Elazhari and M. Elaatmani , *Solid State Communications* **103**(1997)529.
37. K.Ueda, T.Hase, H.Yanagi, H.Kawazoe and H.Hosono, H.Ohata, M.Orita, and M.Hirano, *J.Appl.Phys* **89**(2001)1790.
38. D.B.Rogers, R.D.Shannon, C.T.Prewitt and J.L.Gillson, *Inprganic Chemistry* **10**(1971)723.
39. R.D.Shannon *Acta Cryst.A* **32**(1976)751.
40. K.Isawa, Y.Yaegashi, M.Komastu, M.Nagno,S.Sudo, M.Karppinen, H.Yamauchi, *Phys.Rev.B* **56**(1997)3457.
41. N.Khosrovani and A.W.Sleight , *J.Inorg.Mater*. **1**(1999)3.
42. F.A.Banko, F.P.Koffyberg, *J.Phys.Chem.Solids* **48** (1987)431.

Chapter 4

Synthesis of $AgCoO_2$ and fabrication of p-$AgCoO_2$/n-ZnO heterojunction

Abstract

$AgCoO_2$ thin films with 50% transparency in the visible region were deposited on single crystalline Al_2O_3 and amorphous silica substrates by RF magnetron sputtering. P-type conductivity of $AgCoO_2$ was demonstrated by fabricating transparent p-n junction diode with $AgCoO_2$ film as p-side and ZnO: Al film as n-side using sputtering. Junction thus obtained was found to be rectifying with a forward to reverse current of about 10 at an applied voltage of 3 V. Thus the present study shows that silver delafossite thin films with p-type conductivity can be used for the fabrication of active devices for transparent electronics applications

4.1 Introduction

Transparent Semiconducting Oxides (TSO) have attracted attention for their application to optoelectronic devices especially for blue and UV emitters. Optically transparent oxides with large band gap are intrinsically insulators. Most of the transparent conducting oxides which are being commercially used are n-type. Wide band gap oxides like In_2O_3: Sn (ITO), ZnO, SnO_2 etc. have widely been investigated for the past four decades. The use of TSOs in the fabrication of optoelectronic devices was not materialized due to lack of TSO that exhibit p type conductivity. In 1997, Kawazoe *et al*. reported p-type conducting transparent $CuAlO_2$ films [1]. This was followed by a number of reports of improved p type conductivity in a number of related delafossite materials such as $CuMO_2$ (M=Al, Ga, In, Y, Sc) [2-6]. All oxide transparent p-n junction and ultra violet emitting diodes [7] were successfully fabricated using ZnO and $SrCuO_2$. Rectifying behavior in other oxide based structures has also been reported including p-NiO/i-NiO/i-ZnO/n-ZnO [8], n-ZnO/ p-ZnO [9] and p-$CuYO_2$/i-ZnO/n-ZnO [10]. $CuInO_2$ is the only delafossite structure known to exhibit bipolar conductivity and hence was able to fabricate homojunction $CuInO_2$: Sn/$CuInO_2$: Mg [11]. Doping particularly p type is rather difficult,to be effected in wide band gap semiconductors. [12]. Despite the widespread interest in delafossite materials, silver delafossite films are not extensively investigated. The $AgInO_2$: Sn has been reported to show n-type conductivity and p-type doping was unsuccessful [13]. $AgGaO_2$ thin films grown by PLD has been found to show p-type conductivity [14].

In this work, $AgCoO_2$ has been synthesized and studied in powder and thin film form. The electrical and optical properties of the thin film and rectifying nature of $AgCoO_2$ based p-n junction are reported.

4.2 Experimental

The $AgCoO_2$ delafossite compound was prepared by cation exchange reaction of $NaCoO_2$, which has α-$NaFeO_2$ type structure with silver nitrate. For this initially $NaCoO_2$ has to be prepared by solid state reaction between Co_3O_4 and Na_2O under oxygen flow at 600-700^{0}C for 12h. In the present study a much more simpler technique has been used for the synthesis of $AgCoO_2$ compound. It has been .reported that Ag_xCoO_2 (x<1) has enhanced conductivity due to 3d type holes mixed with O 2p–ligand holes [15, 16]. $AgCoO_2$ powder was prepared by hydrothermal reaction in a Parr bomb at 250^{0}C for 48h.The reagents used were $AgNO_3$, Co_3O_4 and KOH. A 2 inch diameter sputtering target was prepared by pelletizing and heating the powder at 350°C for 5 hours in air. The $AgCoO_2$ films were sputtered in on axis geometry in 80:20; Ar: O_2 mixture at 40 mtorr. The rf power used for sputtering was 100 watts. The substrates were single crystal Al_2O_3 or amorphous silica placed at 4 cm from target and heated to 400^{0}C. The thickness of the films were measured using a stylus profiler (Deltak 6M). The structural properties were studied by x-ray diffraction using Rigaku D-max x-ray diffractometer with Cu K_α line. The high resolution transmission electron micrographs (HRTEM) and selective area electron diffraction (SAED) patterns were recorded using model JEM-2010 UHR of JEOL at an operating voltage of 200 keV. The composition of the films was analysed using the electron probe micro analysis (EPMA). The electrical conductivity was measured in the van der Pauw configuration using the Hall measurement set up. The thermo power measurements were carried out using a home made automated setup

[17]. Transparent p-n heterojunctions fabricated have the structure glass/ITO/n-ZnO/p-$AgCoO_2$. The current density-voltage (J-V) characteristics were evaluated by applying DC voltage to the diode using a Keithley source measure unit (SMU 236). Indium metal was used as the ohmic contact. The glass substrate was coated with sputtered [18] 200 nm thick ITO at a substrate temperature of 150^0C. ZnO: Al was deposited on the ITO coated glass substrate by RF magnetron sputtering at substrate temperature of 150^0C in argon pressure of 10 mtorr [19]. p-n junction was completed by depositing $AgCoO_2$ on glass/ITO/ZnO: Al structure.

4.3 Synthesis and characterisation of $AgCoO_2$ bulk powder and thin films

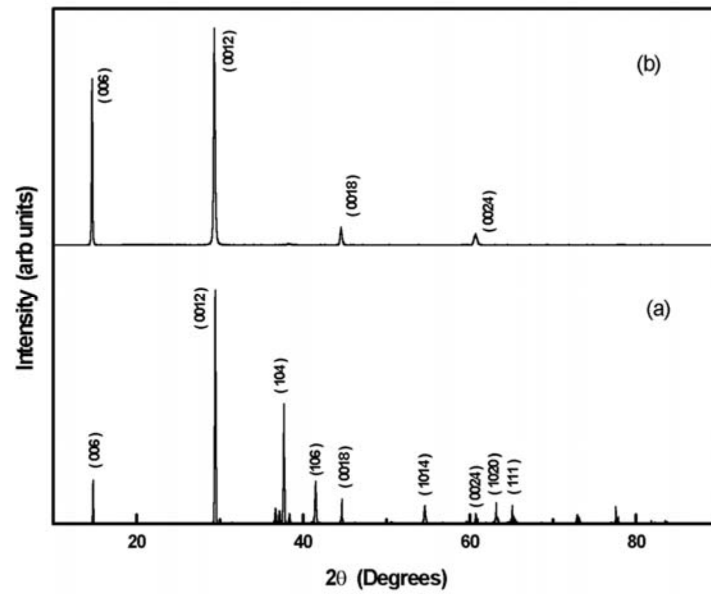

Figure 4.1 X-ray diffraction patterns of (a) $AgCoO_2$ powder and (b).$AgCoO_2$ thin film

X–ray diffraction pattern of the hydrothermally synthesized $AgCoO_2$ powder is shown in figure 4 (a). All The peaks can be indexed by assuming a 6H polytype delafossite structure [20]. However an actual 6H delafossite structure has not been proposed and the observed diffraction pattern can be accounted for a mixture of 2H and 3R forms, a situation commonly observed in delafossite compounds. From EPMA, Ag: Co ratio is obtained as 1.2:1. The $AgCoO_2$ film grown on Al_2O_3 substrate as well as on glass substrate were c–axis oriented, as only the (00l) diffraction peaks were visible (shown in figure 4.1). All diffraction peaks were identified as that of $AgCoO_2$.

The high resolution transmission electron micrograph (HRTEM) of hydrothermally grown $AgCoO_2$ powder is shown in figure 4.2 (a). The lattice spacing amounts to 3.05 A^o, corresponding to (006) planes of the delafossite structure of $AgCoO_2$. The other atomic planes with smaller spacing were not observed. The HRTEM image of the sputtered $AgCoO_2$ thin film grown on carbon coated copper grids at 400^0C under the same growth conditions used for the c-axis oriented films on amorphous silica substrates is shown in figure 4.2 (c). The atomic scale image shows parallel lines of ions at intervals of 2.45 A^o corresponding to (101) planes for most of the grains. The selective area electron diffraction pattern (SAED) of the hydrothermally grown $AgCoO_2$ powder is shown in the figure 4.2 (b). The lattice spacing corresponding to the diffraction pattern was determined with camera constant of the equipment and measuring the radii from the electron diffraction pattern [21]. Diffraction spots corresponding to (110) and (0012) planes of delafossite structure of $AgCoO_2$ were observed. SAED of sputtered $AgCoO_2$ film shows the diffraction spots representing the (012) and (0012) planes (shown in figure 4.2 (d)). The nature of the substrate influences the growth and crystal

structure of the film. The orientation of the films grown on silica and carbon coated grids may be different. However the same deposition conditions as that of $AgCoO_2$ grown on silica leads to the crystalline $AgCoO_2$ films with out any impurity phase. The trials to grow crystalline $AgCoO_2$ films by pulsed laser deposition (PLD) were unsuccessful [22]. The PLD resulted in the amorphous films even in the single crystalline substrate.

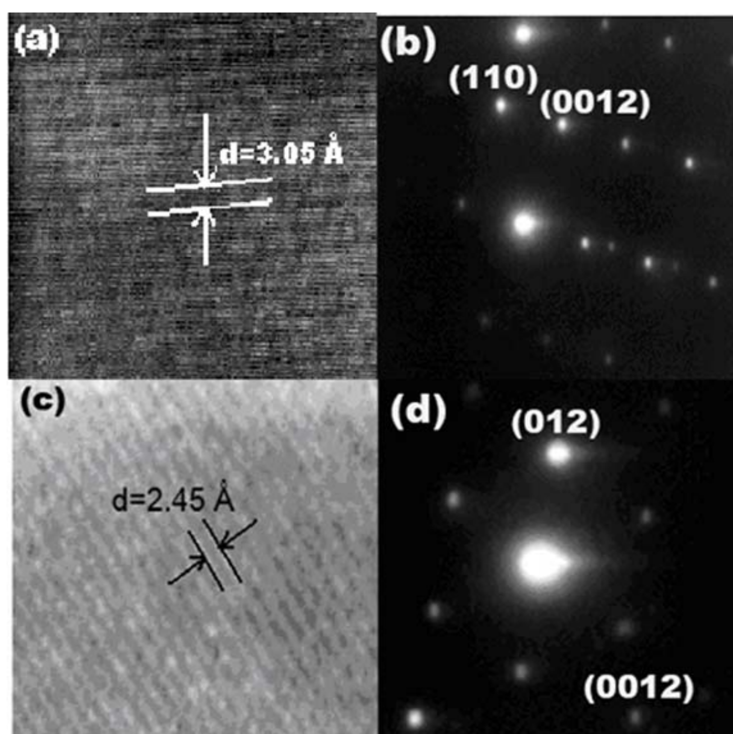

Figure 4.2 (a) HRTEM and (b) SAED of hydrothermaly grown $AgCoO_2$ powder, (c) HRTEM and (d) SAED of $AgCoO_2$ thin film grown on carbon coated copper grid.

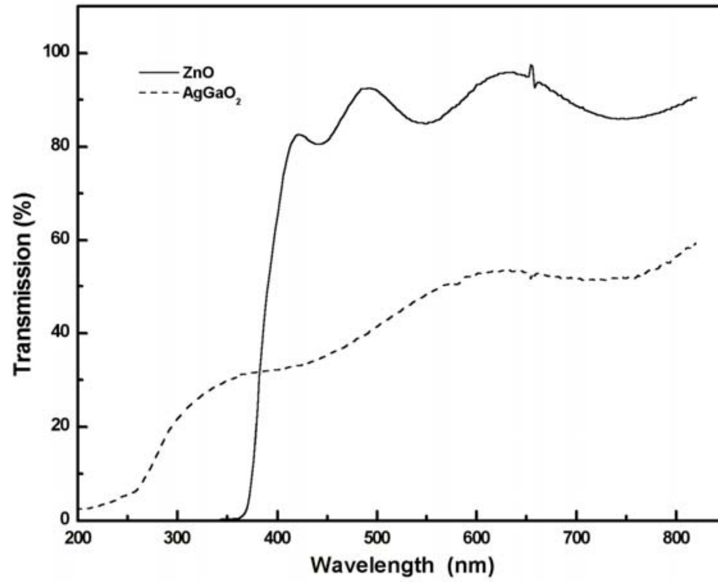

Figure 4.3 Transmission spectra of $AgCoO_2$ and ZnO thin films.

A 150 nm $AgCoO_2$ film shows 40-60% transparency in the visible region while ZnO film gives a transmission of 85% (Figure 4.3). The band gap of $AgCoO_2$ films was obtained by plotting the absorption coefficient α as a function of frequency. Extrapolating the straight line portion of $(\alpha h\nu)^2$ vs. $h\nu$ plot to the energy axis yields the band gap (E_g) and the exponent gives the information about the nature of optical band gap [23]. Band gap of $AgCoO_2$ film was estimated to be 4.15 eV (shown in figure 4.4).

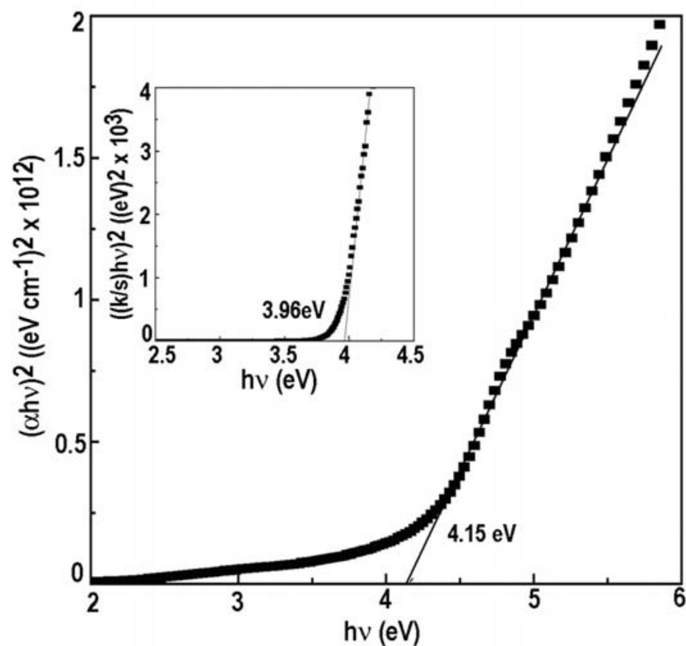

Figure 4.4 $(\alpha h\nu)^2$ vs. hν plot of $AgCoO_2$ thin film and inset shows the $((k/s)h\nu)^2$ vs. hν plot of $AgCoO_2$ powder.

The band gap of $AgCoO_2$ powder sample was estimated by recording the diffuse reflectance spectrum of the samples in the visible region using MgO as the reference. The band gap was found to be ~ 3.96 eV estimated from the plot of $\{(k/s)/h\nu\}^2$ vs. hν (inset of figure 4.4), where k and s denotes the absorption and scattering coefficients and hν the photon energy. The ratio of k/s was calculated from the reflectance spectra via Kubelka–Munk equations [24, 25].

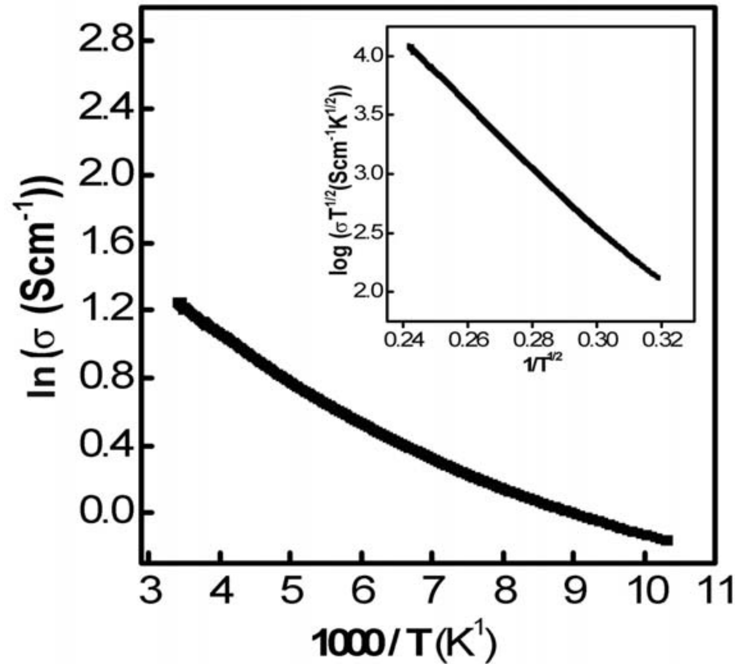

Figure 4. 5 Conductivity log (σ) vs. 1/T and inset shows log (σ $T^{1/2}$) vs. $1/T^{1/4}$ of the $AgCoO_2$ thin film.

The temperature dependence of resistivity shows a semiconducting behavior. The activation energy extracted from the slope of ln (σ) vs. 1000/T plot is 70 meV at high temperature. The room temperature conductivity is 0.2 Scm^{-1}. The ln (σ) vs. 1000/T plot is not well fit by a single line (shown in figure 5.5). However the log ($\sigma T^{1/2}$) vs. $1/T^{1/4}$ plot (inset of figure 4. 5) is close to a straight line suggesting a variable range hopping [26] is dominant in positive hole conduction at the top of valance band which is observed in similar delafossite materials [4, 5]. The Ag^+ ions contributing to the conductivity in thin film of $AgCoO_2$ has been estimated by measuring the transference number using the dc polarization method [27]. The

evaporated gold (1.5 μm) forms the blocking electrode and the variation of conductivity of the Au/$AgCoO_2$/Au structure has been noted under a steady dc potential of 500 mV over a time of thirty minutes (figure 4.6).

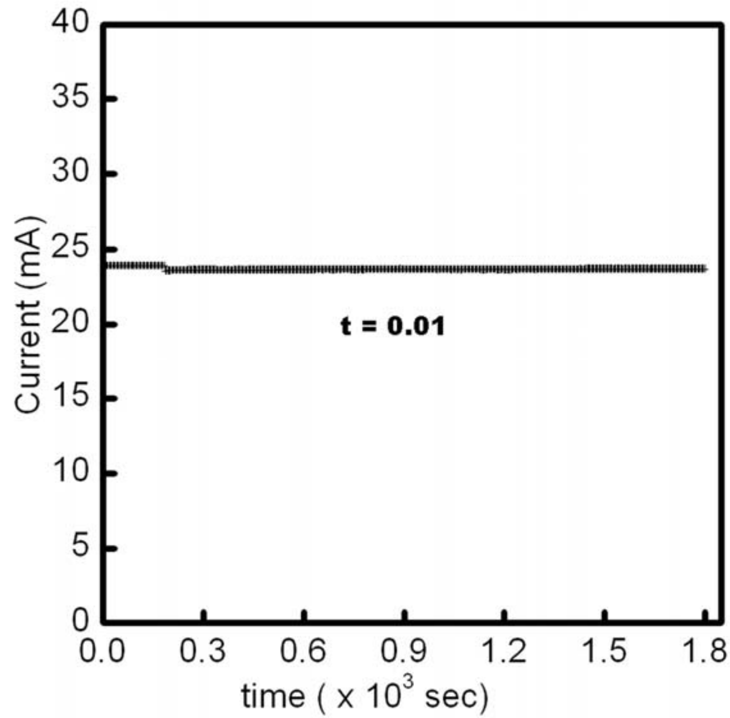

Figure 4.6 Variation of current with time for determining transference number.

The transference number 't' is defined as $t = \frac{\sigma_0 - \sigma_\infty}{\sigma_0}$ (σ_0 is the conductivity at t = 0 and σ_∞ is the saturated conductivity). The variation in conductivity is very small and the estimated transference number is 0.01 indicating the ionic contribution to conductivity is negligible. The thermoelectric power measurement was carried out at room temperature. Figure 4.7 shows the result of

Seeback measurement (S = +220 μV/K) which establishes the p-type nature of the carriers.

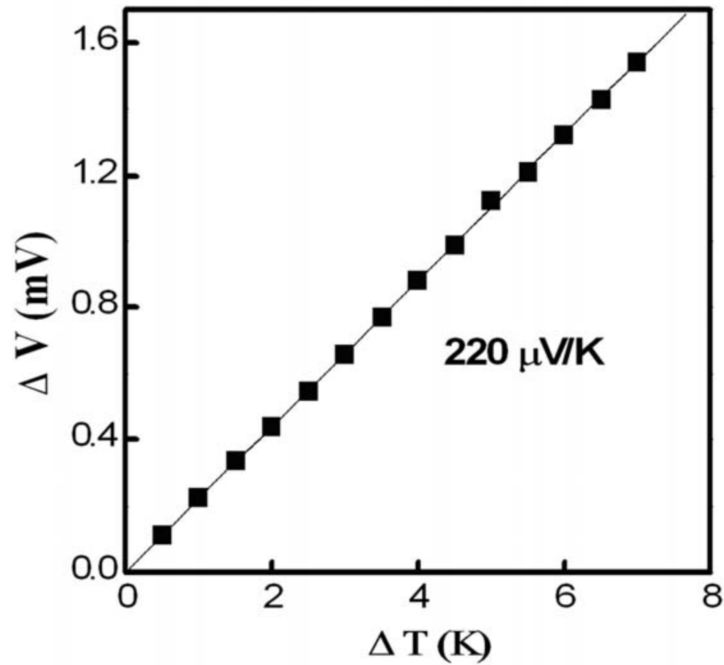

Figure 4.7 The plot of thermo emf (ΔV) vs. temperature (ΔT).

4.4 Fabrication of the all transparent pn junction

Transparent p-n heterojunction fabricated has the structure glass/ITO/n-ZnO/p-$AgCoO_2$. All the layers were grown by rf magnetron sputtering on amorphous glass substrates. The growth of individual layer is described below. The glass substrates were subjected to through cleaning.

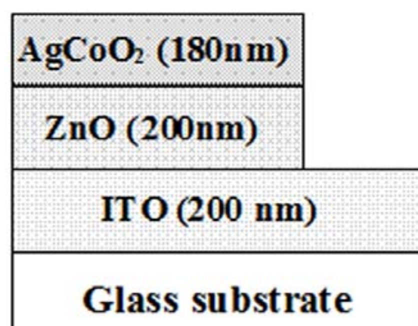

Figure 4.8 The schematic of the transparent n-ZnO/p-$AgCoO_2$ pn heterojunction

4.4.1 Deposition of transparent conducting ITO thin films

Indium tin oxide thin films were deposited by RF magnetron sputtering of ITO target containing 95wt% of In_2O_3 and 5wt% of SnO_2. The target used for sputtering was prepared from In_2O_3 (99.99% pure) and SnO_2 (99.999% pure) powders. The powders were mixed in a mechanical shaker for one hour pressed into a pellet of two-inch diameter and then sintered at 1300^0C for 6 hours in air. Figure 5.9 shows the XRD pattern of the ITO film and ITO target.

The sputtering was carried out in a vacuum chamber in which high vacuum (< $2x10^{-5}$mbar) was created by means of an oil diffusion pump backed by a rotary pump. RF power was delivered to the target material by an rf generator (13.56 MHz) through an impedance matching network. Glass slides of dimension 2.5 cm x 1 cm were used as the substrates. The substrates were kept above the target at a distance of 4cm, which was found to be the optimum condition for the growth of good quality crystalline films [28].

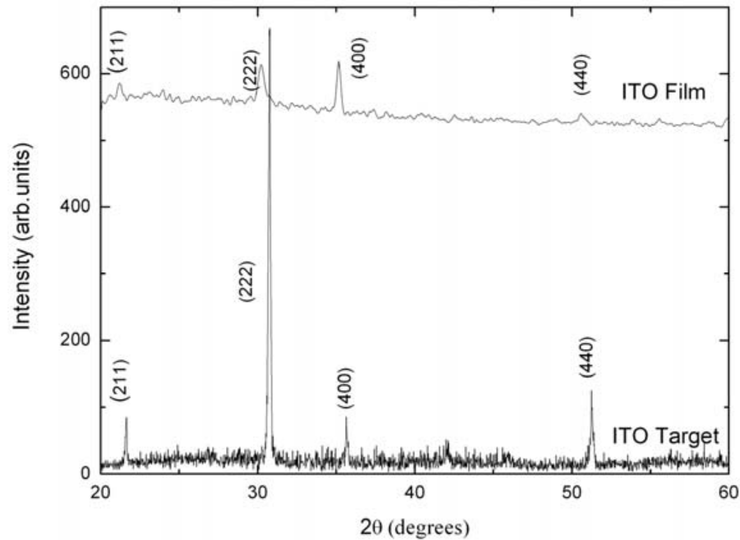

Figure 4. 9. XRD pattern of In_2O_3 powder and ITO target

The influence of substrate temperature, rf power, and annealing temperature on the properties of ITO thin films were analyzed in a previous study in our laboratory [18, 28, 29].The low resistivity was obtained at a substrate temperature of 150^0C. Hence in the present study the substrate temperature for the ITO deposition was chosen as 150^0C and the RF power used was 30W. The argon pressure was adjusted by a mass flow controller and the argon pressure was kept at 0.01 mbar. The target was pre-sputtered for 10 minutes before each deposition in order to remove any contaminants and to eliminate any differential sputtering effects. The sputtering time was adjusted such that all the resulting films used in this study were of thickness 200nm.

The XRD pattern of the ITO films deposited at a target to substrate spacing (T-S spacing) of 4cm is shown in fig 4.9. From the XRD pattern it can be seen that the films deposited at a substrate temperature of 150^0C are

polycrystalline. Films are polycrystalline even though the crystallization temperature of ITO is 150^0C [30]. Peak at $2\theta=30^0$ in the XRD spectra correspond to (222) plane and at $2\theta = 51^0$ corresponds to (440) plane of In_2O_3 [31].

Table 4.1 Properties of ITO thin films as a function of substrate temperature.

Substrate temperature (^{0}C)	Grain size (nm)	Band gap (eV)	Resistivity (Ωcm)	Mobility ($cm^2V^{-1}s^{-1}$)	Carrier density ($x10^{19}$ cm^{-3})
RT	16.8	3.68	.0201	8.46	3.67
100	25.68	3.7	.0065	12.4	7.82
150	26.08	3.8	.0021	17.8	17.1
200	25.2	3.84	.0038	17.6	9.39
250	30.0	3.85	.0064	6.39	17.3

The band gap of the ITO films was calculated from the transmission spectra. By assuming a parabolic band structure for the material, the absorption coefficient and band gap can be related by the expression $\alpha h\nu = A(h\nu\text{-}E_g)^{1/N}$ where E_g is the band gap energy and α is the absorption coefficient corresponding to frequency ν[32]. The absorption coefficient α was determined from the relation, $I = I_0 \exp(-\alpha t)$ where t is the thickness of the sample, I is the transmitted intensity at a particular wavelength and I_0 is the maximum transmitted intensity which is taken to be 100%. This relation gives $\alpha = (1/t)\ln(I_0/I)$. The constant N depends on the nature of electronic transition. In the case of ITO films N is equal to 2, for direct allowed transition [33]. The band gap of ITO films were determined from the plot of $(\alpha h\nu)^2$ vs. $h\nu$ by extrapolating the

linear portion of the curve to the energy axis where αhν is equal to zero. The band gap of ITO films is found to be 3.82 eV, grain size 26 nm resistivity $2.x10^{-3}$ ohm – cm, mobility 17.8 cm^2Vs^{-1}, and carrier concentration $17.1x10^{19}$ cm^3.

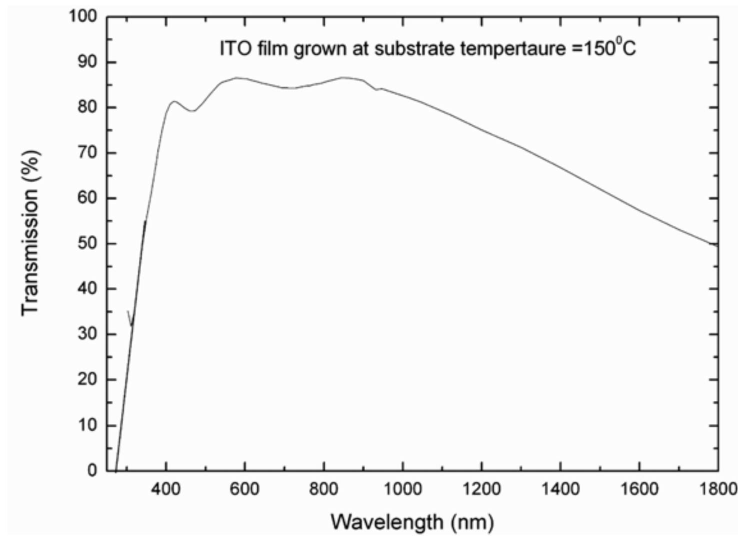

Figure 4.10. The transmission spectra of typical ITO film of thickness 200nm.

4.4.2 Deposition of n-ZnO thin films by sputtering

The sputtering targets were prepared from ZnO powder of 99.99 + % purity . The powder was pressed to form a 2 inch diameter target. The target was sintered at 900°C for ten hours in air. Before depositing the films, the ZnO target surfaces were cleaned by presputtering under the film deposition conditions for 30 minutes.

The sputtering was carried out in high purity Ar gas at substrate temperature of 150°C. The substrate was kept at 3cm above the target. For the growth of transparent and conducting metal oxide thin films it is essential that

non stochiometric metal rich oxide films be deposited [34]. The resistivity was found to increase drastically when oxygen was introduced to the sputtering gas. Fused quartz was used as the substrate.

The x-ray diffraction patterns of ZnO films and targets are shown in figure 4.11. The x-ray diffraction shows only 002 peak indicating that the film is polycrystalline and c axis of the grains becomes uniformly perpendicular to the substrate surface. The surface energy density of the 002 orientation is the lowest in ZnO crystal [34]. Grains with lower surface energy will become larger as the film grows. Then the growth orientation develops into one crystallographic direction of the lowest surface energy. This means that 002 texture of the film may easily form.

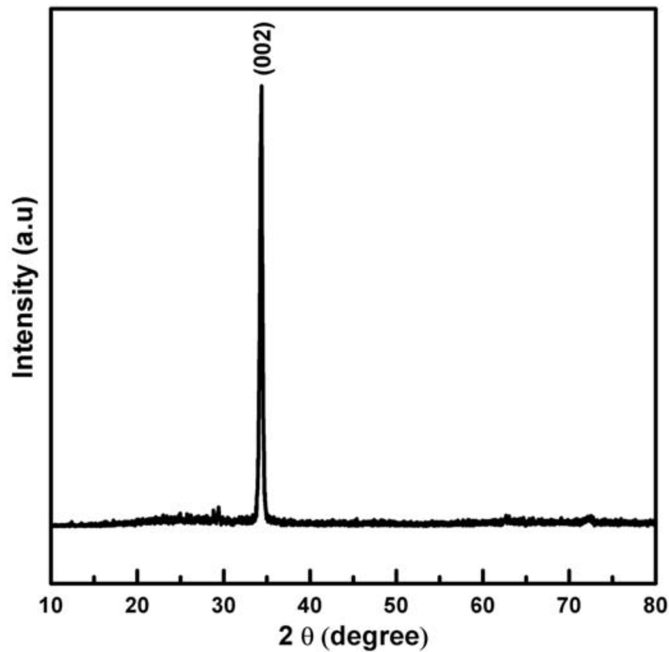

Figure 4.11. XRD pattern of ZnO thin films deposited by rf magnetron sputtering.

ZnO films are highly transparent and shows >85% transmission in the visible region. Figure 4.12 shows the transmission of undoped ZnO thin films. All the films exhibit a transmission >85% in the visible region. The band gap of ZnO films estimated from the plot of $(\alpha h\nu)^2$ verses hν is 3.28 eV.The ZnO films grown on glass substrates are highly transparent and conductive. The Hall mobility was measured to be $\mu = 6\ cm^2\ V^{-1}\ S^{-1}$; conductivity, $\sigma = 50\ Scm^{-1}$ and carrier concentration is $n = 5 \times 10^{19}\ cm^{-3}$

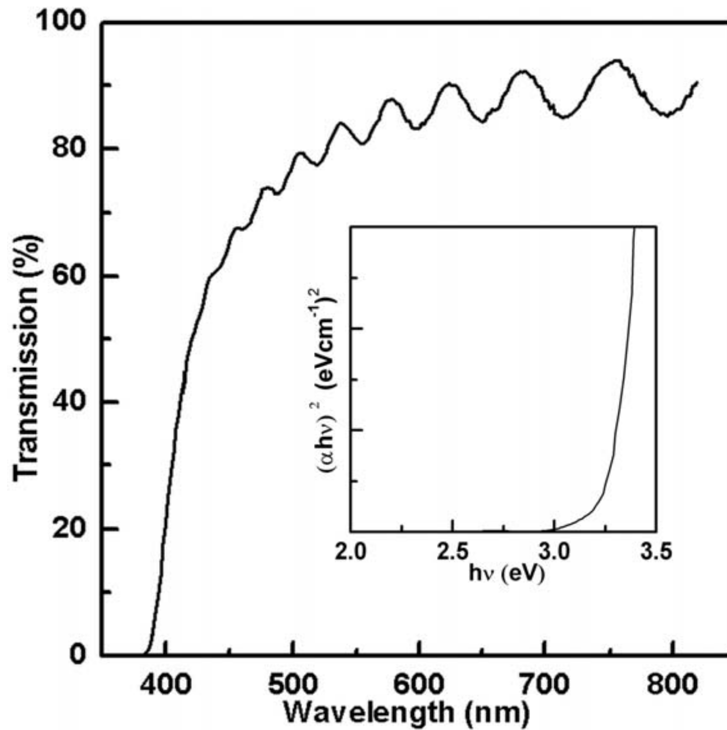

Figure 4.12. Transmission spectrum of ZnO thin films deposited by magnetron sputtering. Inset shows the $(\alpha h\nu)^2$ vs hν plot and the bandgap is 3.28 eV.

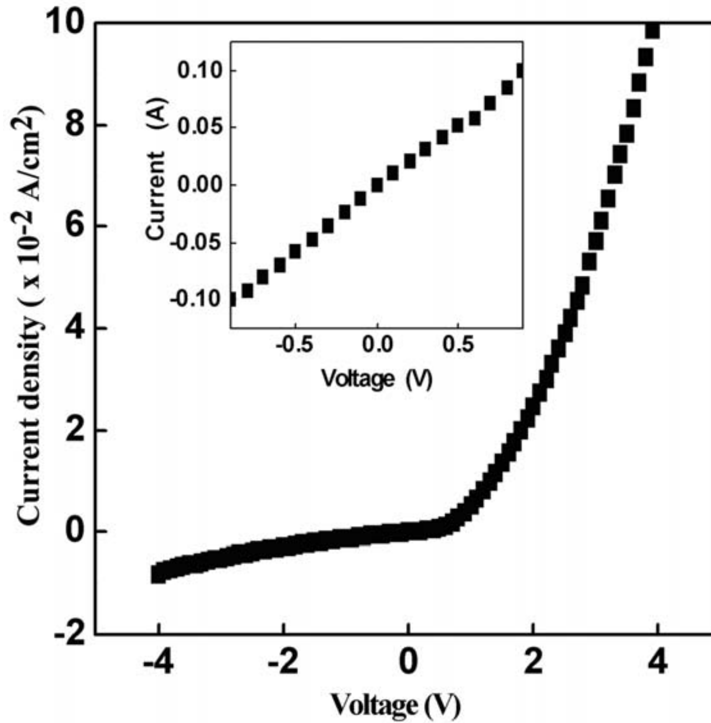

Figure 4.13 Current density - Voltage (J-V) characteristics of $AgCoO_2$/ZnO p-n junction diode and inset shows the I-V characteristics of ZnO/ITO contact

Figure 4.13 shows the typical J-V characteristics of ITO/n-ZnO/p-$AgCoO_2$ p-n heterojunction diode and ITO/ZnO contact is ohmic (shown in the inset of figure 4.13). The J-V characteristics show that the junction is rectifying. The maximum forward to reverse current ratio is about 10 at 3 V and the turn on voltage is 2 V. The diode ideality factor was determined from the slope of the forward bias ln I vs. V (figure 4.14).

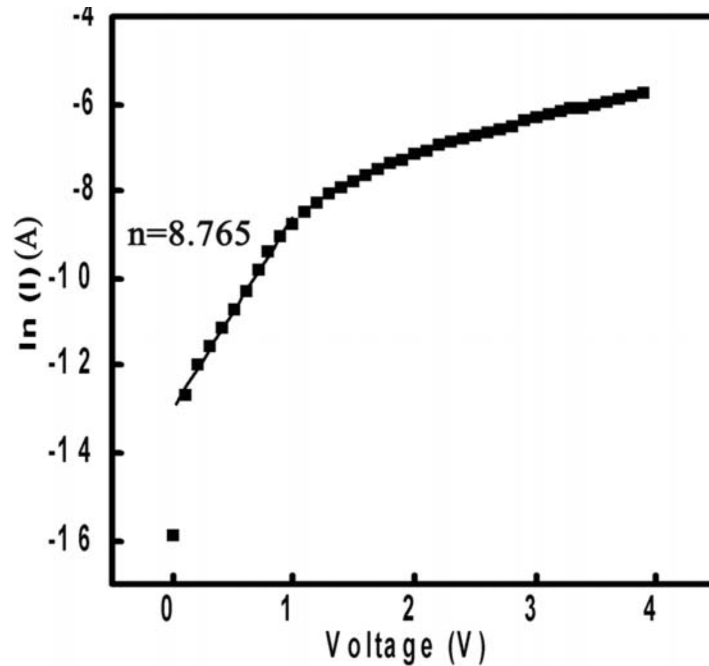

Figure 4.14. ln (I) vs. V plot for determining the ideality factor.

The diode does not confirm to the normal forward bias I-V relation The glass substrate coated with sputtered 200 nm indium tin oxide (ITO) is highly transparent (>85%) in the visible spectrum and has a conductivity 10^{-3} Scm^{-1} [18]. The Hall measurements on $AgCoO_2$ films could not determine the mobility of holes due to very low mobility. Thus the upper limit of mobility was assumed to be ~1 $cm^2V^{-1}S^{-1}$ and using the measured value of room temperature conductivity the carrier concentration n was estimated as ~ 1 x 10^{18} cm^{-3}. Based on the measured band gap of ZnO and $AgCoO_2$ the equilibrium energy band diagram for the p-$AgCoO_2$/n-ZnO/ITO p-n heterojunction can be obtained.(figure 4.15). ITO is n-type TCO which is degeneratively doped having a band gap 3.6 eV with its Fermi level 'E_f' slightly

above the conduction band minimum 'E_c'. The work function of ITO is ~ 4.7 eV [35], the n-type ZnO has band gap 3.3 eV and an electron affinity 4.2 eV [36]. Assuming p-type TCO with work function 7.5 eV, band gap being 4.15 eV and the electon affinity ~3.5 eV, band structure of the p-n heterojunction can be constructed. The carrier concentraton of the n-type ZnO is large and hence the Fermi level must be closer to the conduction band minimum while the p-type $AgCoO_2$ has large hole concentration and the Fermi level must be closer to the valance band maximum. As the p and n materials are brought into contact, a constant Fermi level will be formed at equilibrium. The expected built in voltage based on the band diagram is ~3 eV. The turn on voltage, 2 eV is smaller than the built in potential obtained from the energy band diagram. This can be attributed to the existence of large interface defect states. The interface defect states density can be calculated from the relation $N_{st}= a_2^2-a_1^2/a_1^2a_2^2$ [37] and lattice mismatch is related to $\Delta a/a = 2(a_2-a_1)/a_1^2a_2^2$, where a_1 and a_2 are the lattice constants of ZnO and $AgCoO_2$ respectively. Both ZnO and $AgCoO_2$ films are highly oriented. The X-ray diffraction of ZnO shows only (002) reflection while the X-ray diffraction of $AgCoO_2$ films shows only (00l) reflections. This suggests that both ZnO and $AgCoO_2$ films are highly oriented with their c axis perpendicular to the substrates.

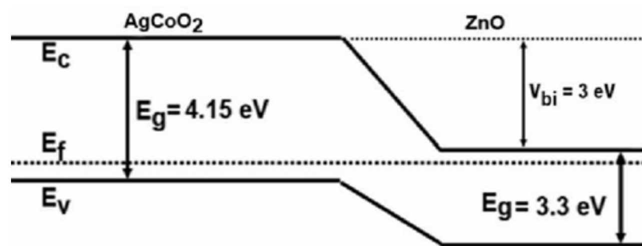

Figure 4.15 Equilibrium energy band diagram of the p–n heterojunction diode fabricated by rf sputtering.

At very small voltages the ideality factor n=8. In the interim voltage n=27 and at higher voltage n=60. The high value of ideality factor in the p-$AgCoO_2$/n-ZnO p n junction can be attributed to poor interface and defects at the interface. According to Wang *et al* [38] the heterojunction diode can be modeled in different bias ranges by a series of diode and resistance. The ideality factor of the device is the sum of ideality factors of the individual junction and may lead to ideality factor much greater than two.

4.5 Conclusion

In conclusion crystalline $AgCoO_2$ thin films with 50% transparency in the visible region were deposited on single crystalline Al_2O_3 and amorphous silica substrates by RF magnetron sputtering. P-type conductivity of $AgCoO_2$ was demonstrated by fabricating transparent p-n junction diode with $AgCoO_2$ as p-type semiconductor and ZnO: Al as n-type semiconductor using sputtering. Junction thus obtained was found to be rectifying with a forward to reverse current of about 10 at an applied voltage of 3 V. Ideality factor of the diode was found to be greater than 1, which could be attributed to the presence of interface defect states.

References

1. H.Kawazoe, M.Yasukawa, H.Hyodo, M.Kurita, H.Yanagi and H.Hosono *Nature* **389(**1997)939
2. K.Ueda, T.Hase, H.Yanagi, H.Kawazoe, H.Hosono, H.Ohta M.Orita and M. Hirano *J. Appl. Phys.* **89(**2001)1790
3. Yanagi H, Hase T, Ibuki S, Ueda K and Hosono H *Appl. Phys. Lett.,***78** (2001)1583
4. M K, Jayaraj ,A.D Draeske, J.Tate and A.W Sleight *Thin Solid Films* **397** (2001)244
5. N Duan, A W Sleight, M K Jayaraj and J.Tate *Appl. Phys. Lett.* **77** (2000)1325
6. A N Banerjee and K K Chattopadhyay *Progress in Crystal Growth and Characterization of Materials* **50(**2005) 52
7. H.Ohta, K.Kawamura ,M.Orita, M.Hirano, N.Sarkura and H.Hosono *Appl. Phys. Lett.***77**(2000)475
8. H Sato, T Minami, S.Takata and T.Yamada *Thin Solid Films* **236(**1993)27
9. T Aoki, Y Hatanaka and Look D C *Appl. Phys. Lett.* **76**(2000)3527
10. R L, Hoffman ,J.FWager, M K Jayaraj and J.Tate *J. Appl. Phys* **90(**2001)5763
11. H.Yanagi, K Ueda, H, Ohta, M Orita, M Hirano and H Hosono *Solid State Commun*. **12**(2001)15
12. Nie, S. H Wei and S. B Zhang *Phys. Rev. Lett.* **88**(2002)66405
13. T Otabe, K .Ueda, A.Kudoh, H .Hosono and H .Kawazoe *Appl. Phys. Lett.* **72** (1998)1036
14. K A Vanaja, R S Ajimsha, A S Asha and M K Jayaraj *Appl. Phys. Lett.* **88** (2006)212103
15. Y.Jshin , J.H Kwak and S.Yoon *Bull. Korean. Chem. Soc*. **18**(1997)775

16. J.S Kng, J.H Kwak, Y.J Shin, S.W Han, K.H Kim and B.I Min *Phys. Rev B* **61** (2002)10682
17. R Manoj, P. Promodan, Johny Isaac and M K Jayaraj Proc. *DAE Solid State Symposium.* **46**(2003)249
18. M Nisha, S Anusha, Aldrin Antony, R.Manoj and M.K Jayaraj *Appl. Surf. Sci*. **252(**2005)1430
19. M K Jayaraj, Aldrin Antony and R.Manoj *Bull of Material Science* **25 (**2002) 227
20. W Stahlin, H R Oswald and Anrg Z *Allg. Chem* **373**(1970)69
21. P.Hirsch, A.Howie, R B Nicholson, D W Pashley and M.J Whelan *Electron Microscopy of thin crystals* (Robert Krieger, New York)
22. R. S Ajimsha, K.A Vanaja, M.K Jayaraj, P.Misra V.K Dixit and L M Kukreja *Thin Solid Films* **515**(2007)7352
23. Yu P Y and Cardona M 1996 *Fundamentals of semiconductor physics and material properties* (Springer, Berlin)
24. P *.J* Kubelka*.Opt. Soc. Am*. **38(**1948) 448
25. P. Kubelka and F *ZTekh* Munk*, Phys* **12***(*1931)593
26. Mott N F 1974 *Metal-InsulatorTtransitions* (Taylor and Francis, London,).
27. V. Thangadurai and W Weppner *Chem. Mater* **14(** 2002)1136
28. Aldrin Antony, M.Nisha , R.Manoj ,and M.K.Jayaraj, *Appl.Surf.Sci* **225** (2004)294
29. M.Nisha and M.K.Jayaraj *Applied Surface Science* **255**(2008)1790
30. Pung Keun Song, Yuzo Shigesato, Itaru Yasui,, Cleva Ow. Yang, and C.Paine David, *Jpn.J.Appl.Phys*. **37**(1998)1870
31. JCPDS card No. 6-416

32. J.Tauc, R.Grigorovici, and A.Vancu *Phys.Stat.Sol(a)***15**(1966)627
33. H.L.Hartnagel, A.L.Dawar, A.K.Jain, C.Jagdish, *Semiconducting Transparent Thin Films*, IOP Publishing Ltd (1995)
34. K.L. Chopra, S. Major and D.K. Pandaya. *Thin Solid Films* **102**(1983)1
35. J.R Sheats, H. Antonisadis, M. Hueshen, W. Lenoard, J Miller, R.Moon D.Roitman and A.Stoking *Science* **273**(1996)884
36. W.Siripala, A.Ivanovskaya, T .F Jaramillo, S.H Baeck and E.W McFarland *Sol Energy. Mater. Sol. Cells* **77**(2003)229
37. D K Zhang, Y C Liu, Y L Liu and H.Yang *Physics B* **351**(2004)178
38. C. X Wang, G W Yang, H .W Liu, Y.H Han, J.F Luo, C.X Gao and G.T Zou *Appl. Phys. Lett.* **84(**2004)2427

Chapter 5

Hydrothermal synthesis of p-type $AgGaO_2$ and fabrication of n-ZnO/p-$AgGaO_2$ pn junction by pulsed laser deposition

Abstract

The synthesis of p-type delafossite $AgGaO_2$ bulk powder materials by hydrothermal method is described in detail. These powder materials have been characterised by various analytical techniques and the phase purity was confirmed. The silver gallium oxide thus synthesised has been used as the target for the growth of thin films by PLD. All oxide transparent ITO/ZnO/$AgGaO_2$ pn junctions have also been fabricated

5.1 Introduction

Delafossite type compounds [1] have general formula $A^IB^{III}O_2$ (A= Cu, Ag, Pt and Pd; B= Al, Fe, Co, Rh, Ga, Sc,In and rare earths). The structure of the delafossite type oxides can be described as the alternate stacking of edge shared BO_6^- octahedral layers and A^+ ion layers perpendicular to c axis (fig1.3chapter 1). Each A^+ ion layer is linearly coordinated by two O^{2-} ions [1]. These delafossites can crystallize in either the rhombohedral 3R (R3m) or hexagonal 2H ($p6_3/mmc$) polytype based on the stacking of the alternate layers of BO_6 octahedra and A^+ cations. This delafossite class of material has been of renewed interest since Kawazoe et al [2] reported p-type conductivity in transparent thin films of $CuAlO_2$. This was followed by reports of observation of p-type conductivity in transparent conducting films of $CuScO_2$ [3], $CuGaO_2$ [4], $CuY_{1-x}Ca_xO_2$ [5], $CuCr_{1-x}Mg_xO_2$ [6] and $CuInO_2$ [7]. Wide band gap semiconductors are difficult to be doped, particularly to p-type [8] and there is no report on p-type silver delafossite in thin film form, except for $AgCoO_2$ [9] The $AgInO_2$ [10] films doped with tin shows n-type conductivity. The synthesis of silver delafossites by conventional solid state reaction of the constituent oxides at high temperature has been found to be unsuccessful. Hence silver delafossites are generally prepared by cation exchange reaction or by hydrothermal synthesis. The presence of trace amounts of metallic silver in the products has been observed in the attempts to synthesize Ag based delafossites [11]. In the present work**,** the synthesis of $\alpha-AgGaO_2$ by a two step process involving the synthesis of β-$AgGaO_2$ by ion exchange reaction followed by the hydrothermal conversion of the β-$AgGaO_2$ into α-$AgGaO_2$.is attempted The trace amount of Ag has been

reduced substantially in the two step synthesis compared to the direct hydrothermal synthesis.

5.2 Synthesis of bulk $AgGaO_2$ powder

β-$AgGaO_2$ was prepared through the ion exchange reaction between β-$NaGaO_2$ and $AgNO_3$. The preparation of β-$AgGaO_2$ involves two steps viz, the synthesis of $NaGaO_2$ precursor and transformation to $AgGaO_2$. The $NaGaO_2$ precursor was synthesized by solid state reaction [12] of stoichiometric amounts of Na_2CO_3 and β-Ga_2O_3. The reaction was carried out by successive heating at 650^0C, 750^0C, 850^0C, 1000^0C, and 1050^0C for 24 h at each temperature. The β-$NaGaO_2$ thus obtained was transformed in to β-$AgGaO_2$ by reacting with excess molten $AgNO_3$ at 280^0C for 24 h under N_2 atmosphere. The $AgGaO_2$ thus obtained has orthorhombic structure. The excess $AgNO_3$ was removed by repeated washing with distilled water and the β-$AgGaO_2$ was then converted in to α-$AgGaO_2$ by hydrothermal reaction in a parr bomb at 250^0C. The reaction was continued for four days. The reagents used were β-$AgGaO_2$ and KOH(1 M) solution..X-ray diffraction (XRD) studies were carried out with Rigaku diffractometer in Brag-Brentano geometry ($\theta-2\theta$) using CuK_α radiation. The electrical conductivity of the sintered pellets was measured from 300 K to 70 K by two probe technique using Keithley source measure unit. Silver paste was used as the electrodes and ohmic nature of the contacts was confirmed before the measurements. Diffuse reflectance spectra of powder samples at room temperature with MgO as reference were recorded using Ocean optics SD 2000 fiber optic spectrophotometer. The thermo power measurements were carried out on the sintered pellets by producing a temperature difference on either side of the pellet and measuring the thermo emf produced.

5.2.1 Characterisation of the $AgGaO_2$ powder material

The x-ray diffraction patterns of the synthesized $NaGaO_2$ and β-$AgGaO_2$ are shown in (Figure 5.1). The orange β-$AgGaO_2$ has orthorhombic structure similar to β-$NaGaO_2$ with a=5.5645 , b=7.1522 and c=5.4697A^0. All the observed peaks can be indexed to that of the β-$AgGaO_2$[13] and $NaGaO_2$ [14]. The structure of 3R α-$AgGaO_2$ is described in space group R3m with Ag at 0 0 0, Ga at 0 0 1/2 , and oxygen at 0 0 z where z=0.1061. The structure of α-$AgGaO_2$ was refined by Rietveld analysis. Figure 5.2 shows the fitting profile calculated by Rietveld refinement, the observed X-ray diffraction data and their difference plot. Rietveld analysis was also carried out with three possible phases of $AgGaO_2$, Ag_2O and Ga_2O_3

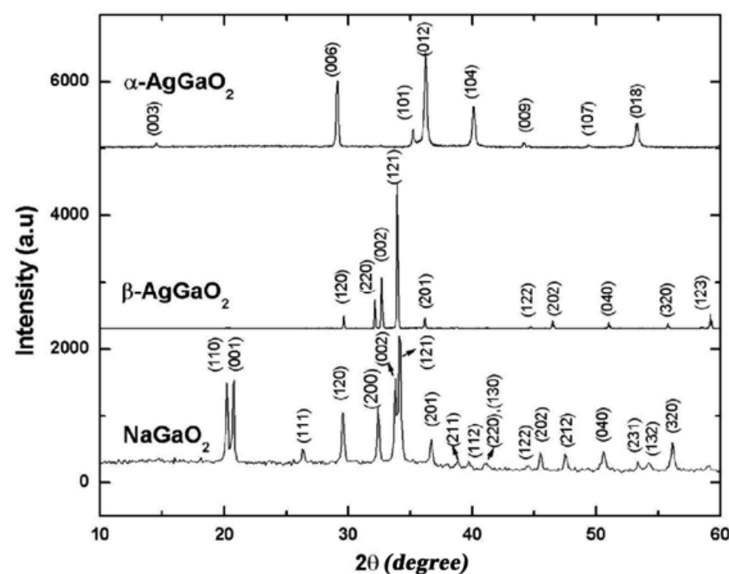

Fig.5.1. Powder X ray diffraction patterns of orthorhombic $NaGaO_2$, β-$AgGaO_2$ and α-$AgGaO_2$.

However, the refinement result did not fit with the observed X-ray diffraction pattern. The structure refinement performed on a single phase of delafossite type confirms the conversion of β-$AgGaO_2$ to α-$AgGaO_2$ by hydrothermal conversion.

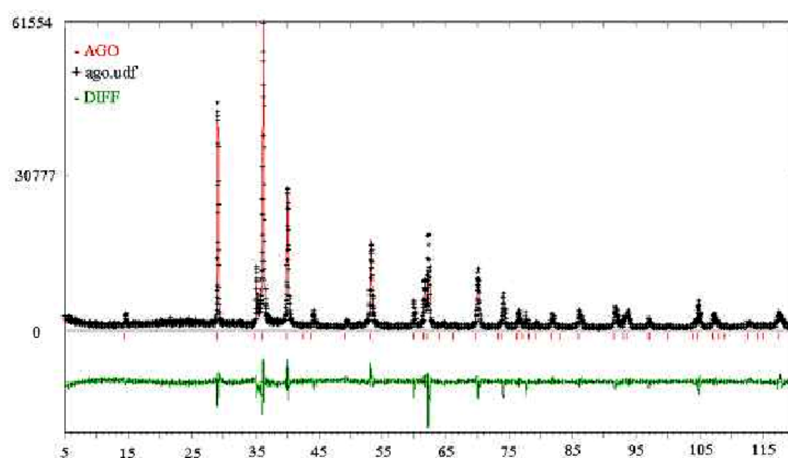

Fig.5.2. Calculated, and difference plots by Rietveld refinement and observed XRD pattern of α-$AgGaO_2$ obtained by hydrothermal reaction.

The scanning electron micrograph (SEM) image in figure 5.3 shows that the particle size of light green α-$AgGaO_2$ crystallite ranges from 1 μm to 3μm.The scanning electron microscopy (SEM) study shows that the morphology of the $AgGaO_2$ compound is hexagonal. The energy depressive X-ray (EDX) analysis shows that the compound is close to stoichiometry with Ag/Ga ratio 1.02. The presence of any secondary phases other than the α-$AgGaO_2$ was not detected by powder XRD. The electron diffraction pattern shown in fig.5.4 can be indexed to the planes of α-$AgGaO_2$.

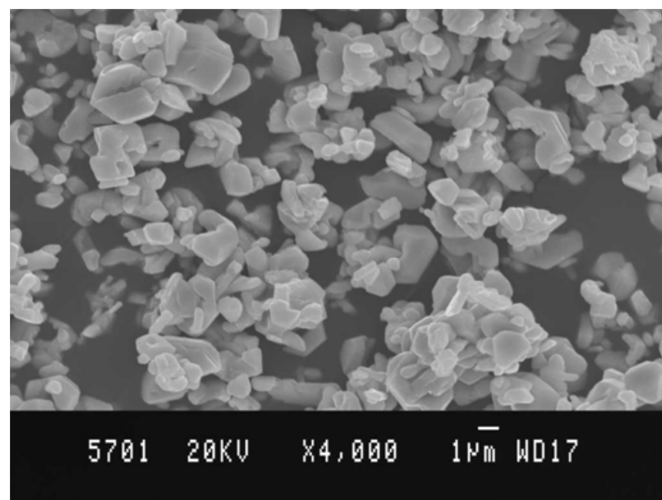

Fig.5.3. The SEM picture of α-$AgGaO_2$ powder grown by hydrothermal reaction

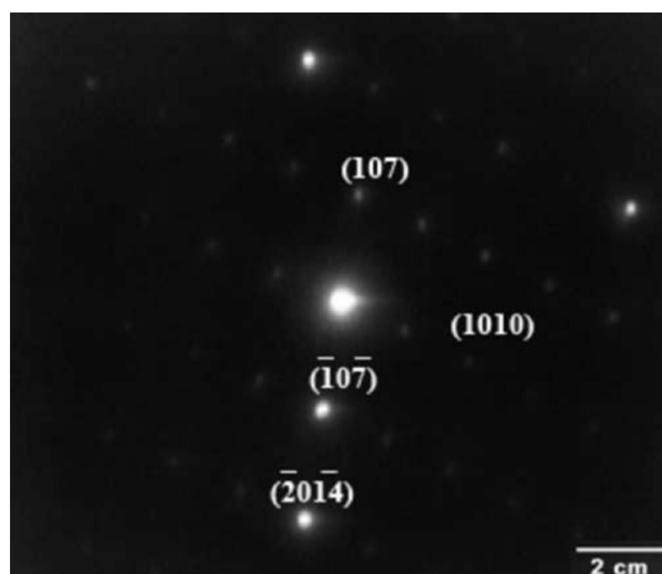

Figure 5.4 The electron diffraction pattern of the $AgGaO_2$ powder grown by hydrothermal reaction.

Inset of figure 5.5 shows the diffuse reflectance spectrum of α-$AgGaO_2$ powder in the visible region using MgO as the reference. The band gap of the α-$AgGaO_2$ powder sample was found to be 4.4eV from the plot of $\{(k/s)h\nu\}^2$ vs hν (fig.5.5) where k and s denote the absorption and scattering coefficients respectively and hν the photon energy. The ratio k/s was calculated from the reflectance spectrum via the Kubelka-Munk equation [15, 16].

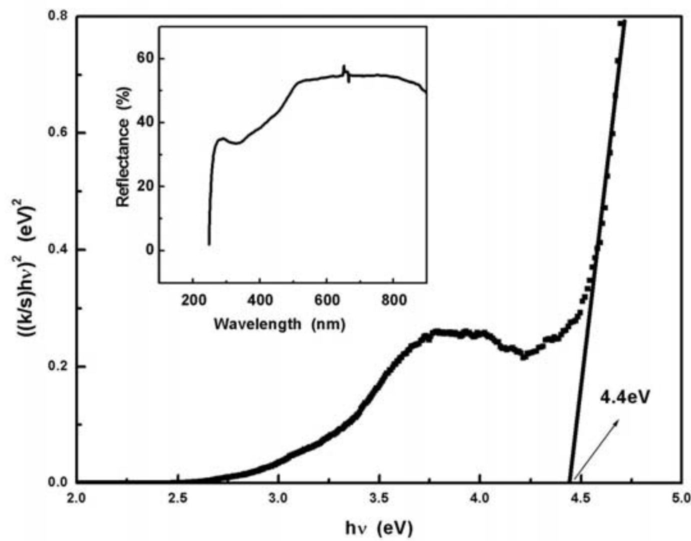

Fig.5.5 Plot of $\{(k/s)h\nu\}^2$ vs hν for α-$AgGaO_2$ giving a band gap of 4.4 eV. Inset shows the diffuse reflectance spectrum of α-$AgGaO_2$.

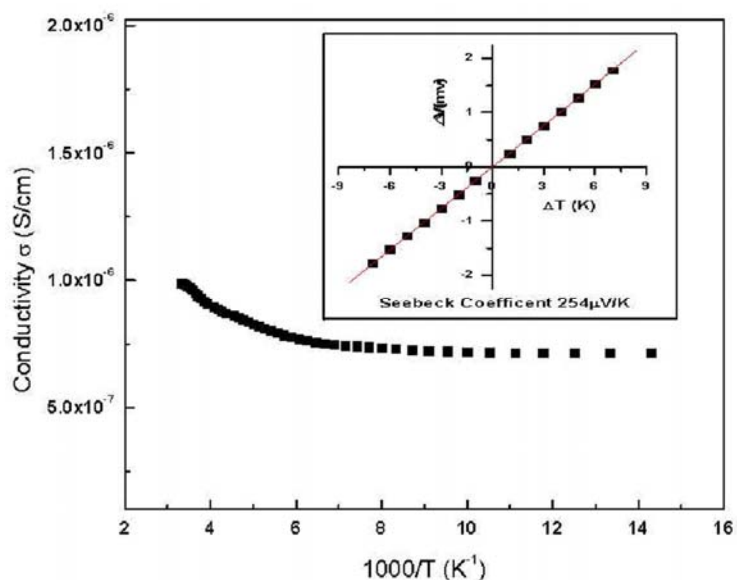

Fig 5.6. Temperature dependence of the dc electrical conductivity of α-$AgGaO_2$. The inset shows the result of Seebeck coefficient measurement of α-$AgGaO_2$

The temperature dependence of the electrical conductivity of undoped α-$AgGaO_2$ was studied in the temperature range of 300 K to 50 K by using sintered pellet of α-$AgGaO_2$. The pellets (1cm diameter) for electrical conductivity studies were synthesized by mixing the α-$AgGaO_2$ powder with poly vinyl alcohol and applying a pressure of 5 tones. The electrical contacts were made using silver paste and the ohmic nature of the contact was confirmed by studying the current voltage characteristic. The conductivity of α-$AgGaO_2$ bulk powder samples at room temperature was ~$1x10^{-6}Scm^{-1}$. The conductivity of α-$AgGaO_2$ samples do not show appreciable dependence on temperature (fig.5.6). At higher temperature, there is an increase in conductivity and the contribution of increased

conductivity seems to have started around room temperature. The temperature dependence of conductivity shows a semiconducting behavior (Fig 5.6). The undoped samples show very low conductivity which can be enhanced by replacing the trivalent Ga ion by divalent impurity or by oxygen intercalation. The oxygen annealing at atmospheric pressure increases the conductivity to $1x10^{-5}Scm^{-1}$. The type of conductivity was determined from the thermoelectric power measurement using the set up similar to the one reported in literature [17] (Inset of Fig.5.6) The positive sign of Seebeck coefficient (+254 μV/K) confirms that holes are responsible for electrical conduction.

5.3 Growth of $AgGaO_2$ thin films by PLD

α-$AgGaO_2$ thin films were prepared on silicon and Al_2O_3 substrates by pulsed laser deposition. The third harmonic (355 nm) of a Q-switched Nd: YAG laser (Spectra physics Quanta ray GCR series) was focused on to a rotating target. The repetition rate of the laser pulse was 10 Hz with pulse width of 9 ns and energy density of the laser was 1 J/cm^2 per pulse. The chamber was initially pumped down to base pressure of 10^{-6} mbar. Oxygen gas was then introduced in to the chamber and the working pressure of oxygen was controlled at 0.01 mbar. The substrate to target distance was kept at 3.7 cm. The substrate temperature was kept at 250^0C for silicon substrates and at 400^0C when Al_2O_3 was used as substrates. The details of experimental set up are discussed in section 2.3.3.The films were allowed to cool down to room temperature at the same oxygen pressure. The thickness of the deposited α-$AgGaO_2$ films was measured using a stylus profiler (Dektak 6M Stylus profiler) as 180 nm. The crystalline nature of the films was identified by x-ray diffraction using CuK_α line.

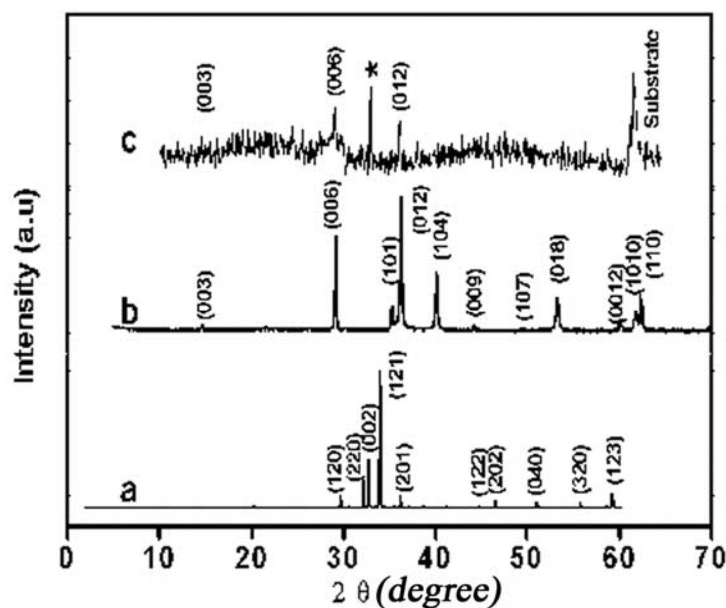

Fig 5.7 The x-ray diffraction patterns of a) α- $AgGaO_2$ powder, b) β-$AgGaO_2$ powder, and c) α-$AgGaO_2$ thin film. * indicates (002) peak of the impurity β-$AgGaO_2$ phase.

Figure 5.7 shows the diffraction patterns of β-$AgGaO_2$ (a) α-$AgGaO_2$ (b) and the thin film(c). The crystalline phase identified in the sample was found to belong to α-$AgGaO_2$ of R3m space group. A small impurity phase was also detected. The high resolution transmission electron micrograph (HRTEM) images of the α-$AgGaO_2$ films grown on carbon coated copper grids, under the same deposition conditions of film growth on silicon substrates are shown in figure 5.8. The nucleation and growth of the film in the form of nanorods with average diameter 20 nm and length up to 270 nm were observed. The atomic scale images of the films (inset of Fig. 5.8) show parallel lines of ions at intervals of 2.225 A^o for most of the grains. This lattice spacing coincides with d spacing

of α-$AgGaO_2$ (104). Similar growth has been observed in nano crystalline $CuAlO_2$ [19]. The d spacing observed does not match with that of Ag_2O or β-$AgGaO_2$. Energy dispersive x-ray analysis shows that the ratio of Ag/Ga is 1.02, which is close to the atomic ratio of α-$AgGaO_2$. The grains in the films grown on silicon substrates may be very small also and such nanoscale particles and small sample thickness may be the reason for the very weak signal in the x-ray diffraction pattern.

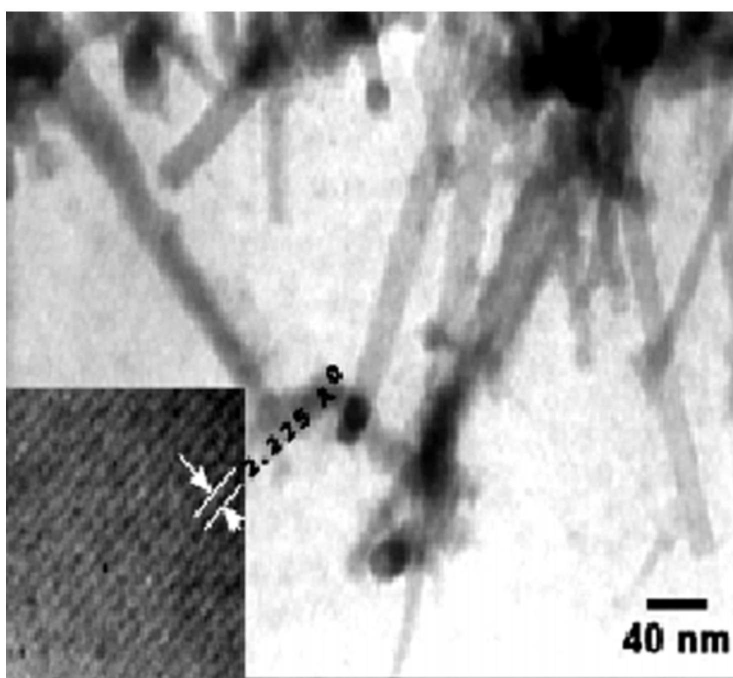

Figure. 5.8. TEM picture of α-$AgGaO_2$ thin film grown on carbon coated copper grid and the inset shows the atomic scale image of the film.

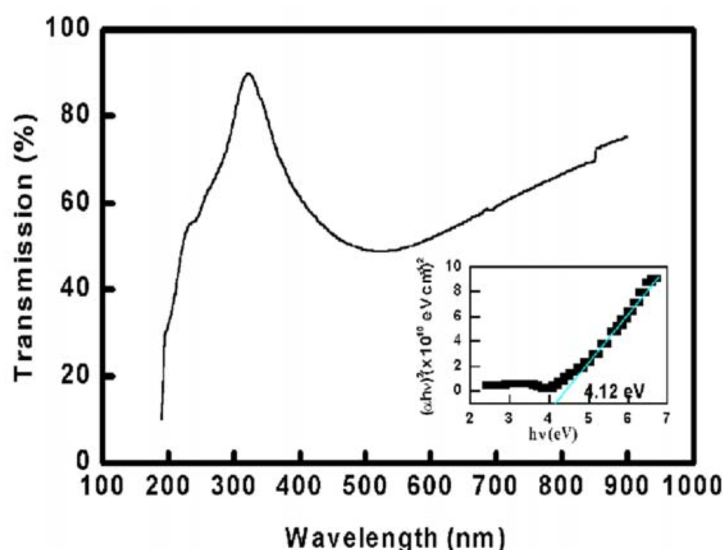

Figure 5.9. Transmission spectrum of the α-$AgGaO_2$ thin film. Inset shows the plot of $(\alpha\, h\nu)^2$ vs $h\nu$.

Figure 5.9 shows the optical transmittance of the α-$AgGaO_2$ films in the visible region. The films have transparency more than 50% in the visible region. The inset shows the plot of $(\alpha h\nu)^2$ vs. $h\nu$, where α is the absorption coefficient and $h\nu$ is the photon energy. The optical gap energy is estimated as 4.12 eV. The dc electrical conductivity of the samples was studied in the temperature range 50 K to 300 K. The room temperature conductivity of the undoped $AgGaO_2$ films was 3.17×10^{-4} Scm^{-1}. The activation energy at high temperature is 68 meV. The σ vs. 1/T plot is not well fitted by a straight line (shown in Fig. 5.10). However the log $\sigma T^{1/2}$ vs. $1/T^{1/4}$ plot (inset of Fig. 5.10) is close to a straight line suggesting that a variable range hopping [20] is dominant in positive hole conduction at the top of valance band which is observed in similar delafossite

materials [4,6]. The contribution from the impurity phase for the conductivity of the film may be very small. The Ag^+ ions contributing to the conductivity has been estimated by measuring the transference number, $t = \frac{\sigma_0 - \sigma_\infty}{\sigma_0}$ (σ_0 is the conductivity at t = 0 and σ_∞ is the saturated conductivity) using the dc polarization method [21]. The evaporated gold (1.5 μm thick) forms the blocking electrode. The variation of conductivity has been noted under a steady dc potential of 500 mV over a time of two hrs. The variation in conductivity is very small (Fig. 5.11) and the estimated transference number is 0.03 indicating the ionic contribution to conductivity is negligible. [21]

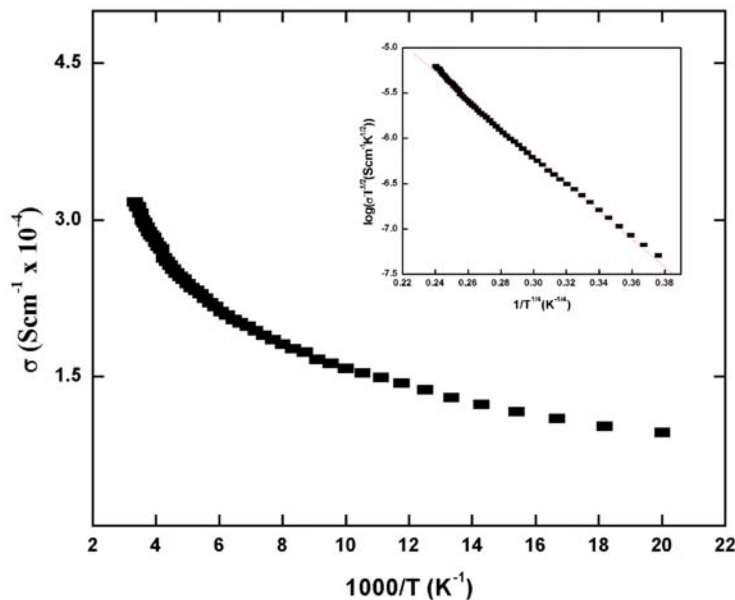

Figure. 5.10 Conductivity σ vs $1/T$ and inset shows log $(\sigma T)^{1/2}$ vs $1/T^{1/4}$ of theAgGaO_2 thin film.

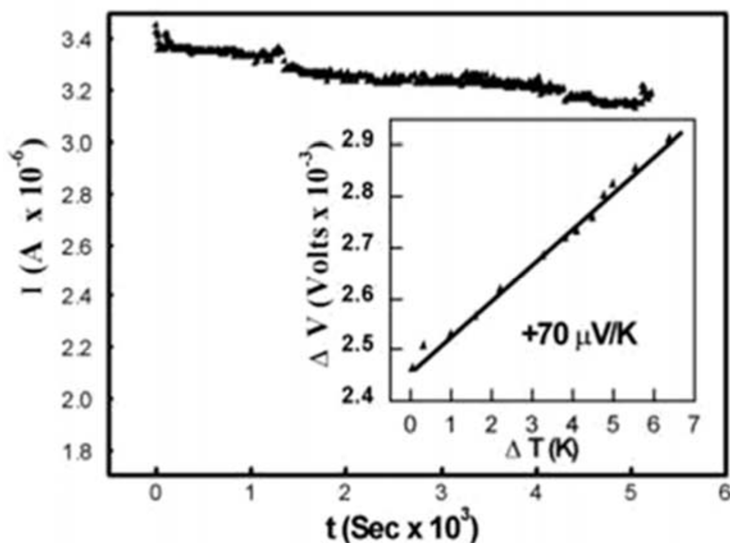

Figure 5.11. The variation of current (I) of $\alpha-AgGaO_2$ under a steady dc potential of 500 mV over a time of two hrs and inset shows the variation of thermo emf of the film with ΔT.

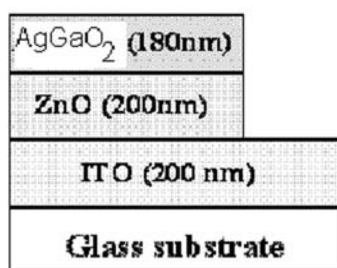

Figure 5.12 The structure of the n-ZnO/p-$AgGaO_2$pn junction

The carriers responsible for conduction are holes which was identified from the Seebeck coefficient measurement. The positive Seebeck coefficient of 70 μVK^{-1} at room temperature indicates that the conduction is p-type. The

possible application of p-type TCO has been demonstrated by fabricating a p-n junction. The transparent heterojunction diodes have a structure, glass/ITO/n-ZnO/p-$AgGaO_2$ as shown in Fig. 5.12.

The indium tin oxide thin film was deposited by rf magnetron sputtering in our laboratory [22]. The parameters used for the deposition of ITO are briefly described here. Indium tin oxide films were deposited by rf magnetron sputtering of ITO target containing 95 wt.% of In_2O_3 and 5 wt.% of SnO_2. The target used for sputtering was prepared from In_2O_3 (99.99% pure) and SnO_2 (99.999% pure) powders. The powders were mixed in a mechanical shaker for 1hour, pressed into pellets of two-inch diameter and then sintered at 1300 ^{0}C for 6 hours in air. The rf sputtering was carried out in a vacuum chamber in which high vacuum of the order of2 x 10^{-5} mbar was created by means of an oil diffusion pump backed by a rotary pump. The rf power was delivered to the target material by an rf generator (13.56 MHz) through an impedance matching network. Glass slides of dimension 2.5 cm x 1 cm were used as the substrates. The substrates were kept above the target at a distance of 4 cm, which was found to be optimum for the growth of good quality crystalline films [23]. Initially the substrate was heated to the required temperature. After attaining the required substrate temperature, high purity argon gas was allowed to flow into the chamber and it was adjusted by a mass flow controller to maintain the argon pressure at 0.01 mbar. The films were deposited at an rf power of 30W. The target was pre-sputtered for 10 minutes before each deposition in order to remove any contaminants and to eliminate any differential sputtering effects. By keeping all other parameters the same, sputtering was carried out for various substrate temperatures ranging from room temperature to 300^{0}C. For films deposited at room temperature, the temperature

of the substrate increased by 20 to 50 degrees during deposition. But when the films were deposited on the preheated substrates, the temperature of the substrate was maintained at the specified value by controlling the power applied to the heating coil. The sputtering time was adjusted such that all the films used in this study were of thickness 220 nm. Table shows the properties of ITO thin films deposited at various substrate temperatures. The lowest resistivity was obtained when the substrate temperature was 150^0C. Hence ITO electrodes for the device fabrication were deposited at a substrate temperature of 150^0C .

The undoped ZnO was deposited on to the ITO coated glass substrates by PLD at an oxygen partial pressure of 10^{-4} mbar and at a laser power of 2 J/cm^2 for 20 minutes resulting in a film of 200 nm thickness. The target to substrate distance was 5.5 cm and substrate temperature was kept at 400^0C. The films were crystalline with (002) planes parallel to the substrate surface, indicating that growth was along c-axis. The ZnO films deposited by PLD have transparency greater than 85% in the visible region, band gap of 3.28 eV, and conductivity of about 44 Scm^{-1}.The conditions for the growth ZnO layer by PLD had been optimized in the laboratory [25]. Depositing the p-type $AgGaO_2$ over the ZnO completed the device. The ITO/ZnO contact is ohmic (inset b of Fig.5.13). The typical current voltage (I-V) characteristics of the p-n heterojunction diode is shown in Fig. 5.13. The n-ZnO/p-$AgGaO_2$ junction shows a rectifying characteristic with the forward current to reverse current ratio larger than 100 at applied voltage of –1.5 to +1.5 volts. The turn on voltage of the device varied between 0.9 volt to 1.1 volt from junction to junction.

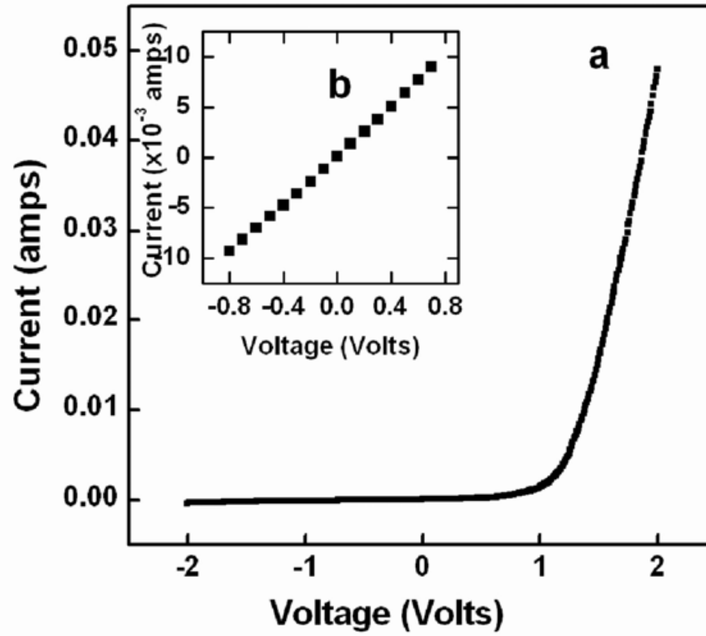

Figure 5.13. The current voltage characteristics for the $AgGaO_2$/n-ZnO p-n heterojunction. Inset shows Ohmic nature of ITO/ZnO contact.

5.4 Conclusion

The single phase α-$AgGaO_2$ bulk powders were grown by a low temperature hydrothermal process. The synthesised samples do not show any impurity phases. The DRS studies show that the material has wide band gap while the thermopower measurements show that the carriers responsible for conduction are holes. These studies indicate the possibility of using this material as p-type material in thin film form for transparent electronics. We have grown wide band gap α-$AgGaO_2$ p-type conducting thin film by pulsed laser deposition. The room temperature conductivity was measured as 3.17×10^{-4}

Scm^{-1}and the optical band gap was estimated as 4.12 eV. The transparency of the PLD deposited α-$AgGaO_2$ film is around 60%. A transparent p-n junction thin film diode on glass substrate was fabricated using p-type α-$AgGaO_2$ and n-ZnO.

References

1. R.D Shannon, D.B Rogers and C.T Prewitt, *Inorg. Chem* **10** (1971)713.
2. H.Kawazoe, M.Yasukawa , H.Hyodo,M.Kurita, H.Yanagi, H. and H.Hosono,*Nature* **389(**1997)389.
3. N..Duan,A.W Sleight,.M.K Jayaraj and Tate*,* *J., Appl.Phys.lett.,* **77** (2000)1325.
4. K.Ueda, T.Hase, H.Yanagi, H.Kawazoe, H.Hosono, H.Ohta, M.Orita and M.Hirano, , *Appl.Phys.Letts.* **89(**2001)1790.
5. M.K Jayaraj, A.D Draeske, J. Tate and A.W Sleight, *Thin Solid Films* **397**(2001)244.
6. R.Nagarajan, A.D Draeseke,A.W Sleight and J.Tate, *J.Appl.Phys* **89** (2001)8022.
7. H.Yanagi,., T.Hase, S.Ibuki K.Ueda, and . H Hosono,., *Appl.Phys.Lett.* **78(**2001)1583.
8. X.Nie, S.H Wei and S.B Zhang, *Phys.Rev.Lett.,* **88**(2002)66405.
9. J.Tate, M.K Jayaraj, A.D Draeseke, T.Ulbrich, A.W.Sleight, K.A Vanaja, R.Nagarajan, J.F Wager and R.L Hoffman, *Thin solid films* **411(**2002)119.
10. T.Otabe, K.Ueda, A.H Kudoh, H.Hosono and H.Kawazoe, *Appl.Phy. Lett.* **72**(1998)1036.
11. D.Shahriari, N.Erman, U.T.M.Haug, M.C.Zarzyczny,L.D Marks, and K.R Popelmeier *J.Phys Chem.Solids* **64(**2003)1437.

12. G.A Korteweg and L.L Van *Reijen J.Phys.Chem solids* **142**(1981) 987.
13. JCPDS Card no. 21-1076.
14. JCPDS Card no 51-1132.
15. P.Kubelka *J.Opt.Soc.Am* **38**(1948)448.
16. P.Kubelka and F.Monk *Z.Tech.Phys* **12**(1931)593
17. D.L Young, T.J Coutts ,V.I Kaydanov *Review of Scientific Instruments 71(2000)462*
18. R. Nagarajan, N. Duan, M. K. Jayaraj, J. Li, K. A. Vanaja, A. Yokochi, A. Draeseke, J. Tate and A. W. Sleight *Intl. J. Inorg. Mater* **3**(2001)265.
19. H.Gong, Y. Wang and Y. Luo *Appl. Phys. Lett.* **76**(2000)3959
20. N. F. Mott, *Metal-Insulator transitions* (Taylor and Francis, London, 1974).
21. V. Thangadurai and W. Weppner *Chem. Mater* **14**(2002)1136
22. M. Nisha, S. Anusha, A. Antony, R. Manoj, and M. K. Jayaraj, *Appl. Surf. Sci*, **252**(2005)1430.
23. A. Antony, M. Nisha, R. Manoj and M.K. Jayaraj, *Appl. Surf. Sci*, **225** (2004)294
24. R. S. Ajimsha, M. K. Jayaraj, and L. M. Kukreja, *Journal of Electronic Materials,* **37**(2008)770
25. R.S, Ajimsha. *Ph.D thesis*, Cochin University of Science and Technology, 2008.

Chapter 6
Summary and scope for future work

Abstract

The chapter gives the summary of the work carried out and a brief outlook for future work in the area of transparent electronics.

6.1 Summary

Transparent electronics is an emerging area. Transparent conducting oxides with electrons as carriers are well known. The carrier concentration in these n-type TCOs can be controlled either by doping or by varying the stoichiometry. However, the progress of the field of transparent electronics is hindered by the lack of suitable p-type TCOs. Recently, co-doping of ZnO has been proposed to achieve p-type conduction [1]. The advantage of co-doping is that an increase in solubility of introduced dopants creates shallow acceptor levels in the band gap. This technique has been applied to ZnO to realize p-type conduction in ZnO thin films [2]. The reproducibility of p-type ZnO remained a difficult task for quite a long time. Recently, the researchers have been successful in establishing techniques that will result in reproducible p-type ZnO and thereby facilitating the fabrication of ZnO based homojunctions. [3-5] In 1997 Kawazoe et al from Tokyo Institute of Technology reported another class of materials in thin film form that exhibits p-type conductivity [6]. Followed by this report there were numerous reports on various copper delafossites, grown in thin film form which are reasonably transparent and conducting [7-10] Wide band gap semiconductors are difficult to be doped particularly to p-type [11] and there is no report on p-type silver delafossite in thin film form, except for $AgCoO_2$ [12] The $AgInO_2$[13] films doped with tin shows n-type conductivity.

In the present studies, various copper delafossite materials viz; $CuAlO_2$, $CuGaO_2$, $CuFeO_2$, $CuGa_{1-x}Fe_xO_2$, $CuYO_2$ and $CuCa_xY_{1-x}O_2$ were synthesised by solid state reaction technique. These copper delafossite materials were grown in thin film form by rf magnetron sputtering technique. In general copper delafossites exhibit good optical transparency. The conductivity of the $CuYO_2$ could be improved by Ca doping or by oxygen intercalation by annealing the

film in oxygen atmosphere. It has so far been impossible to improve the p-type conductivity of $CuGaO_2$ significantly by doping Mg or Ca on the Ga site. The p-type conductivity is presumed to be due to oxygen doping or Cu Vacancies [6]. Reports in literature show, oxygen intercalation or divalent ion doping on Ga site is not possible for $CuGaO_2$ thin films to improve the p-type conductivity. Sintered powder and crystals of $CuFeO_2$ have been reported as the materials having the highest p-type conductivity [14, 15] among the copper and silver delafossites. However the $CuFeO_2$ films are found to be less transparent in the visible region compared to $CuGaO_2$. Hence in the present work, the solid solution between the $CuGaO_2$ and $CuFeO_2$ was effected by solid state reaction, varying the Fe content. The $CuGa_{1-x}Fe_xO_2$ with Fe content, x=0.5 shows an increase in conductivity by two orders, compared to $CuGaO_2$ but the transparency is only about 50% in the visible region which is less than that of $CuGaO_2$.

The synthesis of α–$AgGaO_2$ was carried out by two step process which involves the synthesis of β-$AgGaO_2$ by ion exchange reaction followed by the hydrothermal conversion of the β-$AgGaO_2$ into α-$AgGaO_2$. The trace amount of Ag has been reduced substantially in the two step synthesis compared to the direct hydrothermal synthesis. Thin films of α-$AgGaO_2$ were prepared on silicon and Al_2O_3 substrates by pulsed laser deposition. These studies indicate the possibility of using this material as p-type material in thin film form for transparent electronics. The room temperature conductivity of α-$AgGaO_2$ was measured as 3.17×10^{-4} Scm^{-1} and the optical band gap was estimated as 4.12 eV. A transparent p-n junction thin film diode on glass substrate was fabricated using p-type α-$AgGaO_2$ and n-ZnO.

$AgCoO_2$ thin films with 50% transparency in the visible region were deposited on single crystalline Al_2O_3 and amorphous silica substrates by RF magnetron sputtering and p type conductivity of $AgCoO_2$ was demonstrated by fabricating transparent p-n junction diode with $AgCoO_2$ as p-side and ZnO: Al as n-side using sputtering. The junction thus obtained was found to be rectifying with a forward to reverse current of about 10 at an applied voltage of 3 V.The present study shows that silver delafossite thin films with p-type conductivity can be used for the fabrication of active devices for transparent electronics applications.

6.2 Scope for future work

The pn junction fabricated in the present study shows that, the diode ideality factor deviates very much from normal diode behaviour. This is mainly due to the poor interface between the p and n-type TCOs. The conductivity of n-type ZnO TCO used for the fabrication of pn junction mainly depends on oxygen deficiency, where as the conductivity of p-type delafossite increases on oxygen intercalation. Hence the growth conditions of one are detrimental for the other. It is expected that the epitaxial growth of both n-type and p-type oxide layers will result in a better junction. Since both these oxides have band gap greater than 3 eV, UV light emitting diodes can be fabricated using all oxide transparent heterojunctions. The transparent pn junction can also be used as smart windows which can utilise the ultraviolet part of the sunlight for photovoltaic generation while depending on the plasma frequency of the TCOs IR part can be made reflecting.

The transparent thin film transistor (TTFT) is another active component in the field of transparent electronics. There are numerous reports on TTFT using n-type TCO as the channel layer [16]. The delafossite p-type TCO can be used

for the fabrication of p-channel TTFTs. The main drawbacks of these p-type TCOs are their much lower carrier mobility and high carrier concentration. Various growth techniques have to be employed to get better crystalline films which can lead to better mobility for the carriers. Cu(I), Ru(III) oxide, lanthanum copper oxysulphides ,lanthanum copper selenides etc have been investigated as p-type materials. The hole mobilities of p-type channel layers are very low compared to the electron mobilities of n-type channel layers. Considerable material development remains a task, before high performance devices can be realised. The transparent electronics calls for the development of new materials especially p-type TCOs and growth techniques for realising active and passive components with high performance efficiency. Another research area with high prospects is the study of magnetic impurity doped delafossite materials. The ZnO based dilute magnetic semiconductors which are transparent are widely being investigated for spintronics applications. The transition metal dopants can be easily incorporated into the delafossite materials and this technique offers the possibility of applications in the field of spintronics.

References

1. T.Yamamoto and H.Katayama-Yoshida *Jpn.J.Appl.Phys* **38**(1999)l166.
2. M.Joseph, H.Tabata and T.Kawai *Jpn.J.Appl.Phys* **38**(1999) l1205.
3. D.K.Hwang, K.H.Bang,M.C.Jeong and J.M.Myong *J.Cryst.Growth* **254** (2003)449.
4. S.Tuzemen,G.Xiong,J.Wilkinson, B.Mischuck, K.B.Ucer and R.T.Williams *Physica B* **308-310**(2003)1197.
5. T.Akoi, Y.Hatanaka and D.C.Look *Appl.Phys.Lett* **76**(2000)3257.

6. H.Koawazoe, M.Yasukawa,H.Hyodo, M.Kurita, H.Yanagi and H.Hosono *Nature* **389(**1997)939.
7. N.Duan, A.W.Sleight, M.K Jayaraj and J.Tate *Appl.Phys.lett.* **77(**2000) 1325.
8. K.Ueda, T.Hase, H.Yanagi, H.Kawazoe, H.Hosono, H.Ohta, M.Orita and M.Hirano *Appl.Phys.Letts* **89**(2001)1790.
9. M.K Jayaraj, A.D Draeseke, J.Tate and A.W Sleight *Thin Solid Films,* **397** (2001) 244.
10. R.Nagarajan, A.D Draeseke, A.W Sleight and J.Tate .*Appl.Phys*. **89**(2001) 8022.
11. X .X.Nie., S-H.Wei and S.B Zhang *Phys.Rev.Lett.* **88**(2002)66405.
12. J.Tate, M.K Jayaraj, A.D Draeseke, T.Ulbrich, A.W Sleight, K.A Vanaja,R.Nagarajan,J.F Wager and R.LHoffman *Thin solid films* **411** (2002)119.
13. T.Otabe, K.Ueda, A.H Kudoh, H.Hosono and H.Kawazoe *Appl.Phy. Lett.* **72**(1998)1036.
14. K.Ueda, T.Hase, H.Yanagi, H.Kawazoe H.Hosono, H.Ohata, M.Orita and M.Hirano *J.Appl.Phys* **89**(2001)1790.
15. D.B.Rogers, R.D.Shannon, C.T.Prewitt and J.L.Gillson *Inprganic Chemistry* **10(**1971)723
16. J.F.Wager, D.A.Keszler and R.E.Presely *Transparent electronics*, Springer, (2007)